Høgskulen på Vestlandet

ING5002 - Master Thesis

ING5002

Predefinert informasjon

Startdato:	15-05-2023 12:00 CEST	**Termin:**	2023 VÅR
Sluttdato:	01-06-2023 14:00 CEST	**Vurderingsform:**	Norsk 6-trinns skala (A-F)
Eksamensform:	Masteroppgave		
Flowkode:	203 ING5002 1 MOPPG 2023 VÅR		
Intern sensor:	(Anonymisert)		

Deltaker

Kandidatnr.:	203

Informasjon fra deltaker

Antall ord *:	33364

Egenerklæring *: Ja

Jeg bekrefter at jeg har registrert oppgavetittelen på norsk og engelsk i StudentWeb og vet at denne vil stå på vitnemålet mitt *: Ja

---

Jeg godkjenner avtalen om publisering av masteroppgaven min *
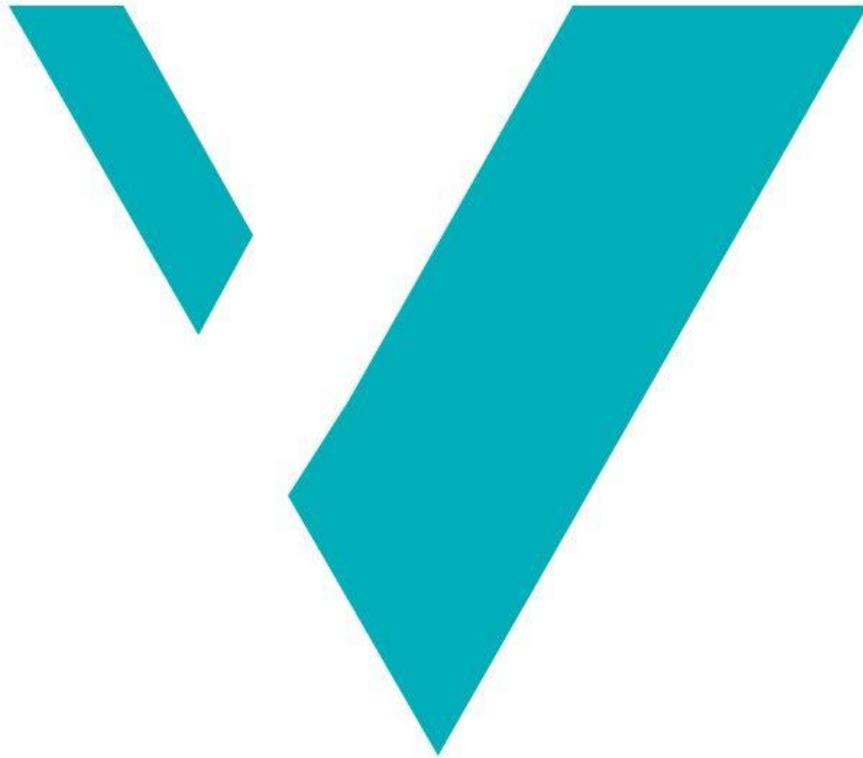
Ja

Er masteroppgaven skrevet som del av et større forskningsprosjekt ved HVL? *

Nei

Er masteroppgaven skrevet ved bedrift/virksomhet i næringsliv eller offentlig sektor? *

Nei

Computational modelling of enclosure fires with exposed timber surfaces

Martin D. Granum

WESTERN NORWAY UNIVERSITY OF APPLIED SCIENCES

MASTER THESIS IN FIRE SAFETY ENGINEERING

HAUGESUND

SPRING 2023

Computational modelling of enclosure fires

with exposed timber surfaces

Master thesis in Fire Safety Engineering

Author:	Author sign.
Martin D. Granum	*Martin D Granum*

Thesis submitted:	
Spring 2023	Open thesis

Tutors: Xiaoqin Hu and Sanjay Kumar Khattri	

Keywords:	Number of pages: 117
Cross-laminated timber (CLT), enclosure fire, FDS, pyrolysis model, numerical modelling, computational modelling, wood structure, fire simulation	+
	Appendix: 18
	Haugesund, June 1st, 2023
	Place/Date/year

Preface

I want to extend my gratitude to my two supervisors, Xiaoqin Hu (Vicky) and Sanjay Kumar Khattri, for their guidance while crafting this thesis. Their expertise greatly influenced the development of the model and the structure of this report, proving essential in bringing this work to fruition.

This thesis served as my gateway to diving into the world of computational modelling of fires, with the ambition of acquiring skills I can integrate into my career as a fire engineering consultant. The completion of this work has fulfilled this aspiration, yet more doors have opened with further questions needed to be answered that I am excited to embark upon.

Lastly, I owe a unique expression of gratitude to my parents. Their unwavering support throughout this pivotal phase of my life extended beyond encouraging words. They provided a comforting home, nourishing meals and exhibited a patience I am immensely grateful for. This journey would not have been the same without their love and support.

Abstract

In an era where sustainable materials like timber are becoming more prevalent in building design and construction, it's crucial to understand and accurately model the behavior of structure fires involving these materials One of the challenges that fire engineers face is being able to predict how the progression of a room fire with exposed wood surfaces develops. This thesis therefore focuses on using computational fluid dynamics (CFD), specifically the Fire Dynamics Simulator (FDS) software, to model enclosure fires involving exposed Cross-Laminated Timber (CLT) surfaces.

The existing body of research exploring the use of CFD software for modelling fires involving exposed timber surfaces is limited. Additionally, the accuracy of results from these studies varies widely. However, interest in this area of research is growing due to its potential in facilitating safe, economically viable, and aesthetically pleasing building solutions. An investigation of the subject is here presented, aiming to contribute to this emerging field and provide insight into existing knowledge, modelling methodology, and result analysis.

FDS was used to model a previously conducted compartment fire experiment involving CLT, based on the work by Bartlett et al. [1]. The simulation incorporated a pyrolysis model provided by Rinta-Paavola & Hostikka [2] to model the release of combustible gases from the exposed timber. Accuracy validation of the FDS model became feasible by comparing the model results with the experimental data. This comparison also facilitated the identification of the model's limitations and provided a basis for subsequent discussions on potential enhancements in the model.

The results from the simulation were inconclusive. The heat release rate (HRR) aligned with the experimental data at an acceptable level, but the temperature readings inside the CLT elements and compartment gas-phase temperature provided insufficient output. The mass loss rate (MLR) from the CLT showed a degree of coherence with experimental data, but the estimations methods to calculate MLR in the experiment by Bartlett et al. gave further insecurities about the accuracy. The most significant limitation of the model was its underperformance in predicting gas-phase temperatures, which in turn impacted other outputs. Suggestions for model improvement include adjusting grid resolution and refining the material properties and the pyrolysis model used for CLT. Additionally, strategies to decrease computational time are strongly recommended, as this can significantly expedite progress in research involving such simulation models.

Sammendrag

I en tid der bærekraftige materialer som tre blir stadig ber utbredt i konstruksjon- og bygningsindustrien er det avgjørende å forstå og nøyaktig kunne modellere brannforløpet knyttet til konstruksjoner med disse materialene. En av utfordringene som branningeniører står ovenfor er å kunne forutsi hvordan brannforløpet i rombrann med eksponerte treoverflater utvikler seg. Denne oppgaven fokuserer derfor på bruk av numerisk fluiddynamikk (CFD), spesifikt programvaren Fire Dynamics Simulator (FDS), for å modellere rombrann der eksponerte overflater av krysslaminert tre (KLT) involveres i brannen.

Eksisterende forskning på bruk av CFD-programvare for modellering av slike branner er begrenset. Imidlertid vokser interessen for dette forskningsområdet på grunn av dets potensiale til å fasilitetere for trygge, økonomisk gunstige og estetisk appellerende bygningsdesign. En nærmere undersøkelse av forskningsområdet presenteres her, med sikte om å bidra med innsikt i eksisterende kunnskap, modelleringsmetodikk og resultatanalyse.

FDS ble anvendt for å modellere et tidligere gjennomført rombrannforsøk av Bartlett et al. [1] hvor romoverflater var bestående av KLT. Modellen inkorporerte en pyrolysemodell utviklet av Rinta-Paavola & Hostikka [2] for å simulere frigivelsen av brennbare gasser fra treoverflatene. FDS-modellen ble validert ved å sammenligne FDS utdataen med eksperimentelle data. Denne sammenligningen gjorde det også mulig å identifisere begrensningene til modellen som gir grunnlag for påfølgende diskusjoner om potensielle forbedringer.

Resultatene fra simuleringen var ikke entydige. Varmeavgivelsesraten (HRR) samsvarte med den eksperimentelle dataen til en akseptabel grad, men temperaturendringene inne i KLT-elementene og røykgasstemperaturer i rommet ga utilstrekkelige resultater. Massetapsraten (MLR) fra KLT viste en viss korrelasjon med eksperimentelle data, men på bakgrunn av metodene benyttet for å beregne MLR i eksperimentet utført av Bartlett et al. var det for mange usikkerheter knyttet til valideringen for å gjøre en sikker vurdering av resultatene. Den mest betydelige begrensningen med modellen var dens evne til å forutsi gassfasetemperaturene, noe som også påvirket kvaliteten for andre resultater. For å forbedre denne modellens nøyaktighet, anbefales det å fokusere på gridoppløsning og videreutvikling av materialegenskaper og pyrolysemodell for KLT. Det anbefales også sterkt å gjennomføre strategier for å redusere simuleringstidene. Dette vil kunne bidra vesentlig til fremdriften av pågående forskning knyttet til slike simuleringer.

1. Table of content

List of Figures

List of tables

1. Introduction

1.1. Background

The building construction industry is a significant contributor to greenhouse gas emissions globally. An estimated 10% of global energy-related CO_2 emissions in 2020 are attributed to manufacturing building materials such as steel and cement [3]. In response, wood, a building material that has previously been underutilised, has gained renewed interest. Although previously unpopular in the construction industry due to its cost and lack of applicability in modern building production in the 20th century, it is now being reintroduced in a new form. Cross-laminated timber (CLT), developed in Central Europe in the 1990s, has demonstrated versatility in various construction types and sustainable properties as a natural carbon absorber [4].

Given the growing interest in CLT, industry professionals, developers, and architects are rapidly incorporating it into new building projects, leaving engineers with the task of designing systems that meet government legislation, industry standards, and the aspirations of architects and developers. The use of CLT in building design poses challenges for fire safety, particularly in the design of high-rise structures where national building codes often require non-combustible structural systems for buildings over five stories [5]. While low-rise buildings may not be required to withstand a complete burnout during a fire, the consequences of structural failure for taller and more complex structures can be magnitudes more significant and, therefore, not an acceptable design option for these buildings [6]. Some governments are updating regulations to allow for more use of mass timber structures; however, in other countries, rules are less specific, leaving more responsibility on designers to ensure that timber structures meet safety standards. Without regulatory guidelines, an analytical approach is deemed necessary to address these challenges [7].

In compartment fires, exposed timber surfaces will alter the input parameters typically considered when designing fire safety, such as temperature, heat release, and fire duration. The greater the amount of exposed timber, the more severe the fire load within the compartment, which can lead to a more intense fire and, thus, higher heat flux and char rate. This creates a feedback loop, a specific and crucial aspect of fires in exposed timber compartments. Consequently, addressing the associated design challenges and adapting design methods to account for the altered fire environment becomes necessary [8].

To understand the risk associated with such buildings, fire modelling can be a valuable tool to implement in building design. Accurate fire modelling can help predict fire behaviour, heat release rates, and charring rates, which in turn guides the design of fire safety measures and structural

systems. Various fire models, such as the Fire Dynamics Simulator (FDS) [9], have been developed and improved over the years, and may be used to simulate compartment fires in buildings with exposed timber surfaces, providing valuable insights into the fire dynamics for such fires.

1.2. Objective and research questions

This thesis aims to model a previously conducted fire test with exposed timber surfaces in FDS and evaluate its accuracy in predicting fire behavior, including heat release rate, gas temperature, solid-phase temperature for CLT and the mass flux of pyrolyzates emerging from CLT. This process entails inputting essential parameters, such as the timber's kinetic properties and the compartment's specific boundary conditions, into the FDS model. The results from the simulation will then be compared to the actual experimental data from the fire test to assess the model's accuracy. The primary objective is to provide insights into FDS's effectiveness in modelling compartment fires with exposed timber surfaces and identify any limitations or areas for improvement in the modelling process.

In keeping with the research objective, a series of inquiries has been articulated, which will be investigated and addressed within the purview of this thesis:

1. What is the model's level of accuracy to experimental data?
2. What are limitations of the model?
3. How can future models be improved for better results?

1.3. Prerequisites

To delimit the scope of this thesis, the subsequent prerequisites are presented:

- A CFD-model of a single room compartment fire with exposed timer surfaces is developed during this work.
- The compartment fire simulation is founded upon a previously executed fire experiment, as documented in existing literature.
- The pyrolysis model employed within the fire model is sourced from literature.
- FDS version 6.7.9 has been deployed for this work.

1.4. Limitations

In order to contextualize the findings of this study, it is essential to recognize several limitations and constraints that pertain to the scope of the research which include, but are not limited to:

1. The investigation primarily concentrates on exposed CLT compartment surfaces and their effect on compartment fires. Consequently, other mass timber products and construction types are not examined, potentially restricting the applicability of the findings to a broader range of construction contexts.

2. The research relies solely on the FDS for fire modelling purposes. Although FDS is a widely used and highly regarded tool, alternative fire modelling approaches may yield different outcomes, and the findings of this study will not be universally applicable to all fire modelling practices.

3. This thesis is based on a single, well-documented, and controlled fire test involving exposed timber surfaces. However, this test may not cover the entire spectrum of potential fire scenarios in buildings with exposed timber surfaces. As a result, the findings will not be universally relevant to all CLT building designs and compartment configurations.

4. The pyrolysis model utilized in the compartment fire model is validated for bench-scale fire tests and may not be applicable for up-scaled model use.

5. The simulation model is subject to the constraints of available computer hardware resources and the timeframe allotted for thesis completion, which may have influenced the resulting outcomes.

1.5. Thesis structure

The organization of this thesis adheres to the conventional IMRAD-structure (Introduction, Methodology, Results, Discussion), with the addition of a theoretical framework preceding the methodology section. This framework provides the reader with foundational knowledge and establishes a context for the subsequent discussion chapter. Moreover, the conclusion is presented as a distinct chapter. A brief overview of the content within each chapter is provided below:

Chapter 2: *Literature review* presents earlier work on similar simulation tasks, an overview of the fire test upon which the fire model is based, and a discussion of the pyrolysis model employed within the fire model.

Chapter 3: *Theory* provides fundamental theoretical background.

Chapter 4:   *Methodology* explain how the compartment fire was modelled.

Chapter 5:   *Results* present extracted data from the simulations.

Chapter 6:   *Discussion* analyse the simulated data and compare them to experimental.

Chapter 7:   *Conclusion* present key findings and suggest for application and further work.

2. Literature review

This literature review aims to provide an overview of the current body of research related to modelling fire in compartments featuring exposed timber surfaces. Initially, the review will offer a brief introduction to wood as a building material, and a succinct discussion of existing calculation methods for modelling compartment fires with exposed timber surfaces. Subsequently, it will summarize existing studies that have conducted simulations of such fires. The review will then introduce the selected fire test modelled for this study, followed by a presentation of the pyrolysis model derived from literature and used in this thesis' model. Note that the figure presented in the literature review are derived from the published articles using WebPlotDigitizer [10] and negligible discrepancies from the original data may be present.

2.1. Wood and Cross-Laminated Timber

This chapter presents wood as a building material.

Wood

Wood is a heterogeneous material constituted mainly of cellulose, hemicellulose, and lignin, with the relative composition of these elements differing among various wood species [11]. Cellulose, the principal constituent in all plant life, possesses a molecular formula of $C_6H_{10}O_5$ and comprises glycosidic linkages. Conversely, hemicellulose a polysaccharide originating from plant cell walls, existing in conjunction with cellulose [12]. Finally, lignin is a polymeric substance that acts as a binding agent for cellulose fibres and other polysaccharide fibres, facilitating the formation of the wood structure [13].

Laminated Timber

Laminated timber elements are wood materials formed from lamellas connected through screwing, nailing, or glueing processes. This novel approach to wood utilization originates in employing edge-tilted lamellas placed adjacently and bonded with a steel rod, initially utilized in constructing stress-laminated timber decks in Canada circa 1975. This technique was later disseminated to Europe around 1990 – the advancement of diverse methods for joining lamellas continued in Switzerland during the 1990s [14].

Laminated timber elements can be classified into the following three distinct categories, and are illustrated in Figure 1:

- - Hollow core elements
- - Edge-tilted elements
- - Cross-laminated elements
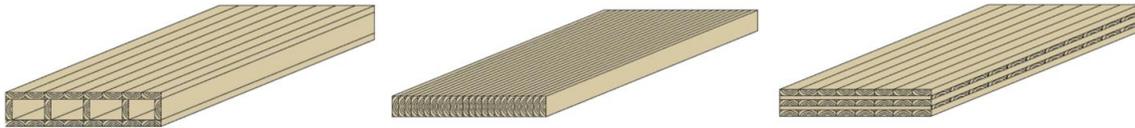
Figure 1 - Illustrations of hollow-core (left), edge-tilted (middle) and cross-laminated (right) elements [14]

Cross-laminated elements (CLT) are the type of laminated elements in which this thesis resolves and is defined in the US as [15]

> *"a prefabricated engineered wood product made of at least three orthogonal layers of graded sawn lumber or structural composite lumber (SCL) that are laminated by gluing with structural adhesives"*

European standard EN16351 defines it as similar without needing fire-resistant adhesives [7].

CLT represent a collective term for components assembled from planks (lamellas) in multiple layers and is the type most used in building assembly [16]. The layers are typically arranged at 90 or 45-degree angles to one another, and bonding agents such as glue or wooden dowels are employed to secure the elements together [14]. CLT is well-suited for a diverse range of structural applications due to its capacity to support loads in three dimensions. Moreover, the manufacturing process allows for the customization of shapes and dimensions, making CLT an ideal material for implementation in modular construction projects [17].

Christian Dagenais et al. [7] highlight that CLT exhibits noticeable inherent fire resistance due to its significant cross-sectional dimensions. These dimensions allow for a steady and consistent charring process, enabling CLT to maintain its load-bearing capacity over extended periods. Consequently, CLT's structural fire resistance can be assessed using design principles similar to those used for timber.

2.2. Fire modelling

Fire modelling is a pivotal component of fire safety engineering, which aims to prevent, contain, and mitigate the effects of fires in structures. This field employs mathematical and computational methods to calculate fire behaviour and predict its impact on buildings. Through its application, fire modelling enables the identification of potential hazards, the design of adequate fire protection systems, and insight into the behaviour of fires in specific building configurations. In mass timber construction, fire modelling is essential due to the potential risk of compartment surface involvement during a fire. It is thus imperative to develop accurate and reliable fire modelling techniques to ensure the safety and structural integrity of tall timber buildings.

Fire safety design, which aims to prevent structural collapse and containment breaches, necessitates estimating the ultimate char depth in mass timber construction by considering the anticipated compartment fire characteristics. Although standards such as Eurocode 5 Part 1-2 [18] and Eurocode 1 Part 1-2 [19] provide guidelines for determining char rates and parametric time-temperature relationships, these general methodologies were developed for compartment fires with non-combustible surfaces. Consequently, they do not adequately account for the many parameters that can change for a compartment fire with exposed CLT and may not accurately predict the charring rates that such fires can produce [7] [20].

Several researchers have proposed strategies to address this issue by employing modified parametric curves that include the influence of combustible compartment surfaces [7]. These include:

- **D. Brandon** [21] introduced an engineering method employing parametric equations and an iterative process to estimate char depth, adjusting the fuel density at each iteration. The charring rate is based on an empirical model derived from various parametric fire tests.
- **Barber et al.** [22] put forth a two-step methodology for CLT, incorporating an additional step to verify the smouldering extinction of CLT by calculating the incident radiant heat flux on timber surfaces and ensuring it remains below a critical value.
- **Schmid & Frangi** [23] developed the Timber Charring and Heat Storage (TiCHS) model, which uses the energy stored in the char layer as a primary characteristic to estimate contributions from structural timber to fire during its fully developed phase, decay phases, and burnout.

An alternative approach to tackling the issue of unpredictable fire development in compartment fires is through numerical simulation. By utilising computational modelling tools, such as FDS,

fire engineers can simulate compartment fires involving exposed timber surfaces with more intricate calculations that account for the pyrolysis process and other factors, including the location of exposed surfaces, room geometry, fire placement, and the dynamic progression of the fire, among others. These models may also be integrated with structural models to simulate the behaviour of the entire structure, encompassing its deformation and collapse under varying fire conditions [24].

There are two main approaches to simulating compartment fires involving exposed timber surfaces in FDS, using *predefined* or *predictive* pyrolysis. As the more straightforward option, the predefined pyrolysis model requires the user to establish a time-dependent heat release curve and assign it to the compartment surface involved in the fire. Conversely, the predictive pyrolysis model entails making material-specific assumptions, including thermal properties and kinetic parameters, to estimate the release of combustible volatiles emerging from the timber surfaces into the simulated domain based on heat transfer to the exposed surfaces. The two approaches are explained in greater detail in chapter 3.5.2.

The existing literature on modelling compartment fires with exposed timber surfaces using computational fluid dynamics (CFD) models is limited. This poor selection might be primarily due to the substantial computational resources these models require. Moreover, the current uncertainties related to these models reduce their usefulness in practical engineering projects, making them less attractive for research. However, the increasing demand for tall timber buildings and their associated fire safety concerns are relatively new. Therefore, as computational power continues to grow, these models will become more appealing for research in the future. The following three chapters present the available literature on the numerical modelling of compartment fires with exposed timber surfaces, including predictive pyrolysis modelling.

2.3. Šálek et al.

In a 2021 academic paper by Šálek et al. [25], the authors introduce a detailed CFD model for a room corner test following ISO 9705-1 guidelines. The model uses oriented strand board (OSB) linings in the enclosure exposed to an initial fire. The primary objective of the investigation was to examine two distinct methodologies for simulating the combustion of the surface linings and to assess the impact of material-specific attributes on the resultant findings. The two divergent approaches encompass predefined and predictive pyrolysis, elaborated in chapter 3.5.2.

Methodologies and Scenarios

The researchers used results from a fire test featuring identical enclosure configurations to validate their simulations. They compared their simulated output results with those from the experiment. The experiment was terminated when the fire reached a flashover for reasons not discussed in the paper. Thus only 412 seconds of experimental data were to be compared to the simulated output. Seven models, Scenario A to G, were executed, each representing a distinct configuration of the OSB fire behaviour.

Scenario A utilized the predefined pyrolysis model, while Scenarios B to G applied the predictive pyrolysis model, with each scenario including different OSB thermal properties. The predictive model is established using the three primary components in wood: hemicellulose, cellulose, and lignin. The researchers explore combinations of specific heat capacity and thermal conductivity values, considering constant and temperature-dependent properties. Additionally, some scenarios purposefully omit the water evaporation process to evaluate its influence on the simulation. See Table 1 for scenario settings.

Results and analysis

The poorest results were found in Scenarios A, C, and F. Scenario A used the predefined pyrolysis model with heat release rate per unit area (HRRPUA) input data, which led to overestimating the experiment by 500-600°C. Scenarios C and F, which used the predictive pyrolysis approach that incorporated water evaporation in the temperature-dependent specific heat capacity, did not reach flashover. As a result, they underestimated the experiment by about 100-350°C. This similarity in outcomes suggests that when water evaporation is included with specific heat capacity, it becomes the dominant factor, preventing fire spread and flashover effect. Figure 2 illustrates the temperature development of a single thermocouple inside the compartment fire.

Table 1 - Scenario A to G settings

Scenario	Pyrolysis	Specific heat	Evaporation included in specific heat	Conductivity
A	Predefined	Constant	No	Constant
B	Predictive	Constant	No	Constant
C	Predictive	Temperature-dependent	Yes	Temperature dependent
D	Predictive	Temperature-dependent	No	Temperature dependent
E	Predictive	Constant	No	Temperature dependent
F	Predictive	Temperature-dependent	Yes	Constant
G	Predictive	Temperature-dependent	No	Constant
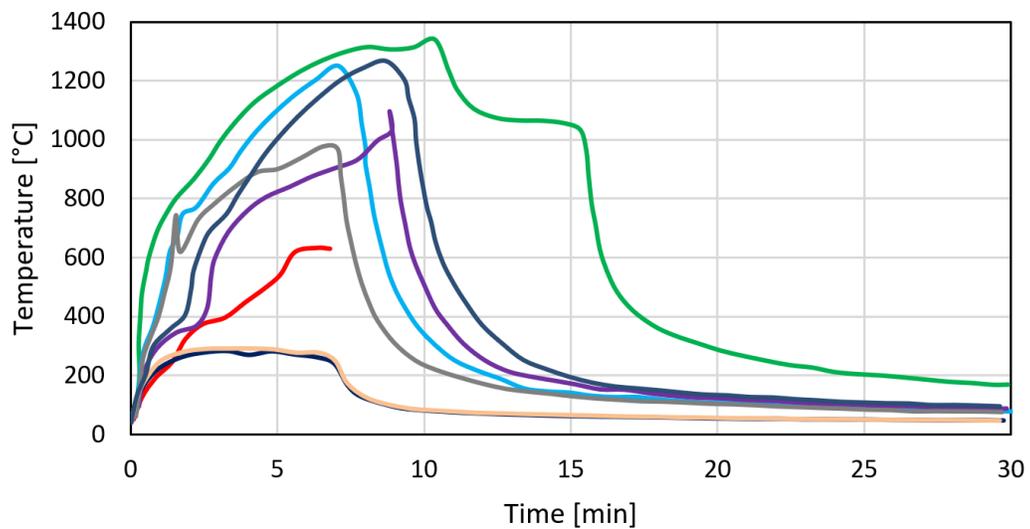
Figure 2 – Time-temperature curve for a single thermocouple inside the compartment [25]

Except for Scenarios C and F, all other scenarios neglected water evaporation and achieved flashover. In Scenario B, constant specific heat capacity and thermal conductivity were employed, exhibiting a temperature progression akin to Scenario G, which utilized constant conductivity and temperature-dependent specific heat capacity. Both scenarios reached temperatures exceeding 1,260°C and overestimated the experimental values. Scenario E combined constant specific heat capacity with temperature-dependent thermal conductivity, resulting in a more rapid initial temperature increase followed by slower growth, ultimately yielding a lower maximum temperature and reduced overestimation. Scenario D adopted temperature-dependent specific heat capacity and thermal conductivity, displaying the slowest initial temperature rise and offering the closest approximation to experimental data, with a maximum overestimation of 300°C.

Conclusion

The study concludes that the predefined pyrolysis model is unsuitable for accurately modelling their compartment fire and that a predictive approach utilizing a large input dataset, including thermal material properties and kinetic parameters, is needed to improve results. When the fire spread and flashover occurred, it was found that the commonly used constant specific heat capacity and thermal conductivity provided poor agreement with experimental data and that temperature-dependent thermal properties should be used instead. The influence of incorporating water evaporation into specific heat capacity was tested and found not to be recommended due to the potential hindrance of fire spread. Instead, adding water as a fourth component in the predictive pyrolysis model and treating it as a separate material that undergoes chemical reaction – evaporation may provide different and more accurate results. A complete input dataset for OSB was provided in the study, and the authors note that obtaining these complete datasets for material burning is difficult and time-consuming. The study recommended using a predictive pyrolysis approach in real-scale enclosure fire scenarios, with extra attention paid to implementing the burning material's thermal properties. The influence of thermal parameters should be further tested in the future, and an optimization-based approach for obtaining thermal properties from smaller experiments may provide promising results. The study suggested the need to validate other wooden-based materials in real-scale experiments to confirm or disprove the need for unique input datasets for each material.

2.4. Brunkhorst & Zehfuβ

In a study akin to Šálek et al., Brunkhorst & Zehfuβ [26] conducted ISO 9705-1 fire tests with exposed or initially protected wooden surfaces. A total of 20 tests were performed to investigate various factors affecting compartment fires with exposed timber linings, including ventilation conditions, the configuration of exposed surfaces, failure of fire protection systems, auto-extinguishment, and the impact of extinguishing measures. One of the experiments were later tried modelled using FDS.

Fire tests and experimental setup

The compartment fire tests were carried out in a standardized room, adhering to ISO 9705-1 guidelines. The room featured an exhaust hood to capture combustion products, and several measurements were taken to analyze the fire's behaviour. Different panel materials were employed to represent exposed and initially protected timber surfaces. Solid timber panels symbolized exposed surfaces, while solid wood panels with a fire protection system represented protected surfaces. The room walls and ceilings were arranged with these panels according to each test's objectives.

The fire sources utilized in the tests were either a propane-gas-operated burner or wooden cribs, representing distinct fire loads. The gas burner's output began at 100 kW, subsequently increasing to 300 kW. The wooden crib maintained an equal mass-to-air ratio, initiating ignition using pans filled with methanol.

Experimental findings

The findings from the experiments highlight that the configuration of timber surfaces significantly impacts fire development and the timing of flashover. When ventilation openings are reduced, a transition to ventilation-controlled fires happens earlier, resulting in lower peak heat release rates but longer durations of fire. This subsequently leads to elevated maximum temperatures and prolonged exposure to these temperatures.

It is found that as the extent of exposed timber increases, the time until flashover occurs diminishes, provided the fire source's heat release rate is sufficient. In these experiments, the geometric arrangement of exposed timber surfaces doesn't significantly affect the outcomes; rather, the heat release rate of the fire source is the primary influencer. Self-extinguishment of

timber surfaces was noted under certain conditions, such as when the mobile fire load is burnt out or extinguished, or when only a single compartment surface was composed of exposed timber.

Factors like the heat release rate of the fire source, the area of the room, and the extent of exposed surfaces considerably influence both the flashover time and the spread of flames to the timber surfaces. In these tests, firefighting measures executed by professional firefighters, using minimal extinguishing agents, proved to be both efficient and effective.

Numerical simulation results and conclusion

Following their fire tests, Brunkhorst & Zehfuß initiated a preliminary investigation using the FDS to replicate one of their experiments. Their study featured two different models: one using predefined pyrolysis and the other employing predictive pyrolysis.

The predefined model used a time-dependent HRR curve, which simulated the burning of exposed surfaces. The data for this was procured from a compartment fire test where the ceiling was composed of exposed wood.

Conversely, the predictive model applied a single-reaction scheme, reducing wood to a singular component material that undergoes pyrolysis. This process produces fuel and char as by-products. An endothermic heat of reaction of 430 kJ/kg was selected, along with a heat of combustion of 14,5 MJ/kg.

The initial fire that was to ignite the combustible surfaces was depicted by a burner surface with a predefined HRR curve. This surface fire represented the combustion process of a 50 kg wooden crib based on a t-squared fire growth curve.

As depicted in Figure 3, contrary to Šálek et al.'s results, the predefined pyrolysis model reasonably matched the experimental data. On the other hand, the predictive pyrolysis model suggested that the wooden surfaces in the model did not ignite, resulting in an absence of supplementary HRR. They did not delve into the reasons for this occurrence, leading to the total HRR calculation falling short of the experimental results. The study concluded that improvements in the modelling level and optimization of reaction parameters for predictive pyrolysis are essential to enhance the accuracy of the simulations.
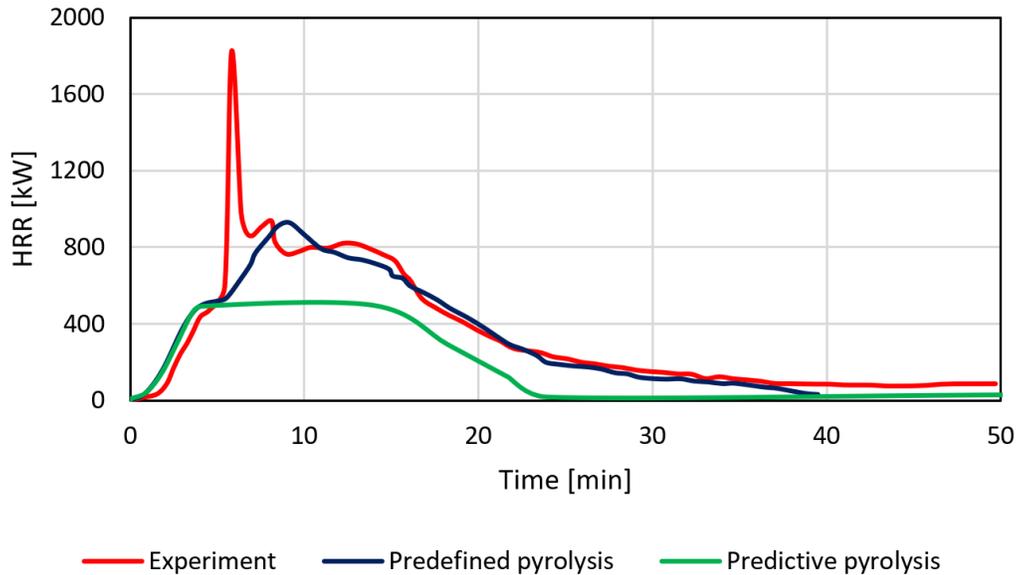
Figure 3 - Experimental and simulated HRR results [26]

2.5. Dixon et al.

Like Šálek et al. and Brunkhorst & Zehuβ, Dixon et al. [20] employs FDS, incorporating the predictive pyrolysis model to simulate compartment fires in which the exposed surfaces contribute to the fire's development. Additionally, they investigate the semi-empirical quantification of requisite fire resistance for building components based on charring depth. Figure 4 below depicts the framework used by the researchers for evaluating the fire resistance level, excluding their additional assessment for establishing a window breakage criterion.
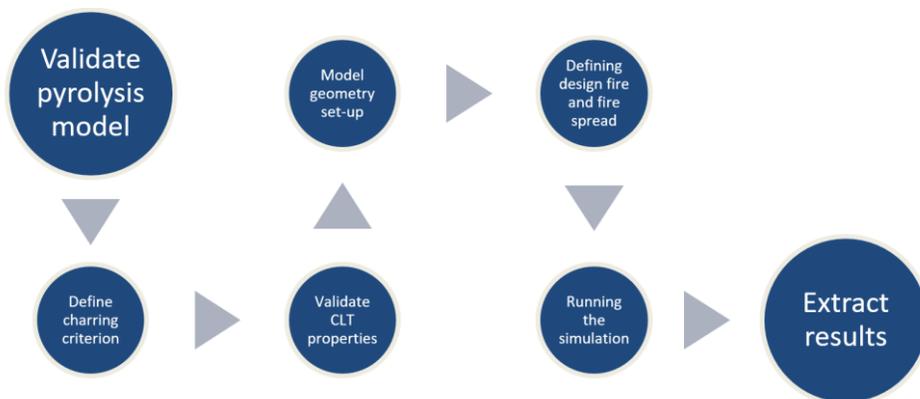
Figure 4 - Dixon et al. methodology framework [27]

14

Methodology

To specify their predictive pyrolysis model, Dixon et al. incorporated the pyrolysis model and thermal properties delineated by Wang et al. [28] They proceeded to validate their model's simulated HRRPUA using experimental data derived from cone calorimeter tests on White Spruce subjected to various heat fluxes, as illustrated in Figure 5. The simulated HRRPUA results were found to align satisfactorily with the experimental findings. These validated results were subsequently integrated into their room-scale models for further validation.
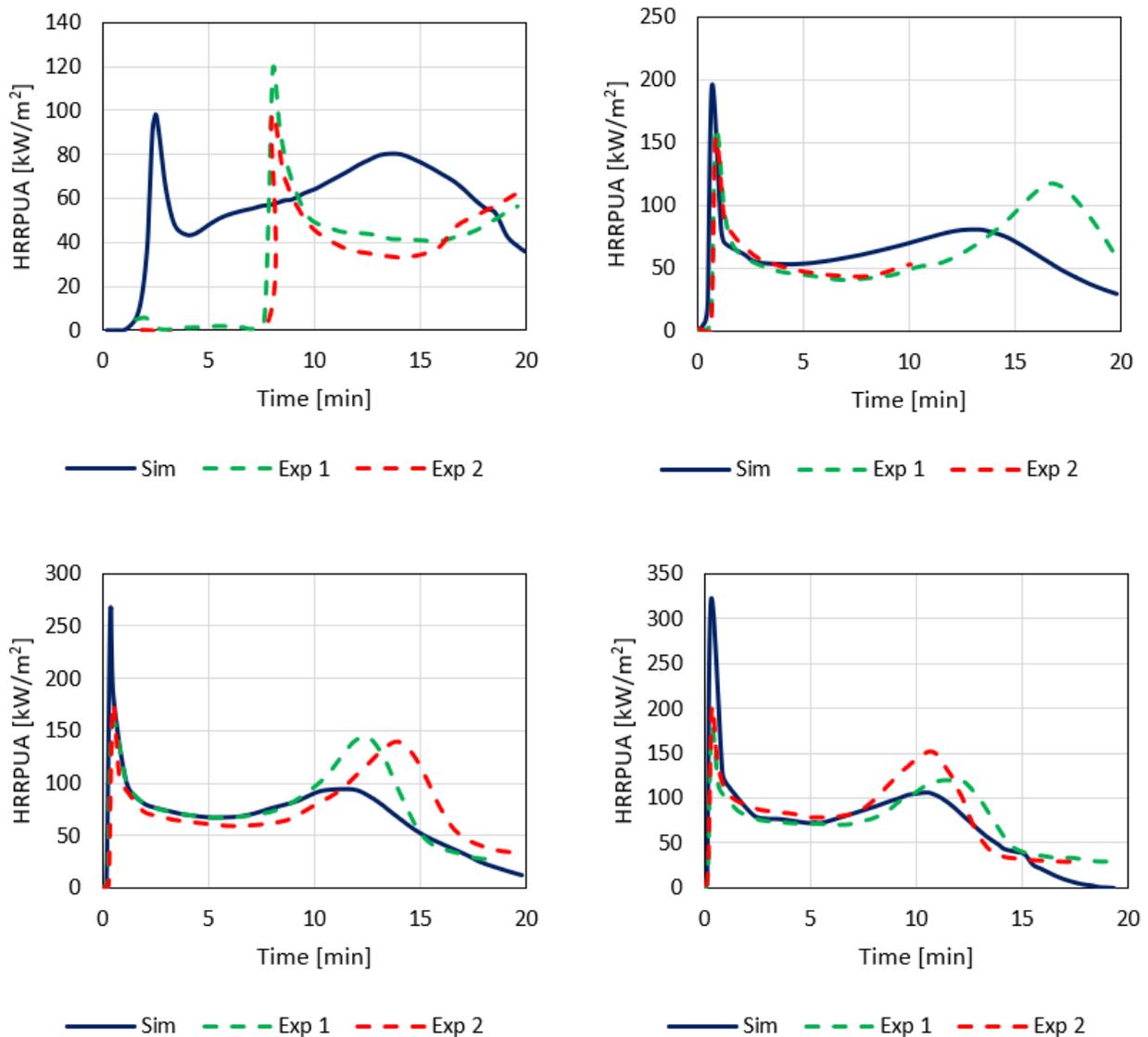
Figure 5 - Experimental and simulated cone calorimeter data at heat flux 20 kW/m2 (top left), 35 kW/m2 (top right), 50 kW/m2 (bottom left) and 65 kW/m2 (bottom right) [27]

15

Akin to this thesis, the selected CLT properties and pyrolysis model underwent validation for room fire simulations by incorporating the parameters into previously conducted room fire tests by McGregor [29]. The simulated data was then compared to the experimental results concerning the total HRR, which also included the heat release contributed by the exposed timber surfaces.

The CLT validation results were in reasonable agreement with McGregor's experimental findings regarding the HRR contribution from CLT. It was also registered continuous burning of the compartment surfaces for some time after the mobile fuel load, were fully consumed. However, some discrepancies exist between the experimental results and FDS simulations, particularly in the HRR behaviour over time and the impact of delamination on HRR and char depth. Figure 6 delineates the outcomes of the validation process, wherein the red curve represents the heat release ascertained from McGregor's experimental data. Concurrently, the green curve corresponds to the predefined design fire, which was intended to initiate combustion of the exposed surfaces. Lastly, the blue curve signifies the cumulative HRR procured from the simulation. The underestimation of char depth in the simulations were attributed to factors such as limitations within FDS, fire source location differences, imperfections in real CLT, and the absence of delamination effects in the model.
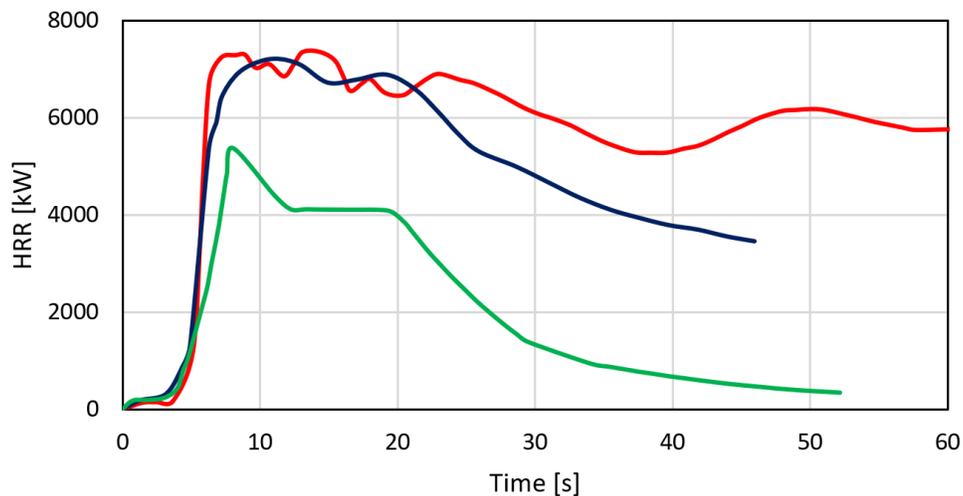
Figure 6 – Comparison of HRR between simulated and experimental data for McGregor's room fire test [27]

The researchers' final model represented an open-plan office with an approximate total floor area of 550 m², featuring an exposed CLT ceiling spanning around 300 m², while beams and columns were assumed to be protected. The initial fire, intended to ignite the combustible surfaces, was based on burning workstations dispersed throughout the office plan. The fire spread mechanism between workstations was addressed by estimating the time needed for fire to propagate between

them, utilizing data from experiments conducted by the National Institute of Standards and Technology (NIST) [30]. Lateral and diagonal fire spread times were approximated at 8 and 10 minutes, respectively. These values were used to simulate a moving or traveling fire across the office floor plate, with the total HRR determined as a time-dependent superposition of individual workstation HRRs.

Results and analysis

Based on the work by Buchanan [31], as acknowledged in Eurocode 5 part 1-2 [18], the charring of CLT elements is presumed to commence at 300 °C. The results from the final model reveal that char depth, as shown in Figure 7, did not surpass 60 mm at any point on the office floor during the 7,200-second (120-minute) simulation. Charring was found to be more significant in areas remote from ventilation openings and the point of fire initiation, likely due to re-radiation and pre-heating. The findings indicate that the performance of timber structures during fire relies on the quantity of load-bearing timber available to withstand fire limit state loads after the required FRL period, which depends on the structural member dimensions and char depth.
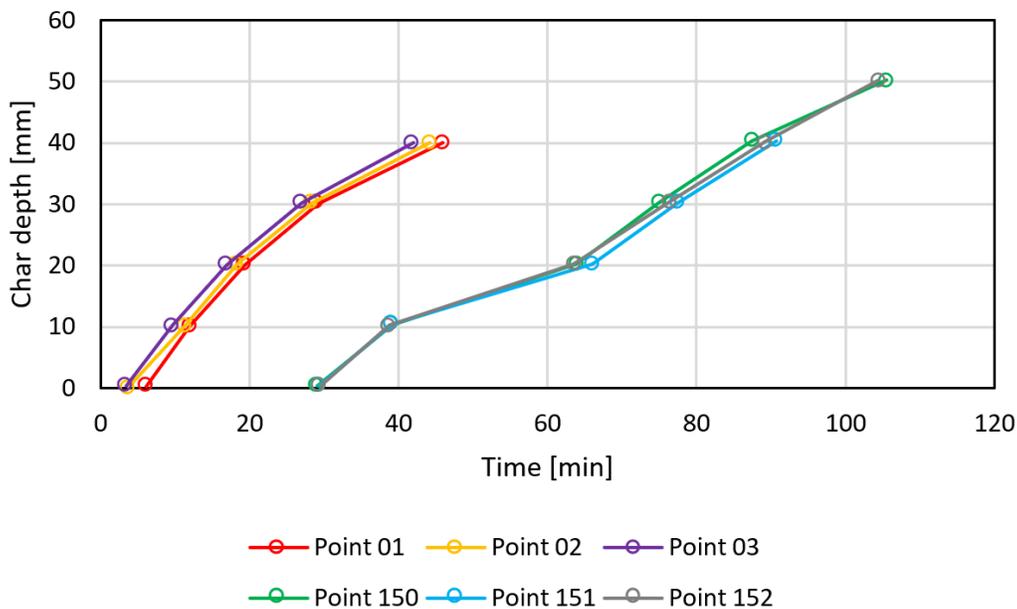
Figure 7 - Char depth at various points during the simulation in the final model [27]

Furthermore, the results demonstrate that fire spread via exposed CLT is rapid compared to the workstation fire, suggesting the need for a workstation fire spread mechanism that incorporates feedback from the compartment environment. The study also observed that longer pre-heating

results in deeper charring, which counteracts the impact of a more rapid and larger fuel load fire. The overall char depth at the most remote points did not exceed 60 mm for the duration of the simulation. The maximum observable contribution to HRR from the CLT occurred at around 2,400 seconds, representing around 10 % of the overall HRR for the office, which significantly impacts the timber pyrolysis and char production within the structure.

Conclusion

In conclusion, the paper presents a preliminary methodology for utilizing FDS to understand fire dynamics within exposed timber compartments and determine the fire resistance level of exposed timber elements. While not yet robust enough to serve as standalone design tools, refining the methodologies and their components could enhance the understanding of fire dynamics and their impact on buildings with exposed timber. The papers acknowledge the significant assumptions made and suggest further work to address limitations, including refining initial fire characteristics, evaluating key input assumptions, and improving correlation to experimental results. Additionally, the functionality of FDS enables the collection of extensive data that can reveal insights into exposed timber fire compartment behaviour, potentially informing timber building design in the absence of large-scale fire tests.

Dixon et al. acknowledge that while FDS has the capacity to accurately model compartment fires involving exposed timber surfaces, they caution that the extended computation time required for such simulations may render it impractical for use in real-time engineering applications.

2.6. Bartlett et al.

In recent years, there has been a growing interest in compartment fire tests involving different levels of exposed and/or protected CLT on walls and ceilings. These experiments have enhanced understanding of fire dynamics in such compartments and the impact of various factors, such as adhesive selection, CLT layer configuration, char layer fall-off, the extent of exposed CLT, fuel load, and the size of openings [7]. This chapter will present the fire test which is chosen as the compartment fire to be modelled in FDS for this thesis.

In a 2017 research article, Bartlett et al. [1] presents a compartment fire test with exposed CLT surfaces. It was one out of five tests carried out by the researchers to investigate the enclosure fire dynamics in such compartments. This test warranted its own publication due to the emphasis on

the self-extinguishment phenomenon, where the fire reaches flashover, progresses to the fully developed stage, and ultimately self-extinguishes upon consuming all mobile fire load, without necessitating human intervention or active system engagement.

The compartment fire presents a robust assessment of FDS modelling due to numerous factors. The fire's brief duration and confined spatial extent significantly diminish the computational time required to simulate the fire. In Bartlett et al. and Hadden et al.'s studies [1] [8] gas-phase and solid-phase temperatures, as well as heat release rates, were comprehensively documented, providing a solid basis for validating the model by comparing these parameters with the simulation results. Moreover, their research offers estimates of the mass flux of volatile compounds produced from the timber surfaces due to pyrolysis, further supplementing the validation parameters. The initial crib fire that initiates the compartment fire is also well-documented, simplifying its representation in the simulation model.

The following description of the fire test comes from Bartlett et al.'s paper [1] and is supported by a related paper presented by Hadden et al. [8].

Test set-up

The experimental arrangement involved a single room compartment with no interior partition as depicted in Figure 25 of chapter 4.2. The back wall and ceiling of the compartment were of exposed CLT, while fire-resistant gypsum plasterboard enclosed the non-exposed front and side wall surfaces. Disregarding encapsulation and the floor system, the compartment's internal dimensions were 2,75 m x 2,75 m x 2,96 m (length x width x height). The configuration factor between the exposed surfaces was approximately 0,20.

The floor system was assembled using high-density stone wool, plasterboards, and medium-density fibreboards, all affixed to a 50 mm timber joist framework. Once the floor system was in place, the chamber's sole entrance measured 1,84 m in height and 0,76 m in width, resulting in an opening factor of 19 m$^{-1/2}$. The CLT components used to construct the chamber were of spruce wood and 100 mm thick, comprising five uniform 20 mm lamellae layers.

In order to focus on the decay phase, a relatively modest mobile fuel load of 127 MJ/m^2 was placed inside the chamber, consisting of four wooden cribs. This was designed to produce a fire that would quickly reach its fully developed stage before transitioning to the decay phase.

To investigate temperature data within the CLT elements and gas temperatures at various positions inside the chamber, thermocouples were employed. Holes of differing depths were drilled into the elements to accommodate the thermocouples. A hood, equipped with oxygen, carbon dioxide, and carbon monoxide analysers, was installed above the test apparatus to facilitate calorimetry and estimate the total HRR.

To examine the HRR contribution from the CLT, a scale was placed beneath the floor system to measure the MLR of the wood cribs. The CLT components were weighed on the same scale before and after the test to approximate mass loss, which aided in estimating the effective heat of combustion from the CLT.

Results

Without further explanation from the authors the initial crib fire was delayed. As indicated in Figure 8, the fire began around 233 seconds into the experiment. The MLR of the cribs, determined by the weights beneath the floor structure, reached an estimated peak of 0,18 kg/s. The crib fire lasted for approximately 13 minutes before the cribs were completely consumed. Additionally, the MLR was utilized to estimate the HRR contribution from the cribs assuming a heat of combustion of 17,5 MJ/kg, which resulted in an approximate peak HRR value of 3000 kW.
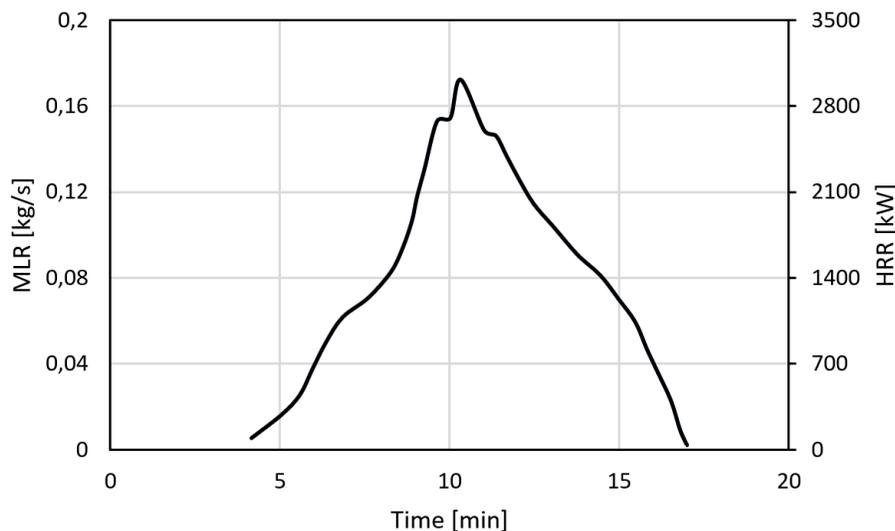
Figure 8 - Measured MLR and estimated HRR of the wooden cribs [8]

In contrast to the other compartment fires which reaches flashover after about 5 minutes, time to flashover for this experiment occurred at 8 minutes and 33 seconds due to the delayed ignition of

the cribs. Flashover was marked by a sudden increase in HRR from 1550 kW to 6210 kW, as depicted in Figure 9. This event happened shortly after the exposed back wall was observed to catch fire.

After flashover, there was a temporary phase of combustion accompanied by external flames through the compartment opening, persisting until the 15-minute juncture, during which the HRR reduced to 4500 kW. After this point, the HRR experienced a swift decline, and culminated in self-extinguishment. There was no plasterboard fall-off observed, however, small local areas on the exposed surfaces did experience delamination which contributed with limited local flaming.
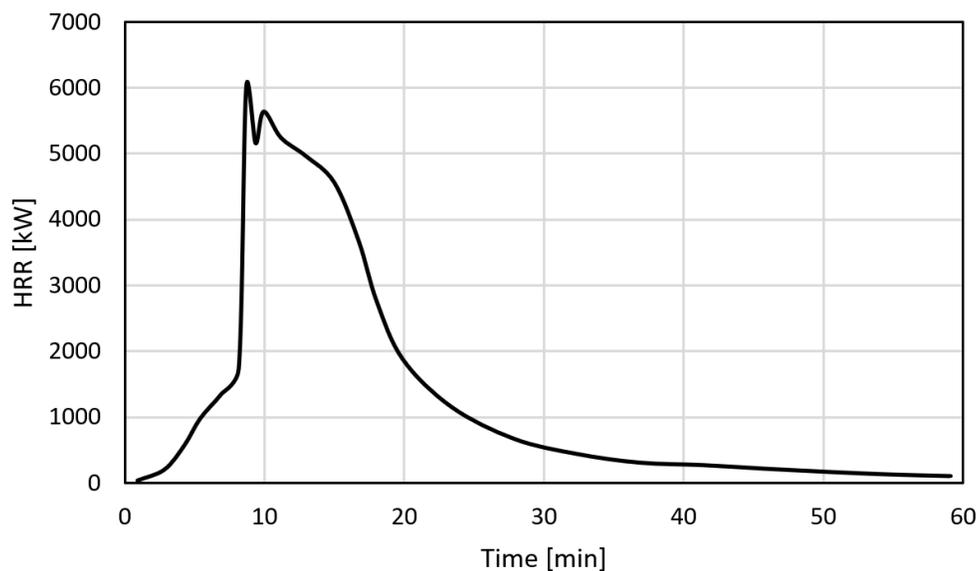
Figure 9 – Total HRR measured through calorimetry [8]

Figure 10 presents the gas-phase temperatures for in the compartment's centre, 220 cm above floor level indicating a decreasing trend starting around the 15-minute mark. The solid-phase temperature profiles of the exposed surfaces presented in Figure 11 also show a decline between 17 and 23 minutes, which indicate the beginning of extinction. The test was concluded at 92 minutes, after which water was applied to extinguish any remaining smouldering.
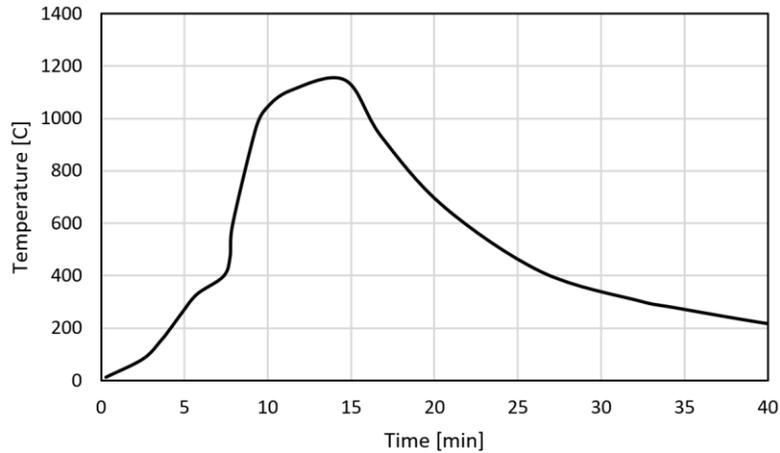
Figure 10 - Gas phase temperature in the centre of the compartment at 220 cm above floor level [8]
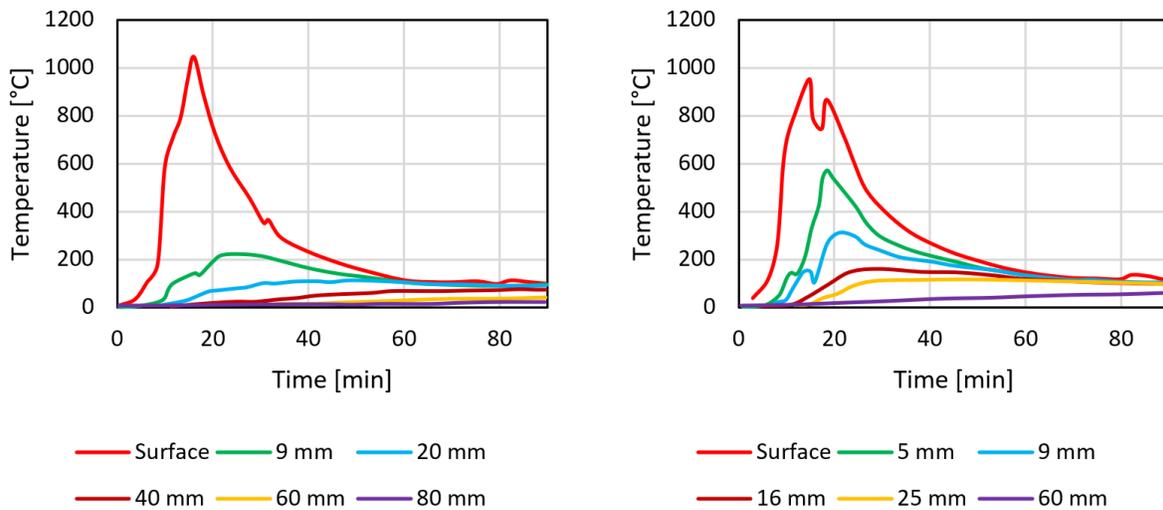
Figure 11 - Temperature profile in back wall (left) and ceiling (right) for various depths of the exposed surfaces [1]

A notable distinction between the fire test under consideration and other compartment fire tests involving exposed timber surfaces is the reported estimation of the MLR for the CLT elements. This is particularly significant as it serves as an additional parameter for comparison with simulation results. The researchers employed two distinct methodologies to estimate the MLR. The first method uses an energy balance by using the temperature data collected inside the CLT elements. This approach is explained in greater detail in chapter 3.2.

The second approach calculates the HRR contributed by the CLT elements by taking the total HRR obtained through calorimetry, subtracting the estimated HRR contributed by the crib fire, and exploiting this value to calculate MLR using Eq. 1. It is assumed by the authors that the heat of combustion is 17,5 MJ/kg.

22

$$\dot{m}'' = \frac{Q_{CLT}}{A\Delta H_c} \qquad \text{Eq. 1}$$

Where

$\dot{m}''$ is mass loss rate per unit area [g/m²s]

Q_{CLT} is HRR contribution from CLT [kW]

A is area of exposed timber [m²]

ΔH_c is heat of combustion of wood [MJ/kg]

Figure 12 illustrate the estimated mass loss rate per unit area (MLRPUA) of the exposed wall and ceiling using the energy balance approach and calorimetry data through Eq. 1. The researchers found that both methods give similar results after an initial peak, which indicate that the energy balance approach may be sufficient to predict extinction.

There were significant discrepancies in peak values because of differences in the effective heat of combustion and the quality of temperature data. However, the method is primarily focusing on the decay phase to see if the calculated MLR can help predict flaming extinguishment, and the discrepancy is therefore not explored in greater detail.

Assuming a normal oxygen concentration and critical MLR of 3,48 g/(m² s) [32] [33], the researchers calculated that it would take about 21 minutes for the fire to go out for the wall and 20 minutes for the ceiling using the energy balance approach. These predictions matched what they saw during the test, with the fire starting to go out around 21 minutes or 17,12 minutes if one adjust for the delayed ignition of the wood cribs.

The process of the fire going out took 3-4 minutes, during which the flames on the outside got smaller and the flaming area inside gradually decreased. Based on these results, the authors believe that the energy balance approach could be helpful for predicting when fires will extinguish in spaces with timber surfaces, assuming no delamination. To achieve this, determining critical MLR for extinction through small-scale experiments and utilizing appropriate input parameters would be necessary. The authors also emphasize the importance of conducting further research to confirm the validity of their findings.
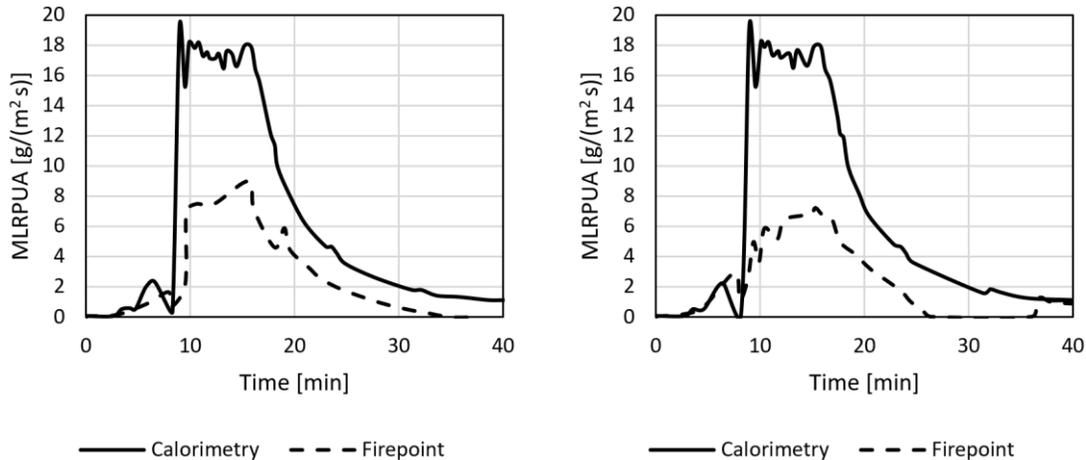
Figure 12 – Estimated MLR from the CLT of the back wall (left) and ceiling (right) [1]

Conclusion

In conclusion, the fire test was a successful attempt to produce a fire which undergoes a fully developed phase before flaming combustion self-extinguish. Utilizing the energy balance approach has demonstrated potential in estimating extinction by employing the calculation at the char-timber interface to determine when the mass loss rate of volatiles attains critical levels for sustained flaming. The comprehensive documentation of HRR and MLR data, temperature profiles, and gas-phase temperature measurements serves as a basis for validating FDS simulation results and offers valuable potential for insights into the strengths and limitations of the fire model.

2.7. Rinta-Paavola & Hostikka

In the fire model presented in this thesis, predictive pyrolysis (see chapter 3.5.2) is selected to simulate the burning of exposed timber surfaces. This method demands many input parameters and relying on general literature values may not consistently produce ideal results. Consequently, a 2021 paper by Rinta-Paavola & Hostikka [2] introduces a pyrolysis model with optimized parameters that, although potentially deviating from literature values, yield improved simulation outcomes in bench-scale tests. The researchers present four different models for the pyrolysis of two Nordic structural timbers, namely spruce and pine woods. The objective of their research was to develop two pyrolysis models for each of these woods, enabling coupled simulations of cross-section reduction and burning rate in numerical fire modelling, specifically employing FDS. Spruce wood was also used for the CLT in Bartlett et al.' experiments.

All models employed the predictive pyrolysis approach. For both wood species, a singular reaction scheme and a parallel reaction scheme were introduced. The single reaction scheme aimed to provide a generalized portrayal of the wood specimen by focusing on one material only, while the parallel reaction scheme recognized the primary triad of wood constituents – hemicellulose, cellulose, and lignin – each possessing distinct decomposition properties. Moreover, to accurately depict the onset of mass loss, a fourth component, extractives, was incorporated into the parallel scheme. Figure 13 illustrate the two reaction schemes presented by Rinta-Paavola & Hostikka.
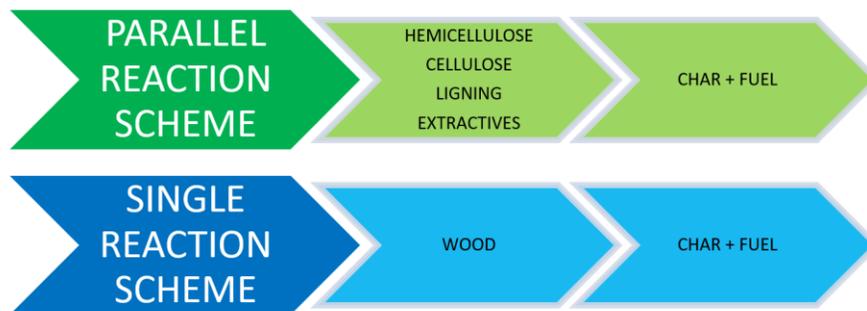
Figure 13 - Parallel- and single reaction scheme [2]

The kinetic models employed in their reaction schemes were established utilizing thermogravimetric data, bolstered by pyrolysis and combustion heat measurements. Heat release models were extracted from small-scale experiments, while cone calorimeter tests were employed to determine physical properties and verify the heat release models. Model validation was executed by juxtaposing simulation outcomes with cone calorimeter experiments under

varying heat fluxes. The final models were manually fine-tuned to closely mimic cone calorimeter tests at 35 kW/m². Consequently, the thermal properties applied in FDS are optimized values that may not align with real-life values but instead produce superior results within FDS.

The following results conclude that the parallel reactions scheme outperforms the single-reaction scheme in reproducing small-scale experiments (TGA, DSC and MCC), but the difference is negligible in predicting heat release and mass loss in cone calorimeter tests. The authors thereby argue that the single-reaction model is the more favourable option for heat release modelling in fires, as simpler models minimize uncertainties resulting from additional input parameters. The study supports the notion that model parameters should not be considered real physical properties but rather model-dependent effective parameters. The single reaction model is preferred in heat release modelling; however, it may not predict local conditions inside timber.

Given this reasoning, the single reaction scheme for spruce is chosen for the pyrolysis of the CLT elements in the model presented in this thesis. Subsequent subchapters will delve into the intricacies of the model and its implementation in FDS. This work replicates the model developed by Rinta-Paavola & Hostikka, to whom all the original credit belongs. Any deviations from their model are duly highlighted in the upcoming sections.

2.7.1. Thermogravimetric analysis

To ensure that the modelled spruce's kinetic properties are consistent with those described in the paper by Rinta-Paavola and Hostikka, a thermogravimetric analysis (TGA) was performed using the FDS. TGA is explained in chapter 3.6. The TGA-mode in FDS can be activated by setting the `TGA_ANALYSIS` flag to 'T' on the `SURF` line for the target analysis. This method is comprehensively described in the FDS User's Guide [34], and an example file can be found in the FDS example directory included with the program download. Figure 5 depicts the TGA setup in SmokeView.
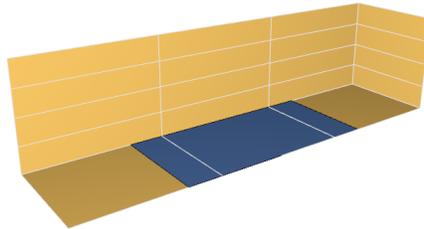
Figure 14 - Illustrative snipping of TGA setup in SmokeView

The analysis was carried out four times with `HEATING_RATE` set to 2, 5, 10, and 20 K/min, following the protocol outlined by the authors to enable comparison with their dataset. In their experiment, the specimens were dried before the analysis, resulting in a measured moisture content of 1.6% and a dry density of 408 kg/m3.

In the FDS version used in Rinta-Paavola & Hostikka's work, the expression of the reaction rate varied slightly compared to the version utilized in this thesis (FDS 6.7.9). In previous versions, the density term on the right side of Eq. 9 in chapter 3.5.2 was divided by the initial density of the layer. For reactions adhering to first-order kinetics ($n_i = 1$), this older formulation is equivalent to

the current one. However, in instances where reactions deviate from first-order kinetics, as in this case, the new value of A_i is articulated as Eq. 2 [34].

$$A_{ij}^{new} = \frac{A_{ij}^{old}}{\rho_s(0)^{n_i-1}}$$

Eq. 2

Where

A_{ij}^{new} is the pre-exponential factor for current FDS version

A_{ij}^{old} is the pre-exponential factor used up to and including FDS 6.7.7

$\rho_s(0)$ is initial layer density [kg/m³]

n_i is reaction order [-]

Table 2 – Pyrolysis reaction Table 2 provides an overview of the input parameters related to spruce and moisture, which pertain to the pyrolysis process. All other parameters remained at their default values, as the analysis primarily aims to validate the kinetic parameters of the pyrolysis model. The pre-exponential parameter (A_i) is adjusted for the current FDS version, considering an initial layer density of 411,9 kg/m³ for the TGA. Moisture vaporization produced 100% water vapor as the reaction byproducts, while the pyrolyzate of spruce yielded 84% fuel gas and 16% char.

Table 2 – Pyrolysis reaction [2]

Material	ρ_i [kg/m³]	A_i [s⁻¹]	E_i [J/mol]	n_i	f_i
Spruce	408	$2,1746 \times 10^{11}$	$1,905 \times 10^5$	1,89	0,984
Moisture	1000	$8,7245 \times 10^{16}$	$1,36 \times 10^5$	3,31	0,016

The findings from the simulated TGA align with those reported by Rinta-Paavola & Hostikka. As they discuss, the single reaction model is capable of accurately predicting the primary mass loss peak's magnitude and location. However, it fails to capture the initial mass loss or the gradual decomposition attributable to lignin at elevated temperatures. Figure 15 contrasts the simulated TGA outcomes conducted in this study with the experimental values, while*Table* 3 presents the peak mass loss values for both simulated and experimental data, the differences between them,

and the percentage of experimental values relative to simulated values, at heating rates of 2, 5, 10, and 20 K/min.
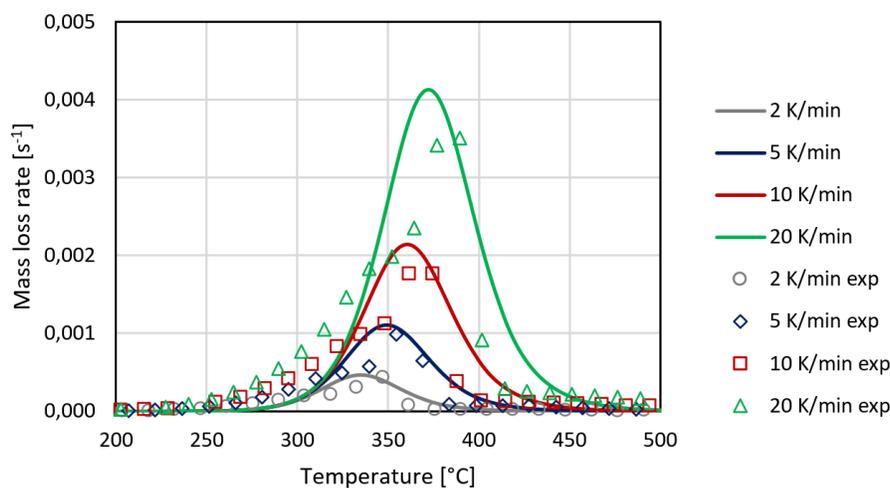
Figure 15 –Simulated and experimental TGA data

Table 3 – Comparison of peak MLR between simulated and experimental TGA data

Heating rate [K/min]	02	05	10	20
Peak MLR sim. [s⁻¹]	0,000463623	0,001107316	0,002137849	0,004126039
Peak MLR exp. [s⁻¹]	0,000441718	0,000990798	0,001766871	0,003503067
Difference	0,000021905	0,000116518	0,000370978	0,000622971
(exp/sim) %	95,28	89,48	82,65	84,90

The objective of the thermogravimetric analysis (TGA) simulation was to validate the decomposition of the modelled spruce and contrast its outcomes with the experimental data from Rinta-Paavola & Hostikka's study [2]. While the single reaction model effectively anticipated the major mass loss peak attributes, it did not account for the initial mass loss or lignin's impact at higher temperatures. Upon comparing the peak mass loss values at various heating rates, discrepancies between the simulation and experimental data were observed, ranging from 2.19×10^{-5} to 6.23×10^{-4}. The experimental values as a percentage of the simulated values spanned from 82.65% to 95.28%. Despite the differences, the simulation results exhibited a substantial degree

28

of agreement with the experimental data, underscoring the model's potential in predicting the decomposition behaviour in wood.

2.7.2. Cone calorimeter test

Following the thermogravimetric analysis (TGA) to confirm the kinetic properties of the modelled spruce, the subsequent step involved simulating a cone calorimeter test, replicating the methodology employed by Rinta-Paavola & Hostikka. This was done to ensure that the model's performance in this thesis aligned with their findings.

Model set-up

Three sets of cone calorimeter FDS simulations were conducted with external heat fluxes of 25, 35 and 50 kW/m². All cases were simulated for 1800 s (30 minutes). Each simulation uses a domain measuring 220 mm × 220 mm × 300 mm to effectively capture the fire plume and minimize heat loss. An obstruction of 100 mm × 100 mm × 33 mm is positioned in the centre of the X and Y axes at the domain's bottom, shown in Figure 16. The top surface of the obstruction (max Z) was given a `SURF` line consisting of 91 % spruce and 9 % moisture. Additionally, a 13 mm layer of ceramic wool was placed beneath the layer of spruce defined on the same `SURF` line for its insulating properties. 10 mm cells were used for gas phase computations, yielding comparable results to a 5 mm cell but with a reasonable computational time.
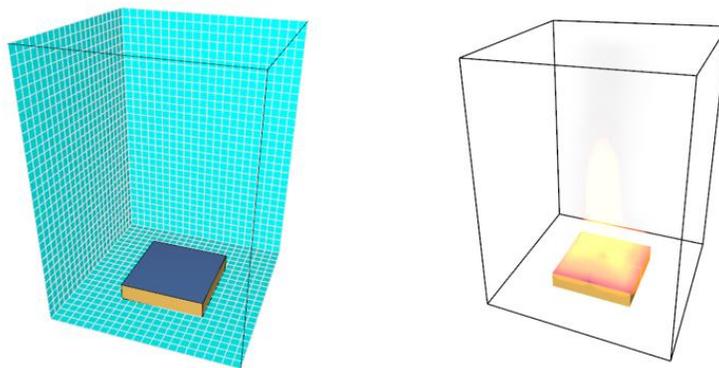
Figure 16 - Snippet of cone calorimeter set-up in SmokeView

In FDS, the solid phase mesh cell size is determined automatically based on the square root of the sample's diffusivity, which may differ from the gas phase cell size. To address the issue of oscillating HRR curve results, the SURF line was modified with `WALL_INCREMENT`, `CELL_SIZE_FACTOR` and `STRETCH_FACTOR` set to 1,0, 0,8 and 1,0 respectively. These are parameters that can enhance the numerical accuracy and stability of the solid phase solution in FDS. `WALL_INCREMENT` equal to 1 forced the solid phase solution to be updated every time step instead of every second, `CELL_SIZE_FACTOR` reduces the mesh cell size in all layers, while `STRETCH_FACTOR` controls the node spacing within the material and creates a uniform mesh for each layer. These adjustments helped minimize spurious fluctuations in HRR due to the pyrolysis reactions.

The thermal parameters for spruce wood used in the model developed by Rinta-Paavola and Hostikka are presented below. The values are briefly discussed, and any discrepancies between the present thesis model and the authors' work are highlighted.

Specific heat capacity

From Rina-Paavola & Hostikka's study, experimental results revealed a linear increase in the specific heat capacity of spruce, ranging from 0.92 kJ/ (kg K) at 30 °C to 1.8 kJ/(kg K) at 230 °C. For determining the specific heat capacity of char, a correlation established by B. Fredlund [35] in her doctoral dissertation was employed, as presented in Eq. 10.

$$c_{p,char} = 1430 + 0{,}355T - \frac{7{,}32 \times 10^7}{T^2} \qquad \text{Eq. 3}$$

Conductivity

Thermal conductivities for both spruce and char were considered as optimized values to achieve the best agreement with the experimental data obtained from cone calorimetry. Consequently, the values were determined to be 0.09 W/ (m K) for wood and 0.22 W/(m K) for char.

This approach, while suitable for the specific experimental context, may introduce potential sources of error when applying the findings to larger scale models. The optimized thermal conductivity values may not accurately represent the inherent variability in these properties,

which could lead to discrepancies when extrapolating to broader applications or different conditions.

Heat of pyrolysis

In a manner akin to determining conductive values, the heat of pyrolysis was ascertained through model fitting to achieve the highest accuracy in the cone calorimeter simulation. As a result, Rinta-Paavola & Hostikka identified the optimal fit for the single-reaction scheme as an endothermic reaction of 19 kJ/kg.

Rinta-Paavola and Hostikka's selection of a 19 kJ/kg endothermic reaction for the single reaction scheme finds support in Atreya's thorough literature review [36]. Atreya compared predictions from a numerical pyrolysis model to experimental data, using a variety of heat of pyrolysis values ranging from +125 kJ/kg to -125 kJ/kg. The analysis demonstrated that both endothermic and exothermic values yielded satisfactory results, contingent upon the test, which led Atreya to advocate for a value of 0 kJ/kg. Considering these findings, the choice of 19 kJ/kg by Rinta-Paavola and Hostikka represents a well-grounded and justifiable decision that closely aligns with Atreya's argument.

Emissivity

Emissivity of char and spruce were set to 0,85 and 0,9 respectively based on a study by Chaos [37]. The study aimed to determine model-specific material properties using inverse modelling and optimization methodologies, much like Rinta-Paavola & Hostikka's study.

A literature review reveals that Janssens' study [38] on the emissivity of char and wood suggested an average emissivity of 0,88 for wood and 1,0 for char under flaming combustion conditions. The values chosen by Rinta-Paavola & Hostikka deviate slightly from the wood emissivity found by Janssens, while the char emissivity exhibits a considerable difference. It is important to note that the values for this simulation have been validated for cone calorimeter tests with acceptable results, providing justification for their use. Nevertheless, employing these values in a larger scenario than a FDS cone calorimeter test could potentially introduce errors, as it is uncertain whether these values would remain suitable when scaling up the model.

Heat transfer coefficient

Ryder and Weckman [39] highlight that a majority of convective heat transfer coefficients found in the literature for cone calorimeter experiments, encompassing various materials such as wood, typically range from 10 to 20 W/ (m² K). In light of this observation, Rinta-Paavola & Hostikka opted to employ an average value of 15 W/ (m² K) as the convective heat transfer coefficient for their simulations, integrating this value into the SURF line for spruce in their FDS simulations.

Opting for a value within this range is reasonable, as it considers the average behaviour of materials under controlled heat flux conditions and streamlines the simulation process by avoiding the need to compute the coefficient. The chosen value of 15 W/ (m² K) provides a balance among potential variations in convective heat transfer behaviour, thus serving as a sensible approximation for the simulation. However, it's essential to be aware that the specific convective heat transfer coefficient for wood might deviate from this assumed value, potentially influencing the accuracy of simulation outcomes. To enhance the representation of wood in simulations, further research and experimental validation may be necessary to adjust this value.

Combustion

The combustion process was modelled as a single-step reaction of $C_6H_{10}O_5$ employing the Eddy Dissipation Concept (EDC). Soot and CO yields were not specified in Rinta-Paavola and Hostikka's study; hence, values of 0.015 for soot and 0.004 for CO (g/g) were adopted based on data from chapter 16 in the SFPE Handbook [40], which pertains to well-ventilated fire product yields.

Rinta-Paavola and Hostikka evaluated the heat of combustion for spruce using Microscale Combustion Calorimetry (MCC) experiments. Although the initial heating rates were set at 20 and 60 K/min, the actual recorded values were 37,4 K/min and 74,5 K/min. Following this, the experiments were simulated in FDS, where the heat of combustion for spruce was adjusted to establish a visual match between the simulated and experimental heat release rate curves, resulting in a heat of combustion per produced mass of gas of 13,75 MJ/kg.

In contrast, Bartlett et al. [1] [8] assumed a heat of combustion of 17,5 MJ/kg. This discrepancy may significantly impact the thesis' model results and is explored in greater detail in Section 6.

Results

Following the completion of all three simulations, the data was processed. The HRR (kW) and MLR (kg/s) values obtained from the CHID_hrr.csv output file were divided by the sample surface area of 0,001 m² to calculate HRRPUA (kW/m²) and MLRPUA (kg/ (s m²)). These values were then compared to the experimental data from the cone calorimeter tests presented by Rinta-Paavola & Hostikka. Figure 17, Figure 18 and Figure 19 below illustrate the comparison between the simulated results ran for this thesis, and the experimental data from Rinta-Paavola & Hostikka's study. It is important to reiterate that the parameters for these simulations were optimized to fit the experimental data of a cone calorimeter test with a heat flux set to 35 kW/m².
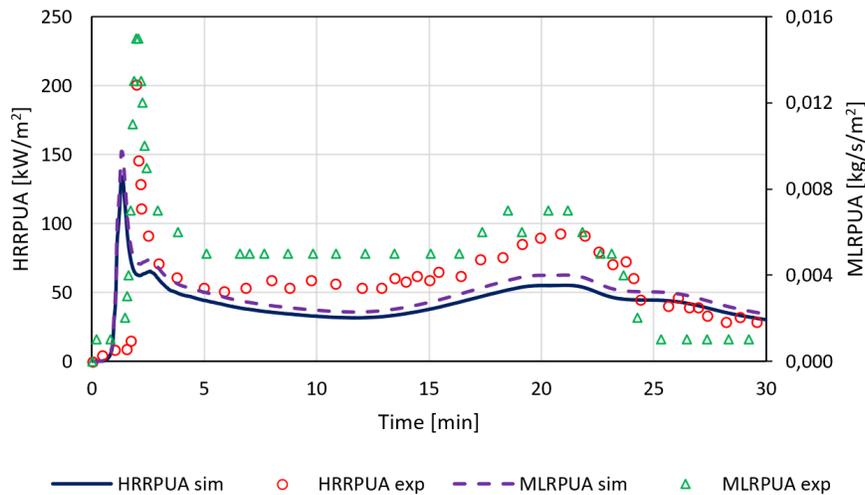
Figure 17 - Comparison between experimental and simulated HRRPUA and MLRPUA for cone calorimeter test at heat flux of 25kW/m²
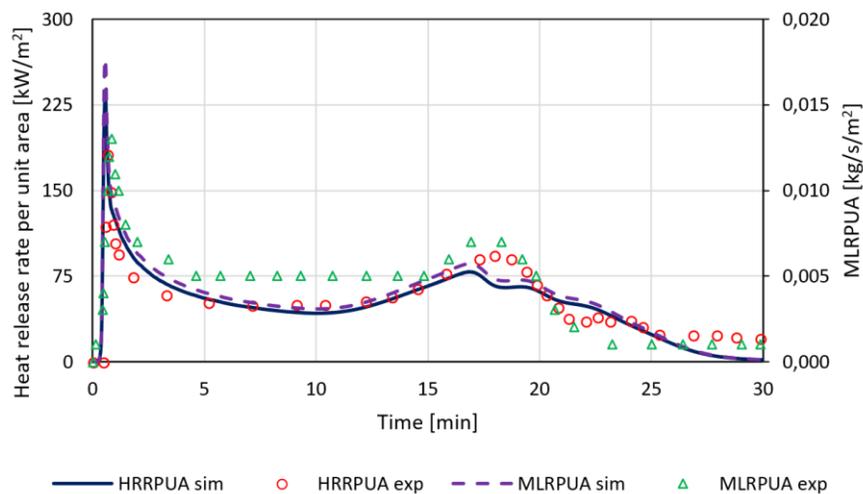
Figure 18 - Comparison between experimental and simulated HRRPUA and MLRPUA for cone calorimeter test at heat flux of 35kW/m²

33
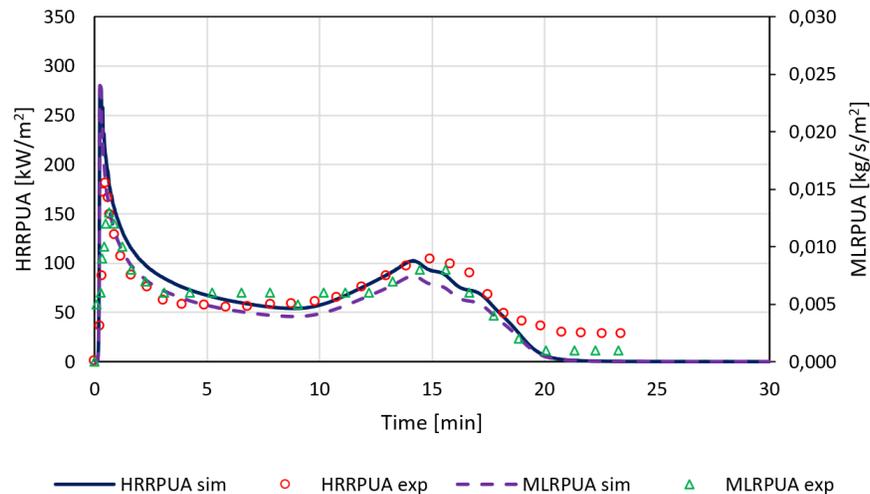
Figure 19 - Comparison between experimental and simulated HRRPUA and MLRPUA for cone calorimeter test at heat flux of 50kW/m²

The results obtained align with expectations as they replicate Rinta-Paavola & Hostikka's research. The 35 kW/m² heat flux demonstrates a strong fit, as this value was the basis for adjusting all parameters. However, the long tail following the second peak for HRR is absent in all simulations due to the model's inability to reproduce the glowing combustion from the char during the decay stage. The simulations for the 50 kW/m² cone calorimeter test also yield satisfactory results, albeit with an overestimation of the first peak and a significantly shorter tail after the second peak. Nevertheless, the location of both peaks and the curve between them are acceptable.

The simulation for the 25 kW/m² cone calorimeter test performs inadequately, which Rinta-Paavola & Hostikka speculate may be due to the sample being exposed to a heat flux closer to the critical value of piloted ignition for wood, at 12 kW/m² [11]. Ignition in the simulation commences earlier than in the actual experiment, with a lower first peak and a barely discernible second peak. The HRR remains relatively low throughout the entire simulation, and the sample does not burn away entirely during the simulated 30-minute period. This outcome introduces additional uncertainties for the upcoming large-scale compartment model and should be acknowledged in subsequent discussions of the results.

In conclusion, this chapter presented the methodology and results of cone calorimeter simulations conducted to validate the modelled spruce's kinetic properties established through thermogravimetric analysis. Three sets of simulations at heat fluxes of 25, 35, and 50 kW/m² were performed, and the outcomes were compared to experimental data from Rinta-Paavola &

34

Hostikka's study. The 35 kW/m² simulation demonstrated a strong fit, while the 50 kW/m² simulation yielded satisfactory results with some deviations. The 25 kW/m² simulation, however, performed inadequately, introducing uncertainties for the upcoming large-scale compartment model.

The thermal parameters used in the simulations were based on Rinta-Paavola & Hostikka's study, with some deviations found in the literature, such as the heat of combustion, emissivity, and heat transfer coefficient. These discrepancies, along with the optimized values for thermal conductivity, may introduce additional sources of error when scaling up the model.

Despite these limitations, the simulations generally aligned with Rinta-Paavola & Hostikka's findings, providing a basis for further investigations and large-scale applications. To enhance the model's accuracy and applicability, future research should focus on refining the thermal parameters, addressing the model's inability to reproduce glowing combustion, and validating the model for a broader range of heat fluxes. Table 4 on the next page summarize the thermal properties utilized in the cone calorimeter test simulations.

Table 4 - Thermal properties used in cone calorimeter test simulation

Material	Spruce	Char	Moisture	Stone wool
Specific heat [kJ/kg K]	0,92 (20°C) 1,8 (230 °C)	$1430+0{,}355T-(7{,}32\times10^7)/T^2$ (absolute temperature)	4,7 (20°C) 6,7 (230 °C) [41]	1,13
Conductivity [W/m K]	0,09	0,22	0,6	0,04 (20°C) 0,06 (200 °C) 0,11 (400 °C) 0,17 (600 °C) 0,26 (800 °C) 0,38 (1000 °C)
Density [kg/m3]	408	59	1000	65
Emissivity [-]	0,9	0,85	0,9	0,9
H_C [kJ/kg]	$1{,}375\times10^4$	-	-	-
H_r [kJ/kg]	19	-	2500	-

3. Theory

This chapter aims to provide a comprehensive understanding of the fundamental theories and concepts that underpin the study of compartment fires with exposed timber surfaces. By examining the various aspects of fire dynamics and the specific properties of engineered wood, the chapter establishes the groundwork for the numerical simulation and analysis conducted in this thesis.

3.1. Flaming combustion of timber

Timber exposed to high temperatures in an oxygen-limited environment may lead to pyrolysis, where the complex organic compounds within the timber break down into simpler molecules, producing volatile gases, tars, and a carbon-rich residue known as char. The flammable gases produced within the wood element will, via diffusion, move to the surface of the wood and mix with the ambient air. As the flammable gases accumulate at the surface, a mixture of pyrolyzate and oxygen from the air will reach a flammable concentration and oxidate. If the flow of volatiles out from the wood element is adequate, a sustainable flame appears. The flame will work as a secondary external heat source and heat the timber through radiative and convective heat transfer, further sustaining the pyrolysis process [42].

As the timber burns, a char layer develops between the flaming solid surface and the pyrolysis region within the element. With an increasing char depth, the heat transfer to the virgin wood becomes lesser and consequently, so does the production of volatiles. Suppose the MLR of flammable gases from the wood is reduced to a critical value. In that case, there will no longer be a flammable mixture of air and volatiles for continuous burning and self-extinguishment of flaming combustion will occur [33] [42]. Following is a closer examination of the critical processes involved in the flaming combustion of timber.

Pyrolysis

Pyrolysis constitutes a thermally driven decomposition process that transpires when materials like wood encounter elevated temperatures. This process, involving both chemical and physical alterations, is critical for elucidating materials' ignition, combustion, and extinction dynamics. As polymers disintegrate into smaller gas-phase molecules, sufficient heat generation via combustion is required to sustain a continuous reaction [42]. Upon exposure to heat, timber's inherent natural

polymers, mainly hemicellulose, cellulose, and lignin, undergo degradation, yielding byproducts including inert and combustible gases, liquid tars, carbonaceous char, and inorganic ash [43]. Hemicellulose is usually the first component to start pyrolysis, followed by cellulose and lignin. Pyrolysis can be categorized into several phases, encompassing dehydration and gradual pyrolysis below 200°C, the initiation of pyrolysis up to 300°C, and accelerated pyrolysis beyond 300 °C [44]. It is crucial to distinguish between pyrolysis, an endothermic process, and combustion, as the former does not necessitate the presence of an oxidizer [45].

Charring

Low-temperature charring phenomena involve mass loss at temperatures below 200°C, with pyrolyzate consisting mainly of non-combustible volatiles [46] [44] [45]. High-temperature charring phenomena involve the thermal decomposition of wood's three main components at varying temperature ranges and rates, influenced by factors such as heating rate, species and moisture content [45]. Pyrolysis rates rapidly increase between 300°C and 500°C, forming residual char [44]. While general agreement exists on the order in which constituent polymers react, their chemical processes, and char yields, the literature displays significant variation in fundamental properties like decomposition temperatures. These differences may be partially attributed to variations in species, heating rate, and testing methods, highlighting the importance for designers to be aware of the chemical processes determining timber's thermal and mechanical properties when exposed to fire [45]. While charring is generally simplified as pyrolysis occurring at 300 °C for structural applications, it must be recognized that multiple stages within the pyrolysis process can affect a timber member's load-bearing capacity [45].

The process of charring significantly impacts the heat transfer mechanisms of virgin wood material due to the resulting alterations in physical properties and the development of cracks [46]. As the heat conductivity of char is lower than that of virgin wood, and the formation of cracks occurs, the radiative heat transfer mechanism through char pores becomes the dominant mode of heat transfer into the wood sample [47]. As a result, this can introduce more significant levels of uncertainty in heat transfer analyses where assumptions of one-dimensional heat transfer are applied [48].

Evaporation of moisture

Moisture transport influences the formation of three distinct zones: a dry zone where pyrolysis occurs, a dehydrating zone, and a wet zone. As temperatures approach 100°C, free water evaporates, and some water vapour migrates deeper into the timber, re-condensing and increasing local moisture content [49]. The interplay between dehydration and pyrolysis is affected by heat flux, with the simultaneous occurrence at higher heat fluxes [50]. This results in moisture impeding the temperature rise, typically up to 115 °C [45], due to energy consumption for evaporation and cooling effects from the convective mass flow of water vapour. As a result, bound water is generally released at higher temperatures, around 240 °C [51].

Ignition

Ignition occurs when oxygen interacts with pyrolysis products, leading to a swift exothermic reaction. This discussion focuses on flaming combustion, which is distinct from smouldering combustion. Ignition can be divided into two categories: piloted ignition, which requires an external spark or flame to activate gaseous substances, and unpiloted ignition, which relies solely on heating to supply the necessary energy for ignition [45].

Two criteria are typically used to define ignition: critical heat flux and critical surface temperature. The former pertains to the minimum heat flux required for ignition, while the latter refers to the lowest surface temperature that can initiate ignition. These criteria have some variability, with piloted and unpiloted ignition critical heat flux values ranging from 10 to 13 kW/m² and 25 to 33 kW/m², respectively. Critical surface temperature results display more significant variation; however, ignition consistently occurs at temperatures significantly lower than in fires. It is crucial to recognize that various factors influence ignition properties, such as experimental setup, sample orientation, ambient temperature, and heat transfer mode. Moreover, wood characteristics like density, moisture content, thickness, configuration, and duration significantly impact the heat required for ignition [45].

Combustion

Following ignition, flaming combustion occurs at the wood surface. This involves mixing the volatile pyrolysis gases from the wood surface with ambient air. In contrast, smouldering combustion occurs through solid-phase char oxidation [45]. The literature gives a heat of

combustion for wood between 15 and 20 MJ/kg [52], where the combustion of these volatiles contributes to increased heat transfer into the solid wood, accelerating the pyrolysis process [53]. Heat fluxes from the flaming of timber were found by Petrella [54] and Tewarson and Pion [55] to range from 23,9 kW/m² to 77,5 kW/m², depending on the type of timber. However, it was discovered that unlike other types of liquid and solid fuels where flaming will greatly contribute to further combustion, the heat losses from burning timber will be equal to or greater than the flaming heat flux. Meaning a flame cannot sustain without an external heat source supporting heat transfer into the specimen. Consequently, a continuous external heat transfer from the fire, such as from other burning surfaces or mobile fuel loads, must be present to ensure persistent flaming combustion [56].

The pyrolysis rate significantly influences the combustion rate, exhibiting a full initiation during the onset of flaming combustion [52]. However, as the char layer, which possesses lower thermal conductivity than unburned wood, forms, it attenuates the combustion rate until pyrolysis penetrates deeper into the timber material [44]. Eq. 4 gives the net heat flux at the wood surface, excluding the contribution for smouldering combustion from char [45].

$$\dot{q}''_{net} = \dot{q}''_e + \dot{q}''_f - \sigma(T_s^4 - T_\infty^4) - h_c(T_s - T_\infty) - k\frac{\partial T}{\partial x}$$

Eq. 4

Where

$\dot{q}''_{net}$ is net heat flux [kW/m²]

$\dot{q}''_e$ is external heat flux [kW/m²]

$\dot{q}''_f$ is heat flux from flames [kW/m²]

σ is Stefan-Boltzmann constant [W/m²K⁴]

T_s is surface temperature [K]

T_∞ is ambient temperature [K]

h_c is convective heat transfer coefficient [W/m²K]

k is thermal conductivity [W/mK]

$\frac{\partial T}{\partial x}$ is temperature gradient with respect to the spatial coordinate x [K/m]

Flame extinction

Flaming combustion goes extinct when the flame loses more heat than it produces. This can happen when the amount of pyrolyzates being released drops below a critical MLR [45]. Critical MLR of volatiles from a solid fuel is the lowest value of pyrolyzate flow that must be present to have continuous flaming. For example, Emberly et al. [57] quantified the worst-case scenario for critical MLR for European Spruce to be 3,93 ± 0,45 g/m²s and critical heat flux for the extinction of flaming surface to be in order 43,6 ± 4,7 kW/m². However, it is stated that the properties of firepoint will vary with the wood species and therefore needs to be specified for each product if one is to estimate self-extinguishment.

The interface surface between char and timber is the point of interest when analysing the MLR of the pyrolyzates. In this pyrolysis region, the incoming heat plays two distinct roles. Firstly, it participates in pyrolysis, wherein the material decomposes into residue and flammable gases. Secondly, it conducts further into the unpyrolyzed, dried timber, which is not yet involved in the pyrolysis process, and causes the vaporisation of any residual moisture. MLR of pyrolyzates can be expressed through the net heat flux at the region of pyrolysis and the amount of heat needed to produce volatiles, as formulated through Eq. 5 [1] [33].

$$\dot{m}'' = \frac{\dot{q}''_{net}}{L_v}$$

Eq. 5

Where

$\dot{m}''$ is mass loss rate of pyrolyzates [g/m²s]

$\dot{q}''_{net}$ is netheat flux [kW/m²]

L_v is heat of vaporization [kJ/g]

The heat of vaporization L_v is the amount of heat needed to vaporize an amount of fuel at its vaporization point, meaning that the energy spent heating the fuel to its vaporization point is not included [58]. The heat of gasification L_g found through experimental testing includes the heating of the fuel from ambient temperatures and determined by Tewarson and Pion to be 1,82 kJ/g for timber. L_v can therefore be calculated from Eq. 6 and is around 1,1 kJ/g for wood [55].

$$L_v = L_g - \int_{T_\infty}^{T_p} C_p dT$$

Eq. 6

Where

L_v is the heat of vaporization [kJ/g]

L_g is heat of gasification [kJ/g]

C_p is specific heat capacity [kJ/kgK]

T_p is pyrolysis temperature [K]

T_∞ is ambient temperature [K]

Summary

To summarize, in this chapter on flaming combustion of timber, the processes of pyrolysis, charring, evaporation of moisture, ignition, combustion, and flame extinction are examined. Pyrolysis, an endothermic process, occurs when timber is exposed to high temperatures, breaking down its complex organic compounds into simpler volatile molecules. Charring, the formation of a carbon-rich residue, affects heat transfer mechanisms in virgin wood. Moisture content influences the formation of distinct zones, which impacts the interplay between dehydration and pyrolysis. Ignition occurs when oxygen interacts with pyrolysis products, initiating an exothermic reaction. Flaming combustion takes place at the wood surface and is sustained by continuous external heat transfer. Flame extinction occurs when the flame loses more heat than it produces, leading to self-extinguishment.

The subsequent chapter expands on these foundational principles to discuss the calculation method for MLR of CLT, as employed by Bartlett et al. [1], in predicting self-extinguishment of flaming combustion within the compartment fire central to this thesis.

3.2. CLT mass loss rate estimation

In the compartment fire study conducted by Bartlett et al. [1], as discussed in Section 2.6, the authors suggest that the prediction of extinction for flaming CLT surfaces can be achieved by

estimating the MLR of volatiles from the CLT surfaces and knowing the critical MLR for sustained flaming combustion.

From prior experiments [32], the researchers determined that the self-extinguishment of spruce timber occurs when the rate of pyrolyzates falls below 3.48 g/ (m² s), which is deemed the critical MLR. Eq. 5 from Section 3.1 can subsequently be employed to estimate the MLR in the pyrolysis region. The net heat flux, $\dot{q}_{net}^{''}$, relies on both conductive heat transfer through char and conductive heat transfer into dry timber. Char formation is presumed to transpire at 300 ⁰C [55], and the heat fluxes can be represented through a discretized version of Fourier's Law [22]. From this, Bartlett et al. presents Eq. 7 to estimate the MLR from the CLT surfaces.

$$\dot{m}^{''} = \frac{1}{L_v}\left[k_c\frac{T_c - 300}{\Delta x_c} - k_w\frac{300 - T_w}{\Delta x_w}\right] \qquad \text{Eq. 7}$$

Where

$\dot{m}^{''}$ is MLR of pyrolizates [g/m²s]

T_c is temperature of char [K]

T_w is temperature of untouched wood [K]

L_v is heat of vaporization [kJ/g] (see Eq. 6)

k_i is thermal conductivity [kW/mK]

Δx_c is the char thickness [m]

Δx_w is the untouched wood thickness [m]

In the experiment, thermocouples were placed within the CLT elements at different depths. Eq. 7 was thereby applied to the temperature readings. Temperature gradients were extracted from the temperature data and char depth was derived from interpolation of the temperature profile. Thermal conductivity for char and wood were assumed 0,25 and 0,18 W/(mK) respectively [52]. Using this approach, they get the results presented in Figure 12 in chapter 2.6.

3.3. Compartment fires

Compartment fires are characterized by four different stages; the ignition-, growth-, fully developed- and decay phase. Different phases have different characteristics which separate them

from each other, like temperature, type of fuel burning, fuel-controlled regime burning or ventilation-controlled regime burning, and what type of heat transfer that is dominant. It is not given that a fire will undergo all phases, as there are numerous variables that can affect the course of development, i.e., activation of automatic extinguishment systems, no available fuel, oxygen concentration etc. Figure 20 illustrates a characteristic time-temperature curve for all phases a compartment fire can go through [59].

Figure 20 – Development of compartment fires [59]

A key-difference between compartment fires and outside fire situations is the smoke layer that emerge for a compartment fire. Flames and smoke give off substantial amounts of radiation which heat unburnt fuel and increase the fire size. A larger fire will increase the production of smoke, and if production is greater than the mass flow of gases out of the compartment, the smoke layer will continue to grow and radiation intensity increase. If this process is allowed to continue, flashover will occur, and the fire is fully developed [59].

Flashover is a phenomenon which occurs when there is a rapid transformation in the enclosure fire dynamics from growth phase to a fully developed fire. It is also often presented as the switch from a fuel-controlled regime to a ventilation-controlled regime. There is an ongoing discussion on how to define flashovers, but typically one of the following criteria must be present [60] [59]:

- Smoke layer temperature exceed 600 °C
- Radiative heat flux at ground level exceeds 20 kW/m^2
- Visible flames outside fire compartment

For a fully developed fire, also coined "steady phase", the fire has reached its maximum magnitude of HRR and burning is typically dependent on ventilation that is available (ventilation-controlled

44

regime). This means that a percentage of the flammable gases within the fire compartment don't have access to oxygen and won't combust. Flammable gases are led with the mass flux of smoke outside and ignited when met with a satisfying oxygen concentration [59]. All available fuel is partaking in pyrolysis for this phase, gas temperatures can reach up to 1 200 °C and the condition details for this period are crucial for structural design purposes [7].

Consequently, when the amount of fuel available decrease, the production of flammable gases from pyrolysis lessens and the fire enters a decay phase. Temperature begins to drop and often times a fuel-controlled regime appear. Meaning that there is sufficient ventilation in the compartment and all flammable gases produced can combust within the compartment. For a traditional compartment fire where available fuel consist of room interior and room surfaces are incombustible, the fire can be assumed to extinguish when all combustible interior is consumed [59].

3.4. Compartment fires with exposed timber surfaces

When it comes to compartment fires featuring exposed timber surfaces, the fire dynamics differ significantly from those with non-combustible linings. The most notable differences include [61]:

- higher heat release rates
- faster times to flashover
- increased gas temperatures
- an extended decay phase with higher temperatures

In contrast to compartment fires with non-combustible linings, fires in compartments with exposed timber surfaces may not extinguish even after all interior combustibles have been consumed. The exposed timber surfaces will participate in the fire and continue burning if there is enough heat transfer to the pyrolysis region within the CLT elements [8] [62]. The heat transported into the elements during the decay phase is typically due to convective heat from the burning surface itself [17] and radiative heat from adjacent or opposite exposed timber surfaces of ceilings and walls. Adequate heat exchange between exposed surfaces can prolong the fully developed phase, otherwise self-extinction may occur [8].

An additional risk for compartment fires with exposed and/or encapsulated timber surfaces is delamination and encapsulation failure. Delamination is fall-off of lamellas during a fire which can be caused by glue line failure, debonding or char fall-off. Encapsulation failure is failure of

protective layers, such as gypsum plasterboards, to appropriately safeguard the underlying timber and exposing it to fire [17]. Both mechanisms contribute to virgin timber being exposed to the fire which increase charring and heat release rate [63] [8]. This can also prevent drastically delay extinguishment or prevent self-extinguishment overall [17]. Figure 21 illustrates how the fire progression can develop with exposed and/or encapsulated timber surfaces [64].
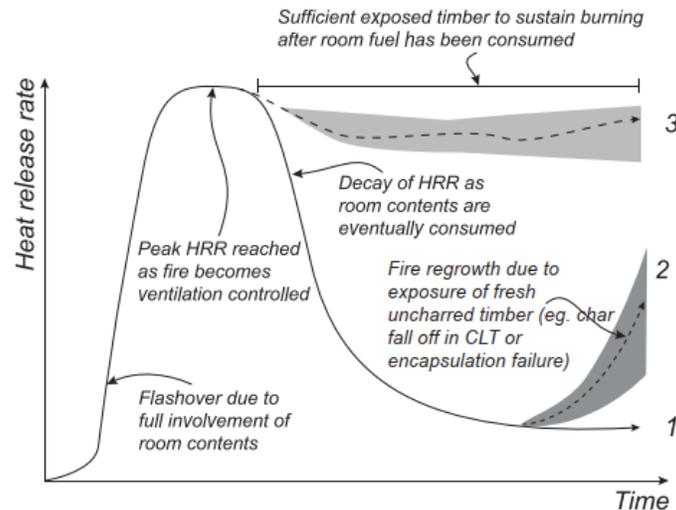
Figure 21 – Heat release rate for compartment fires with exposed CLT surfaces [64]

3.5. Numerical simulation

Computational fluid dynamics (CFD) is a modelling technique employed across numerous engineering fields to analyze fluid flow. It involves solving the fundamental laws of mass, momentum, and energy conservation in three dimensions over time by dividing the volume of interest into smaller sub-volumes and applying the conservation laws to each. The Navier-Stokes equations are conservation laws, and account for viscous forces in fluid flow. Various commercially available CFD codes exist to solve these equations and examine fluid flow. These codes typically feature a pre-processor, allowing users to define geometry, grid, physical phenomena, fluid properties, and boundary conditions to be modelled; a solver that approximates the unknown flow variables for a given time step and solves the resulting algebraic equations; and a postprocessor that enables the display of input and output data in various forms, such as grid displays, vector plots, contour plots, 2D and 3D surface plots, and particle tracking [59].

The Fire Dynamics Simulator (FDS) [9], developed by the National Institute of Standards and Technology (NIST) and Technical Research Centre of Finland (VTT), is a freely available CFD

model. FDS primarily focuses on smoke and heat transfer and is employed for addressing fire engineering issues and as a tool for investigating combustion and fire dynamics principles [65] [34]. FDS is considered a "fire model" because it incorporates features describing various aspects of fires, such as gaseous fuel and oxygen combustion, thermal radiation transport through hot gases, material decomposition, and the activation of sprinklers and smoke detectors [65].

FDS is an extensive model encompassing various sub-models that account for a wide range of parameters. The following sections of this chapter will offer a concise overview of the most significant aspects of the FDS model relevant to this study, drawing upon information from the FDS user's guide [34] and technical reference guide [65].

3.5.1. Combustion model

FDS utilizes combustion models to determine the heat release rate per unit volume by summing the product of mass production rate of a species and the species' heat of formation, as shown in Eq. 8. The default combustion model in FDS, called "Single-Step, Mixing-Controlled Combustion," assumes instantaneous, complete mixing of lumped species, which represent mixtures of individual species. For more complex reactions involving carbon monoxide and soot formation, a generalized approach is needed.

$$\dot{q}''' = -\sum_\alpha \dot{m}_\alpha''' \, \Delta h_{f,\alpha}$$

Eq. 8

Where

$\dot{q}'''$ is heat release rate per unit volume [kW/m^3]

$\dot{m}_\alpha'''$ is mass production rate of species α [kg/m^{3}s]

$\Delta h_{f,\alpha}$ is heat of formation of species α [kJ/kg]

The mixing time plays a crucial role in turbulent combustion, as it influences the rate of chemical reactions. It can be affected by various physical processes such as diffusion, advection, and buoyant acceleration. The reaction time scale model accounts for these processes and selects the fastest one to control the flow time scale.

The default combustion model in FDS requires user-specified parameters, including fuel species, chemical formula, CO yield, soot yield, and heat of combustion. FDS automatically generates lumped species (`AIR`, `FUEL`, and `PRODUCTS`) based on these parameters.

3.5.2. Pyrolysis model

FDS offers a *predefined* and a *predictive* approach to represent the pyrolysis process in the simulated environment.

Predefined Pyrolysis

The predefined pyrolysis is commonly employed to predict temperature variations and smoke movement within a specified domain caused by a fire. To conduct these simulations, users can define time dependent HRR and define the surface area where this HRR will emerge. FDS uses this information to determine the quantity of combustible gases entering the domain and igniting. Alternatively, the user can specify a time dependent rate at which combustible gases shall enter the simulated domain This predefined pyrolysis model can be implemented using a "burner" `SURF` line applied to a `VENT` or an obstruction surface.

Upon reaching the specified ignition temperature, the surface effectively becomes a source of gaseous fuel emissions. The heat release can also be configured to cease once the given mass of the burning surface has been fully combusted. This pyrolysis model needs the user to assume a heat release rate for the burning object, which can be obtained from sources such as literature and/or various bench-scale and large-scale fire tests.

Predictive Pyrolysis

The predictive pyrolysis model is used in this thesis' investigations and is a more sophisticated approach for examining the combustion of solid materials under heat exposure. Contrary to the predefined pyrolysis model, combustible gases are introduced into the simulation space through the breakdown of solid materials due to heat conduction. This more complex pyrolysis model in FDS estimates the amount of flammable gases entering the domain based on the solid's heating and various competing chemical reactions, which may also generate other solid and gaseous byproducts, such as char and water vapor. This is calculated by FDS using Arrhenius function to estimate a reaction rate, shown in Eq. 9.

$$r_i = \rho_{s,i}^{n_i} A_i \exp\left(-\frac{E_i}{RT_s}\right)$$

<div align="right">Eq. 9</div>

r_i is reaction rate of the ith component

A_i is pre-exponential factor

E_i is activation energy

n_i is reaction order [-]

R is universal gas constant

T_s is temperature where the reaction occurs

$\rho_{s,i}$ is density of the ith component of the layer

Note that the density of the ith material component in the layer, $\rho_{s,i}$, is determined by dividing the mass of the component by the layer's volume. As a result, $\rho_{s,i}$ will increase when the ith component is produced as a residue from another reaction or decrease if the component breaks down.

In contrary to the predefined pyrolysis model, which employs a minimal set of parameters to depict burning, the advanced model considers several factors that affect the burning rate. In this model, the burning rate of a solid material is influenced by kinetic values specified by the user, its density, emissivity, absorption coefficient, specific heat capacity, and other during combustion. It also considers the material's temperature throughout the burning process, which is ascertained by analysing conductive heat transfer within the material. This method involves the use of multiple parameters, the gathering of which can be time-consuming. To collect this data, researchers employ a variety of tools and techniques. These include thermogravimetric analysis (TGA) and the cone calorimeter, which are specifically used to gather information about the material's thermal properties.

3.5.3. Conductive heat transfer

In a room fire, enclosure surfaces are subjected to both radiative and convective heat. A portion of this heat is conducted into the solid material through the conductive heat flux. These solid surfaces might consist of multiple layers composed of various materials, which may undergo thermal decomposition reactions as heat is conducted through them, changing their chemical composition through the predictive pyrolysis model described above. FDS presumes that conductive heat

moves perpendicularly to the solid surface and can be represented by a one-dimensional heat conduction equation for the solid phase temperature. Eq. 10 is relevant for conductive heat transfer into the solid perpendicular to the surface calculated by FDS [65].

$$\rho_s c_s \frac{\partial T_s}{\partial t} = \frac{\partial}{\partial x}\left(k_s \frac{\partial T_s}{\partial x}\right) + \dot{q}''_{s,c} + \dot{q}''_{s,r}$$

Eq. 10

Where

ρ_s is density [kg/m³]

c_s is specific heat [kg/ (kJ K)]

T_s is temperature [K]

t is time [s]

x is position [m]

k_s is thermal conductivity [kW/(mK)]

$\dot{q}''_{s,c}$ is heat loss due to pyrolysis [kW/m²]

$\dot{q}''_{s,r}$ is radiative absorption and emission [kW/m²]

The one-dimensional assumption has limitations, as it does not account for radial heat dispersion or heating multiple sides of an obstruction. There are also constraints on the geometry of an obstruction when calculating heat transfer. FDS employs obstructions, which are three-dimensional solid objects that hinder flow, to represent various elements in a model. These can encompass walls, floors, and ceilings, as well as any other material object [66] [34].

Constructing an obstruction within FDS involves several stages, including defining materials, using these materials to create surfaces, and ultimately incorporating these surfaces into the obstruction. The material properties, such as density, specific heat, and conductivity, play a crucial role in determining standard heat conduction properties [66] [34].

3.5.4. Grid resolution

Grid resolution is a critical aspect of CFD simulations, as it determines the level of detail captured by the numerical model. In the context of fire simulations in FDS, the non-dimensional expression $D^*/\delta x$ is presented in the FDS User's Guide [34] as an indicator than can be employed to help quantify grid resolution, which influences the accuracy and computational efficiency of the results.

The grid cell size, δx, refers to the dimensions of each cell in the computational mesh used to discretize the simulation domain. The choice of grid cell size is essential, as a finer mesh offers better resolution and accuracy but demands more computational resources.

The expression $D^*/\delta x$ represents the ratio of the characteristic fire diameter (D^*) to the size of a grid cell (δx). A cell size δx deemed appropriate for a large fire may not necessarily be suitable for a smaller fire due to the smaller D^* value. A particular value of $D^*/\delta x$ considered optimal for a large fire might also be effective for a small fire, though this is not guaranteed, as the value of D^* decreases with the reduction of the fire. If HRR increases over time, the value of $D^*/\delta x$ also rises. If $D^*/\delta x$ is assessed to be sufficiently fine for the maximum anticipated HRR, the cell size may still prove inadequate during the initial growth phase of the fire. The characteristic fire diameter, D^* is formulated as in Eq. 11.

$$D^* = \left(\frac{\dot{Q}}{\rho_\infty c_p T_\infty \sqrt{g}} \right)^{\frac{2}{5}} \qquad\qquad \text{Eq. 11}$$

Where

$\dot{Q}$ is total HRR [kW]

ρ_∞ is ambient air density [kg/m³]

c_p is specific heat capacity of air at constant pressure [J/kgK]

T_∞ is ambient temperature [K]

g is acceleration due to gravity [m/s²]

Although recommendations on suitable value ranges for $D^*/\delta x$ can be found in various scholarly publications [67], the FDS Validation Guide provides $D^*/\delta x$ values for several contexts [68], which may serve as an initial point of reference when establishing mesh resolution. Nonetheless, directly applying these values without additional research is ill-advised.

It should also be noted that the D^*-approach is thought of as a metric for quality of gas phase fluid flow and may not be adequate for simulations which involves closely assessing conductive heat transfer into solid material to predict pyrolysis, which demands higher resolution for accuracy [69].

The determination of an ideal cell size or the precise value of $D^*/\delta x$ for a specific scenario remains inconclusive, except for performing a mesh sensitivity analysis. This analysis involves conducting a series of simulations with varying grid resolutions to identify the point at which the outcomes no longer change significantly as the mesh is refined. By performing mesh sensitivity analysis, researchers can ascertain the optimal grid resolution that balances the need for accurate results and computational efficiency. Ultimately, a mesh sensitivity analysis stands as the principal approach for identifying the appropriate mesh resolution.

3.6. Thermogravimetric analysis

Thermogravimetric Analysis (TGA) is an analytical technique used to investigate the thermal behaviour of materials during decomposition and pyrolysis processes. Using an analyser apparatus like the one depicted in Figure 22, TGA measures the mass loss in a sample as a function of temperature or time under controlled heating conditions, providing insights into thermal stability, composition, and kinetic parameters [11].

Figure 22 – Example of a thermogravimetrical analyser [70]

Explained in chapter 3.1, pyrolysis is the thermal decomposition of solid material in an oxygen-free environment, producing volatile gases, non-volatile char, and ash. Estimating kinetic parameters, such as activation energy and pre-exponential factors, is essential for developing models that describe pyrolysis processes for fire safety engineering.

Estimating kinetic parameters using TGA involves

- preparing a small, homogeneous sample with a known mass,
- placing it in a TGA instrument, and
- determining the heating rate and temperature range based on material properties and analysis objectives.

Mass loss is measured as the sample is heated, resulting in a thermogravimetric curve that can be used to analyze decomposition stages, such as drying, devolatilization, and char oxidation [71].

Thermogravimetric data is subjected to mathematical models to extract kinetic parameters, such as the Flynn-Wall-Ozawa, Kissinger-Akahira-Sunose, or Coats-Redfern methods. These models involve fitting experimental data to theoretical equations to calculate activation energy, pre-exponential factor, and reaction order [72].

The estimated kinetic parameters are incorporated into pyrolysis models. The model's predictive performance is assessed by comparing its predictions with experimental results from other relevant studies or independent data sources [2]. In summary, TGA is an effective technique for estimating the kinetic parameters of pyrolysis processes and improving the accuracy of computational models used in various applications.

3.7. Cone calorimeter test

The cone calorimeter test, standardized under ISO 5660 [73] and ASTM E1354 [74], evaluates the fire performance of materials, including their response to heat exposure, ignition, and combustion properties. This test is used in academic research and industry applications to gather information about heat release rate, ignitability, mass loss, and smoke production of materials under controlled heat flux conditions. The results can be used among other to develop fire-resistant materials, fire protection systems, and fire safety design and regulations [75].

The cone calorimeter, illustrated in Figure 23, comprises a conical radiant heater, sample holder, load cell, exhaust system, and sensors and instruments for measuring parameters during the test. A square specimen with 100 x 100 mm dimensions and an appropriate thickness is placed in the sample holder beneath the conical radiant heater. The heater emits a controlled heat flux, typically 10 to 100 kW/m², onto the sample surface, simulating thermal exposure experienced in fire scenarios [76].
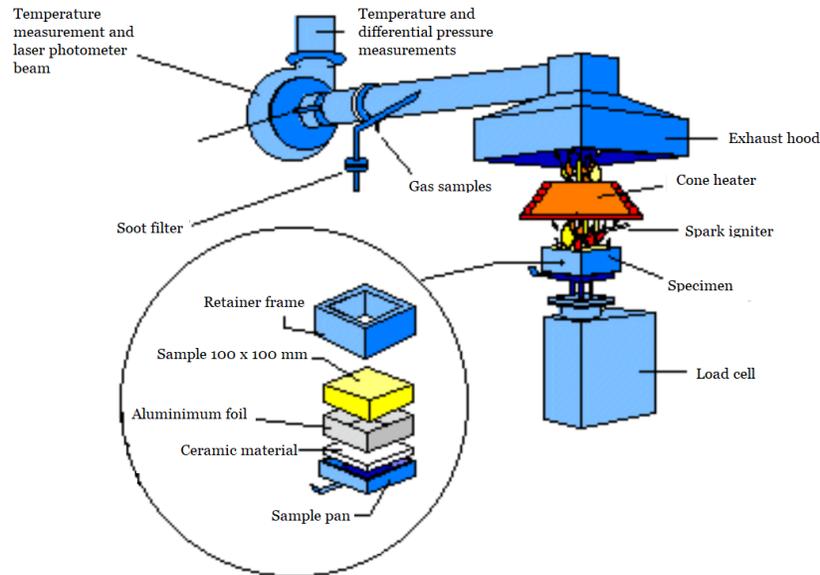
Figure 23 - Illustration of an ISO 5660 cone calorimeter, original drawing from SINTEF-report [77] is retouched with English annotations

As the material is exposed to the specified heat flux, pyrolysis, ignition, and combustion may occur. The load cell monitors the mass loss of the sample during the test, providing information on the material's decomposition and combustion rates. The exhaust system above the sample captures gases and smoke produced during the test. Sensors and instruments measure HRR, time to ignition, total heat release, effective heat of combustion, MLR, and smoke production rate, among other parameters [76].

HRR is determined by measuring oxygen consumption in exhaust gases using oxygen depletion calorimetry. This method relies on the principle that the HRR is proportional to the oxygen consumed during combustion. The HRR can be calculated by monitoring oxygen concentration in exhaust gases and comparing it to the initial concentration [75].

Analysis of cone calorimeter test results can yield an understanding of the material's fire performance, including its potential impact on fire growth and severity [75]. Additionally, the data can be used to validate and refine mathematical models predicting (such as simulated pyrolysis) [2], the fire behaviour of materials and assemblies, contributing to improvements in fire safety engineering and design [75].

4. Methodology

This chapter offers a thorough explanation of the compartment fire model created to evaluate FDS's capability to predict compartment fires with exposed timber surfaces. The methodology is divided into several sections, covering the choice of the pyrolysis model, the compartment model geometry setup, the initial crib fire, and the device configuration for data collection. Furthermore, the chapter addresses the mesh sensitivity analysis conducted to examine the impact of mesh resolution on simulation results.

The pyrolysis model and the compartment fire test, which are key to the simulation model in this thesis, are detailed in chapter 2.7 and 2.6 respectively. The full FDS script ran for this thesis is given in the Appendix.

4.1. Choosing pyrolysis model

The accurate representation of pyrolysis reactions in compartment fires with exposed timber surfaces is essential to obtain reliable results in FDS simulations. This section discusses the process of selecting a suitable pyrolysis model for simulating exposed CLT elements in the compartment model, the rationale behind the chosen model, and the uncertainties associated with its implementation.

Rinta-Paavola & Hostikka's study [2] introduces two methods for simulating pyrolysis in FDS, specifically for structural spruce and pine timber: the single reaction scheme and the parallel reaction scheme. Considering that the experiments conducted by Bartlett et al. [1] employed CLT made of spruce wood, Rinta-Paavola & Hostikka's model was deemed suitable for this study.

The single reaction scheme was selected for modelling the pyrolysis of exposed CLT elements in the compartment model due to its relative simplicity and comparable performance to the parallel reaction scheme. This scheme simplifies the pyrolysis process by defining a single wood material and generalizes values for the best fit.

The single reaction scheme posits that the reaction of the single wood material generates two byproducts: 84% char and 16% fuel gas. To account for moisture in wood, an additional component, water, is incorporated into the scheme. The moisture content is informed by R.M. Hadden et al.'s research [8], which reported a 12% moisture content for the CLT elements at the beginning of the compartment fire test. However, to maintain consistency with Rinta-Paavola & Hostikka's model and to avoid introducing discrepancies, a moisture content of 9% is used in the

large-scale model. A graphical representation of the single reaction scheme can be found in Figure 24.
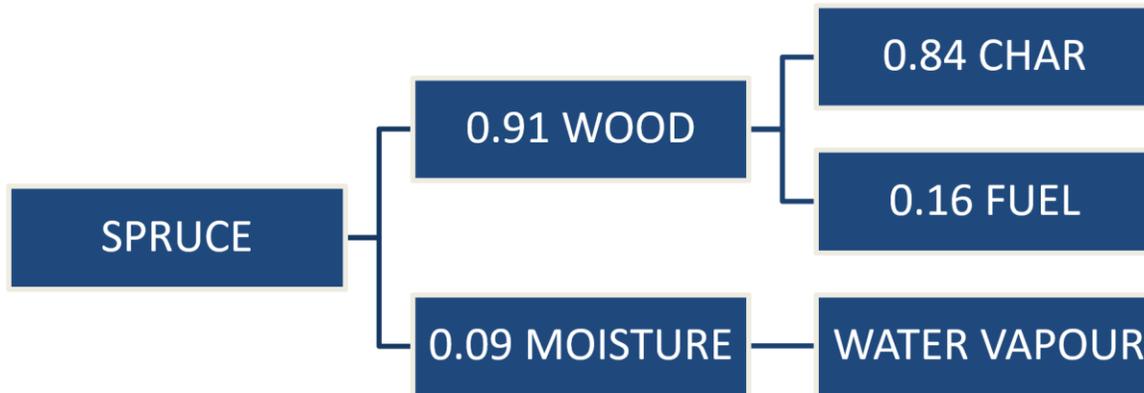
Figure 24 – Single component reaction scheme

The selection of the single reaction scheme for modelling pyrolysis introduces uncertainties related to the simplifications and assumptions made in the model. By generalizing the pyrolysis process, the single reaction scheme may not fully capture the complex reactions associated with the decomposition of wood components such as hemicellulose, cellulose, and lignin. Furthermore, the use of a 9% moisture content, as opposed to the 12% reported by R.M. Hadden et al. [8], may also contribute to uncertainties in the simulation results.

To assess the impact of these uncertainties on simulation accuracy, a parameter sensitivity analysis can be conducted, comparing various parameters such as moisture content, single- and parallel reaction schemes, and other relevant parameters. This analysis would help in determining the extent to which the simplifications made in the single reaction scheme and the variations in other parameters affect the model's predictions. However, it is important to note that such a study is not within the scope of this thesis but is relevant for future work.

In conclusion, the selection of the single reaction scheme for modelling pyrolysis in exposed CLT elements was informed by its simplicity and comparable performance to the parallel reaction scheme. However, the inherent uncertainties associated with this simplified model must be considered when interpreting the simulation results. Conducting a parameter sensitivity analysis can provide valuable insights into the impact of these uncertainties on the accuracy of the FDS simulations.

4.2. Model geometry

Initially, the model geometry was established based on the comprehensive descriptions provided by Bartlett & Hadden et al. [1] [8]. The primary goal was to ensure that the model closely resembled the actual experimental setup, thereby minimizing potential sources of error or uncertainties that could arise from the physical domain and reducing the need for assumptions.

The single-room compartment was constructed using four wall obstructions and two box obstructions, strategically positioned at the centre of the X and Y axes at the base of the domain. The internal dimensions accurately reflected the experimental measurements when the encapsulation was implemented, with dimensions of 2,72 × 2,72 × 2,77 meters (W × L × H). Additionally, an opening was situated at the bottom centre of the front wall, measuring 1,84 meters in height and 0,76 meters in width. Snippets of the compartment model can be seen in Figure 25 for illustrative purposes. The blue walls represent gypsum plasterboard, and the beige walls represent CLT.
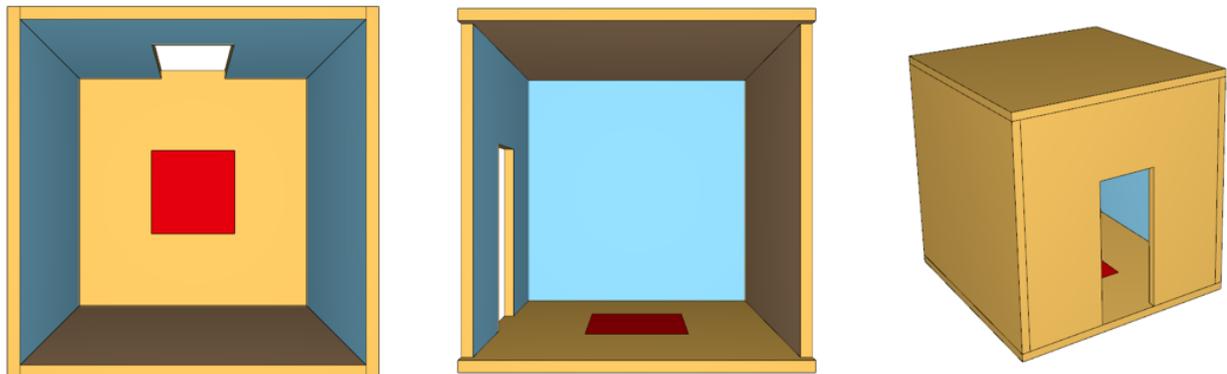
Figure 25 - Snippets of model geometry from PyroSim

Outside the opening the simulated domain is expanded 1,9 metres from the compartment front and 6,0 meters above ground level. This to capture the fire plume and the accompanying combustion reactions which occur outside the compartment and contribute to total HRR during the fire.

4.3. Thermal properties of compartment surfaces

To characterize the thermal attributes of the interior compartment surfaces, four SURF lines were defined: one for the exposed ceiling, one for the exposed rear wall, one for the flooring system, and one for enclosed surfaces. The exposed CLT SURF lines consisted of a single 100 mm layer

composed of 91% spruce and 9% moisture, using the same material parameters as those applied in the cone calorimeter test simulations. Separate SURF lines were assigned to the exposed ceiling and wall to facilitate the analysis of distinct MLR emanating from each surface and is closer described in chapter 4.4. The encapsulation SURF line consisted of a 25 mm (12,5 mm × 2) fire-rated gypsum plasterboard with a 100 mm CLT structure behind it. The floor SURF line was made up of a single 50 mm layer of stone wool insulation. The thermal properties for gypsum plasterboard and stone wool were consistent with those assumed by Bartlett et al., as detailed in Table 5 along with their respective references.

Table 5 - Thermal properties of encapsulation and insulation

Thermal properties	Plasterboard	Stone wool insulation [78]
Conductivity [W/m K]	0,24 [79]	0,039
Specific heat capacity [kJ/ (kg K)]	0,95 [80]	0,7
Density [kg/m³]	784 [79]	164

The SURF lines were subsequently assigned to their corresponding obstruction surfaces. The back wall and ceiling utilized exposed CLT, while the left, right, and front walls were given encapsulation. The floor was assigned stone wool. All other obstruction surfaces were set to the default, which is INERT.

All SURF lines were attributed BACKING='VOID'. In FDS, BACKING='VOID' means that the back side of a wall or obstruction is assumed to be in contact with an empty space (air gap) at ambient temperature. This condition affects how heat is transferred through the obstruction, as the heat will be lost to the empty space behind the obstruction [34], and allows the user to place obstructions at the mesh boundary.

4.4. Reactions

The development of an accurate reaction model is crucial for producing reliable outcomes. This section outlines the process of defining the reaction model, the rationale behind the chosen model, and the uncertainties associated with its implementation.

The studies by Bartlett et al. and Rinta-Paavola & Hostikka present differing heat of combustion values for wood, with Bartlett et al. suggesting a value of 17,5 MJ/kg and Rinta-Paavola & Hostikka proposing 13,75 MJ/kg. To account for these discrepancies and minimize unwarranted assumptions, three distinct reactions are incorporated into the model: `CRIB PYROLYZATE`, `CEILING PYROLYZATE`, and `WALL PYROLYZATE`.

The reactions produced from the wall and ceiling pyrolyzates are the same, but to examine the MLR for each surface individually, it is necessary to identify two different fuel components and, consequently, two separate reactions. `CRIB PYROLYZATE` represents the reactive species introduced into the compartment space through the `BURNER` and is assigned a heat of combustion value of 17,5 MJ/kg in alignment with Bartlett et al. Conversely, `CEILING PYROLYZATE` and `WALL PYROLYZATE` signify the reactive species generated by the `SPRUCE` material via pyrolysis, possessing a heat of combustion value of 13,75 MJ/kg as described by Rinta-Paavola & Hostikka. The `REAC` lines are given below for illustrative purpose.

```
&REAC

    ID='CRIB PYROLYZATE',

    HEAT_OF_COMBUSTION=1.75E+4,

    FUEL='CRIB PYROLYZATE',

    SPEC_ID_NU='AIR','CRIB PYROLYZATE','PRODUCTS',

    NU=-27.8760872419788,-1.0,33.0901597290989/



&REAC

    ID='WALL PYROLYZATE',

    HEAT_OF_COMBUSTION=1.375E+4,

    FUEL='WALL PYROLYZATE',

    SPEC_ID_NU='AIR','WALL PYROLYZATE','PRODUCTS',

    NU=-27.8760872419788,-1.0,33.0901597290989/
```

```
&REAC

    ID='CEILING PYROLYZATE',

    HEAT_OF_COMBUSTION=1.375E+4,

    FUEL='CEILING PYROLYZATE',

    SPEC_ID_NU='AIR','CEILING PYROLYZATE','PRODUCTS',

    NU=-27.8760872419788,-1.0,33.0901597290989/
```

To accommodate multiple reactions within a single simulation, necessitates the specification of reactions through 'complex stoichiometry.' Consequently, the oxidation process between fuel and air must be delineated. As previously noted in Section 2.7, the assumed CO and soot yields are 0.004 and 0.015, respectively. In FDS, soot is represented by the chemical formula 'C,' and the stoichiometric balance is established as follows (rounded to four decimals):

$$C_6H_{10}O_5 + 27,8761(0,2076\,O_2 + 0,0095\,H_2O + 0.0004\,CO_2 + 0.7826\,N_2)$$
$$\rightarrow 33,0902(0,1591\,H_2O + 0,1748\,CO_2 + 0,0007\,CO + 0,0061\,C + 0,6593\,N_2$$
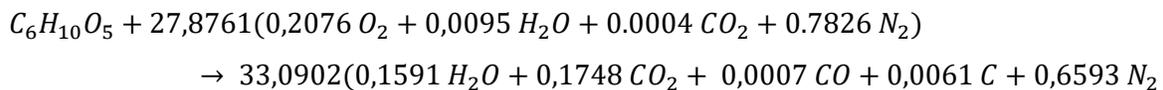
4.5. Initial fire

The experimental fire test was initiated by ignition of four wooden cribs spread evenly on the compartment floor. The four wooden cribs were represented in the large-scale simulation model by one BURNER, employed to a 1 m² VENT positioned in the centre of the compartment and specified with a mass loss curve based on the burning characteristics of the cribs provided in Bartlett & Hadden et al.'s research with maximum MLR being 0,17 kg/s.

To ensure that the simulated burner accurately represented the crib fire, a simulation was conducted using a 10 cm mesh resolution and assigning all surfaces as INERT. The focus of this analysis was solely on the HRR from the burner, rather than the contribution of other surfaces. Heat of combustion was set to 17,5 MJ/kg as assumed by Bartlett et al. As shown in Figure 26, the simulated and experimental data compare well.

The experimental curve is derived from the published study paper using WebPlotDigitizer [10] and is interpolated for a fixed time step of 10 seconds. The paper explains that the ignition and fire propagation of the wooden cribs experienced a delay, and based on the provided figures, this delay

is presumed to occur 233 seconds into the recorded time. In order to conserve computational resources, the time origin is shifted to 233 seconds.
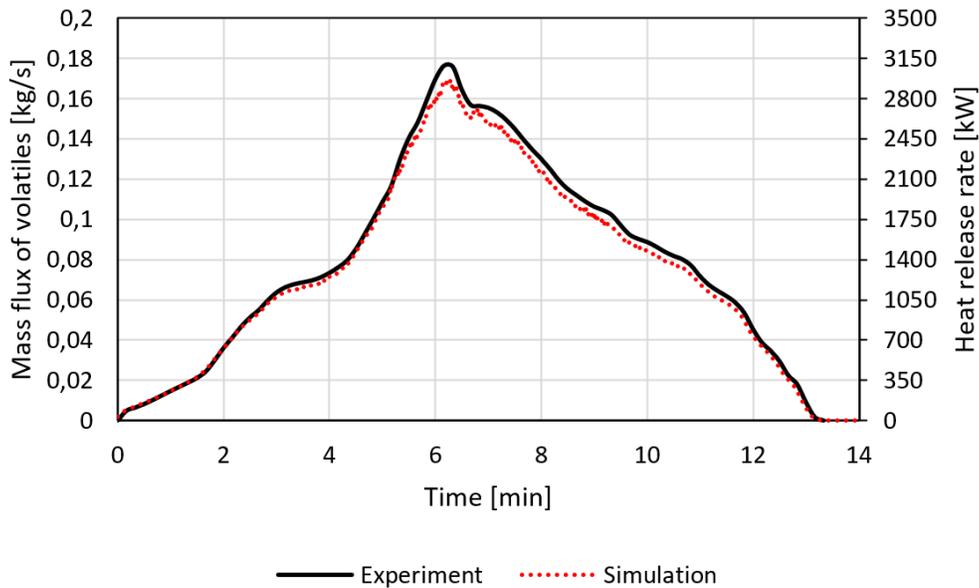
Figure 26 - Comparison between experimental and simulated crib fire data

4.6. Device configuration

To gather data from the simulations, both solid- and gas-phase devices were positioned within the domain. The primary interest was in comparing the data to the results presented by Bartlett et al. Consequently, the devices were situated as closely as possible to the experimental configurations detailed in their research. Figure 27 demonstrates the placement of devices on both walls and ceilings, as well as the gas-phase temperature devices.

The solid-phase devices, located on both exposed and encapsulated surfaces within the compartment, measured the incident heat flux to which the surface was exposed, and the temperature at the solid surface and at various depths within the solids in millimetres. The gas phase devices were spread uniformly in the room to measure the room temperature at 70, 120, 170, 220 and 270 mm above floor level. MLR of pyrolyzates emerging from each surface is automatically presented in the CHID_hrr.cvs file by FDS.
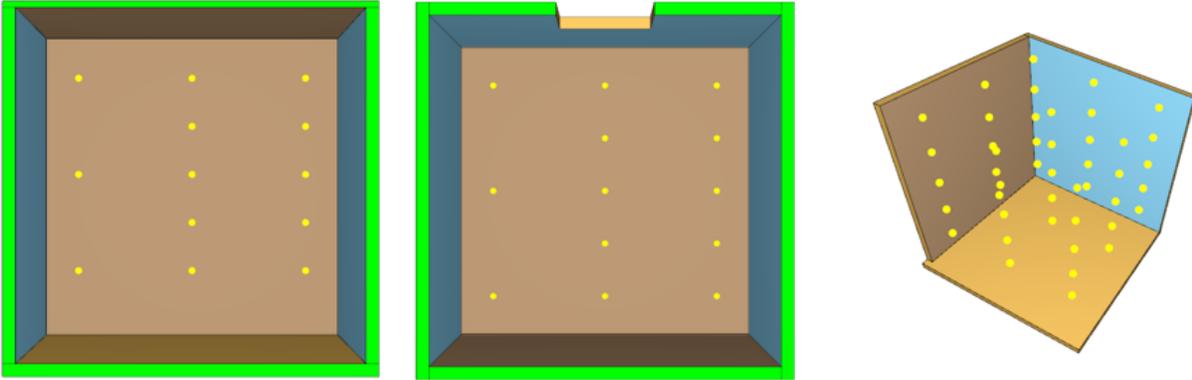
Figure 27 - Snippets of device placements from PyroSim

4.7. Mesh sensitivity analysis

The successful depiction of fire dynamics in CFD models, like FDS, hinges upon the selected grid resolution. Therefore, this research incorporated a mesh sensitivity analysis to gauge the influence of grid resolution on the output of simulations. The analysis accounted for computational efficiency, simulation accuracy, and the practical constraints of computational resources, simulation duration, and the capabilities of the FDS software.

In this study, four grid resolutions were employed: 100 mm, 80 mm, 50 mm, and 25 mm. The choice was informed by Rinta-Paavola & Hostikka's cone calorimeter tests, which yielded results comparable to experimental data at a 10 mm grid resolution. However, implementing a 10 mm resolution for the compartment model was deemed too resource-intensive and therefore, was not pursued.

Section 3.5.4 explains that the D*-approach provides an assessment of the grid resolution necessary for accurate gas phase fluid flow modelling. The mesh cell sizes employed in this study, although considered suitable for fluid flow modelling, required refinement to accurately capture the complex pyrolysis process within the CLT elements [2].

Table 6 present the four simulations. The table also includes $D^*/\delta x$ values with HRR $\dot{Q} = 6000\,\text{kW}$ (based on HRR reported by Bartlett et al.), ambient air density $\rho_\infty = 1{,}204$ kg/m³, specific heat capacity for air $\rho_\infty = 1{,}005$ kJ/(kg K), ambient temperature $T_\infty = 293$ K and gravitational force $g = 9{,}81$ m/s². $D^*/\delta x$ values are considerably high and sufficient to capture both the initial stages of the fire and the peak HRR emanating from the fire plume through the compartment opening.

Table 6 – Mesh resolutions for mesh sensitivity analysis

Cell size, δx [m]	$D^*/δx$	Number of cells
0,10	19,63	86 400
0,08	24,55	171 000
0,05	39,27	691 200
0,025	78,55	3 859 200

The mesh sensitivity analysis involved running simulations at each grid resolution, maintaining consistent boundary conditions and material properties, to discern the impact of grid size on predicted fire dynamics. Temperature and HRR were the parameters chosen for comparison across the simulations, with higher convergence levels indicating reduced sensitivity to grid resolution.

Despite the potential for inherent uncertainties in the simulation results due to limitations imposed by time consumption due to the workings of the FDS software, the mesh sensitivity analysis provides valuable insights into the effect of grid resolution on simulation accuracy. It highlights the necessary detail level for accurate predictions when applying the predictive pyrolysis model in large-scale simulations. It also underscores the importance of balancing computational efficiency with accuracy in FDS simulations.

5. Results

This chapter showcases the outcomes of the simulations carried out for this thesis. Initially, the results from the mesh sensitivity analysis are introduced. Following that, the simulation which is deemed most appropriate to compare to the compartment fire experimental data is explored in-depth, providing detailed findings.

5.1. Mesh sensitivity analysis

Four simulations were conducted with varying grid resolutions of δx = 0,1 m, 0,08 mm, 0,05 m, and 0,025 m, while keeping all other parameters constant. The resulting temperature and HRR development for each simulation is here presented, and a consequent discussion follows.

It should also be noted that the models with grid resolutions of δx = 0,1 m, 0,08 mm, 0,05 m were run for 2400 seconds each. However, due to computational constraints, the model with a grid resolution of δx = 0,025 m was only run for 900 seconds.

5.1.1. Gas phase temperature

The development of temperature in the compartment are analysed and compared for the grid resolutions. Temperatures were measured at several points throughout the compartment. Figure 28 presents the temperature at 220 cm above floor level averaged from nine measurement points evenly spread out. The measurements show a rapid increase in temperature that reaches around 550 °C after about 210 seconds (3,5 minutes) for all simulations, before a slower temperature increase develops. This increase follows until the 750-seconds (12,5 minutes) mark when the temperature starts to decrease. During these 540 seconds the average temperature for the different grid resolutions spans between 745 °C and 830 °C. The average and peak temperature for this time frame is listed in Table 7. The average difference in percentage between the grid resolutions are listed in

Table 8.

Surprisingly, the most significant differences were observed between the grid resolutions δx = 0,025 and δx = 0,05, showing a 10.79% variation in average temperature and a 10.64% difference in peak temperature. On the other hand, the smallest temperature differences were found between δx = 0,1 and δx = 0,025, with a difference of 2.38% in average temperature and a 5.87% difference

in peak temperature. The finest grid resolution (δx = 0,025) resulted in the lowest average and peak temperatures. While the reason for these outcomes is not entirely clear, the overall findings suggest that the chosen grid resolutions do not significantly affect the compartment temperatures. As such, a grid resolution of δx = 0,1 m is considered sufficient for predicting gas-phase temperatures within the fire compartment.
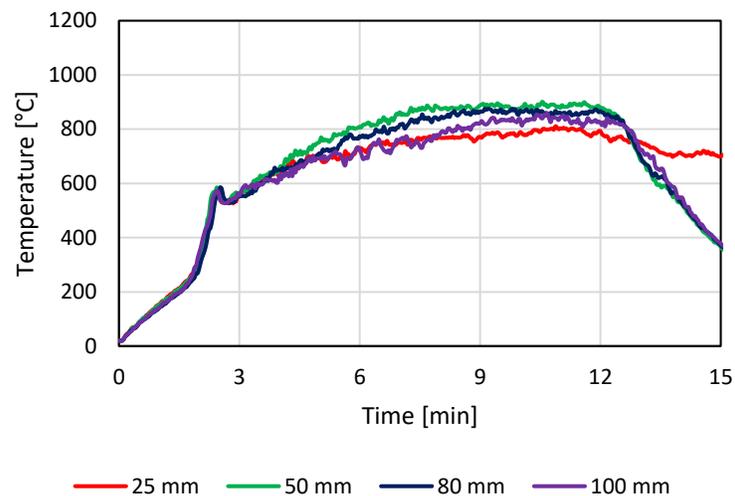
Figure 28 - Gas phase temperature at 220 cm above floor for grid resolutions 25, 50, 80 and 100 mm

Table 7 – Mesh sensitivity analysis. Average and peak temperature in the timeframe between 210 and 750 seconds

Compartment temp. 220 cm above floor	Average and peak temperature for each grid resolution [°C]			
	δx = 0,1 m	δx = 0,08 m	δx = 0,05 m	δx = 0,025 m
Average temp.	763	803	830	745
Peak temp.	859	875	901	810

Table 8 – Mesh sensitivity analysis. Grid resolution comparison

Compartment temp. 220 cm above floor	Average temperature difference between grid resolutions [%]					
	0,1 vs 0,08	0,1 vs 0,05	0,1 vs 0,025	0,08 vs 0,5	0,08 vs 0,025	0,05 vs 0,025
Average temp.	5,10	8,41	2,38	3,31	7,49	10,79
Peak temp.	1,84	4,77	5,87	2,93	7,72	10,64

5.1.2. Heat release rate

The progression of total HRR throughout the simulations are also analysed and compared for each grid resolutions. FDS captured the HRR of all combustion reactions occurring within the computational domain meaning both inside and outside the compartment. However, it is worth noting that observed from visual output data when the fire plume extended the farthest from the compartment opening, a fraction of the combustion reactions escaped beyond the simulated domain and thus were not included in the results - a trend observed across all grid resolutions.

In a typical mesh sensitivity analysis, the "steady-state" HRR would be the primary point of comparison. However, given that the chosen fire scenario does not achieve a steady-state HRR, the focus is instead shifted towards peak HRR.

Figure 29 present total HRR for each grid resolution. HRR values initially present a consistent growth until around the 75-second mark, at which point a more significant increase becomes apparent. This accelerated growth persists until the 360-second mark (6 minutes), marking the attainment of peak HRR. Following this peak, all grid resolutions display a rapid decrease in HRR, except for grid resolution $\delta x = 0,025$.

Grid resolution $\delta x = 0,025$ demonstrates a significantly higher peak HRR compared to the other grid resolutions. Moreover, it maintains this heightened HRR for a more extended period before experiencing a considerable decline, after which it stabilizes once again for a brief time.

Peak HRR for all grid resolutions are listed in Table 9. The difference in percentage between each simulation is listed in Table 10. The peak HRR discrepancy between the coarsest grid resolutions ($\delta x = 0,1$ and $\delta x = 0,08$) is a mere 1,53%. It can also be seen that HRR for these two grid resolutions converge well throughout the entire course of fire. However, a significant change is observed when comparing $\delta x = 0,05$ resolution with both $\delta x = 0,08$ and $\delta x = 0,1$. The difference in peak HRR escalates to 7,9% and 9,43%, respectively. Such a substantial deviation suggests that the transition to a finer grid resolution may significantly alter the fire environment.

This observation is further amplified when the finest grid resolution ($\delta x = 0,025$) is compared with $\delta x = 0,1$, $\delta x = 0,08$ and $\delta x = 0,05$. The percentage variation in peak HRR among these resolutions' surges to 25,69 %, 24,18 %, and 16,36 % respectively, further underscoring the impact of grid resolution on the fire model's output.
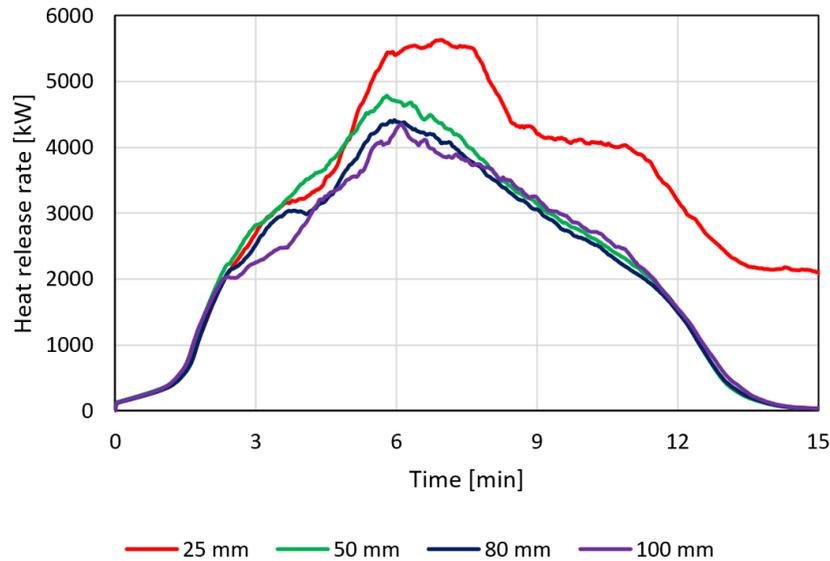
Figure 29 – Mesh sensitivity analysis. Total heat release rate for grid resolutions 25, 50, 80 and 100 mm

Table 9 – Mesh sensitivity analysis. Peak HRR for each grid resolution

Total HRR captured by	Peak HRR for each grid resolution [kW]			
	$\delta x = 0,1$ m	$\delta x = 0,08$ m	$\delta x = 0,05$ m	$\delta x = 0,025$ m
Moving average	4 346	4 413	4 776	5 627
Measured	5 086	4 801	5 305	6 030

Table 10 – Mesh sensitivity analysis. Grid resolution comparison

Total HRR captured by	Peak HRR difference between grid resolutions [%]					
	0,1 vs 0,8	0,1 vs 0,05	0,1 vs 0,025	0,8 vs 0,5	0,08 vs 0,025	0,05 vs 0,025
Moving average	1,53	9,43	25,69	7,90	24,18	16,36
Measured	5,77	4,22	16,98	9,97	22,69	12,79

A reasoning for this discrepancy in HRR may be found if looking at the mass flux of combustible pyrolyzates emerging from the exposed timber wall and ceiling. Figure 30 present the mass flow of pyrolyzates emerging from the ceiling (left) and wall (right) due to the kinetic parameters added to the `MATL` line for spruce. Grid resolution $\delta x = 0,025$ has an obvious greater mass flux of combustible species added to the simulated domain which will increase the amount of heat

67

released when combusted. The MLR for grid resolution δx = 0,05 were also slightly greater than both δx = 0,1 and δx = 0,08 and may explain the noticeable percentage difference in HRR.
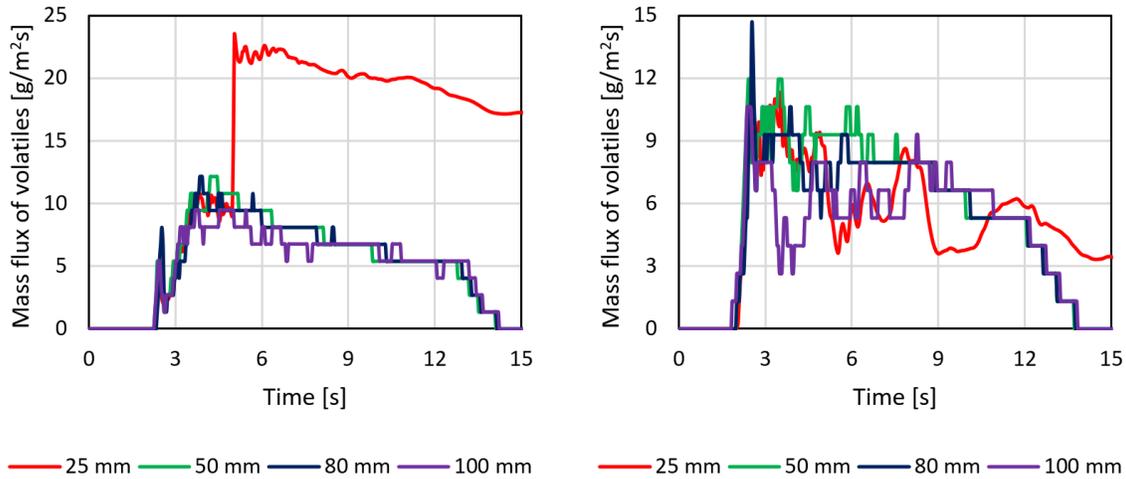
Figure 30 - Mesh sensitivity analysis. Mass flux of pyrolyzates from exposed timber ceiling (left) and wall (right) for grid resolutions 25, 50, 80 and 100 mm

The evaluation of HRR for each grid resolution introduces contrasting perspectives compared to the conclusions derived at for the analysis of gas temperatures. The gas temperature results for each resolution suggest that a point of convergence is attainable at δx = 0,1. However, the analysis of HRR suggests that the three coarser grid resolutions neglect critical aspects of the fire in relation to the pyrolysis modelling. This analysis further reveals that the selection of nominal grid cell sizes chosen for the mesh sensitivity study were not sufficiently small to determine a definitive convergence point. This is due to the uncertainty regarding whether grid cells smaller than δx = 0,025 would generate substantially different outputs or if grid cell sizes between δx = 0,05 and δx = 0,025 would converge to the same outputs as δx = 0,025 resolution.

The distinct HRR behaviour associated with δx = 0,025 resolution implies that coarser grid resolutions may not fully capture all essential aspects of the fire dynamics. This mesh sensitivity analysis emphasizes the importance of grid resolution in accurately modelling a fire scenario, specifically in the context of pyrolysis modelling. The results indicate that smaller grid cell sizes contribute to higher MLR of pyrolyzates from the exposed CLT elements, subsequently leading to a higher, more sustained HRR, a phenomenon not captured at coarser resolutions. These observations strongly suggest that the grid cell sizes selected for this study were perhaps too large, complicating the search for a resolution at which point results begin to converge.

Considering these findings, it is recommended for future mesh sensitivity analyses, particularly when using predictive pyrolysis, to consider implementing finer grid resolutions than $\delta x = 0,025$ to identify the point of convergence. The results suggest that a grid cell size smaller than $\delta x = 0,05$ is necessary to adequately capture the pyrolysis phenomena in the CLT. While these finer resolutions may require more time, they have the potential to provide a more detailed and accurate portrayal of the fire scenario and is necessary in determining the convergence point.

As previously stated, the selection of grid size was primarily informed by the time constraints inherent in this study. Consequently, further mesh sensitivity analysis using finer grid sizes was not undertaken. Nevertheless, the simulation outcomes derived from the $\delta x = 0,025$ grid resolution seem promising, as it appears to alter the fire dynamics with higher and longer HRR as is observed in real world fires when exposed timber surfaces are participating into a compartment fire setting.

In summary, despite the inability of the mesh sensitivity analysis to identify a grid resolution where results converge, it underscored the crucial impact of grid resolution on simulation outcomes. This is especially true when utilizing the predictive pyrolysis model. Considering this thesis's emphasis on capturing intricate details in modelling compartment fires involving exposed timber surfaces, it was decided to proceed with the analysis using the simulation results obtained from the $\delta x = 0,025$ resolution. This resolution was selected due to its unique ability to somewhat capture the exposed timber surfaces considerably influence on the development of the fire scenario.

5.2. Final model results

Based on the mesh sensitivity analysis, the simulation with nominal grid cell size of $\delta x = 0,025$ was chosen as the model to be further analysed for its performance to predict fire dynamics in compartment fires with exposed timber surfaces. The following subchapters present a brief overview of the simulation process, the simulated results for total HRR, gas-phase compartment temperatures, temperature profiles within the exposed timber surfaces, incident radiative heat flux, and finally the mass flux of volatiles that were introduced into the compartment due to heating of the CLT elements.

5.2.1. Details of simulation

The models for this thesis were simulated using FDS version 6.7.9. The final simulation run, with a grid resolution of δx = 0,025 m, had a total of 3 859 200 grid cells, divided into 18 different meshes (MPI processes), and utilized 4 OpenMP Threads. Due to time constraints, the simulation was terminated upon reaching the 15-minute mark (900 seconds), at which point it had been running for more than 700 hours (over 29 days).

A significant amount of computation time was consumed by inter-mesh communication. Therefore, it can be speculated that fewer meshes might have helped reduce this computational burden. Additionally, coarser meshes could have been employed in regions where pyrolysis was not occurring, such as outside the compartment. This could potentially have saved some computation time. Nonetheless, an accurate representation of pyrolysis in the CLT required a grid resolution with high detail. Combined with the use of the `CELL_SIZE_FACTOR=0.8` (see chapter 2.7.2), and the broad CLT compartment surfaces, a considerable number of grid cells was required. This led to these simulations being highly demanding in terms of computation.

Figure 31 on the next page presents visualizations of the temperature data obtained from the compartment's middle at each 100-second interval. This serves to depict the fire's progression during the 15-minute simulation. The crib fire, which initially introduces fuel into the compartment, begins at the 0-second mark and increases its fuel injection rate. After the 6-minute (360 seconds) mark, the crib fire's rate decreases and by 790 seconds, it stops adding fuel. This cessation is noticeable in the 800 and 900-second visualization frames, where there is a significant drop in temperature compared to previous frames.
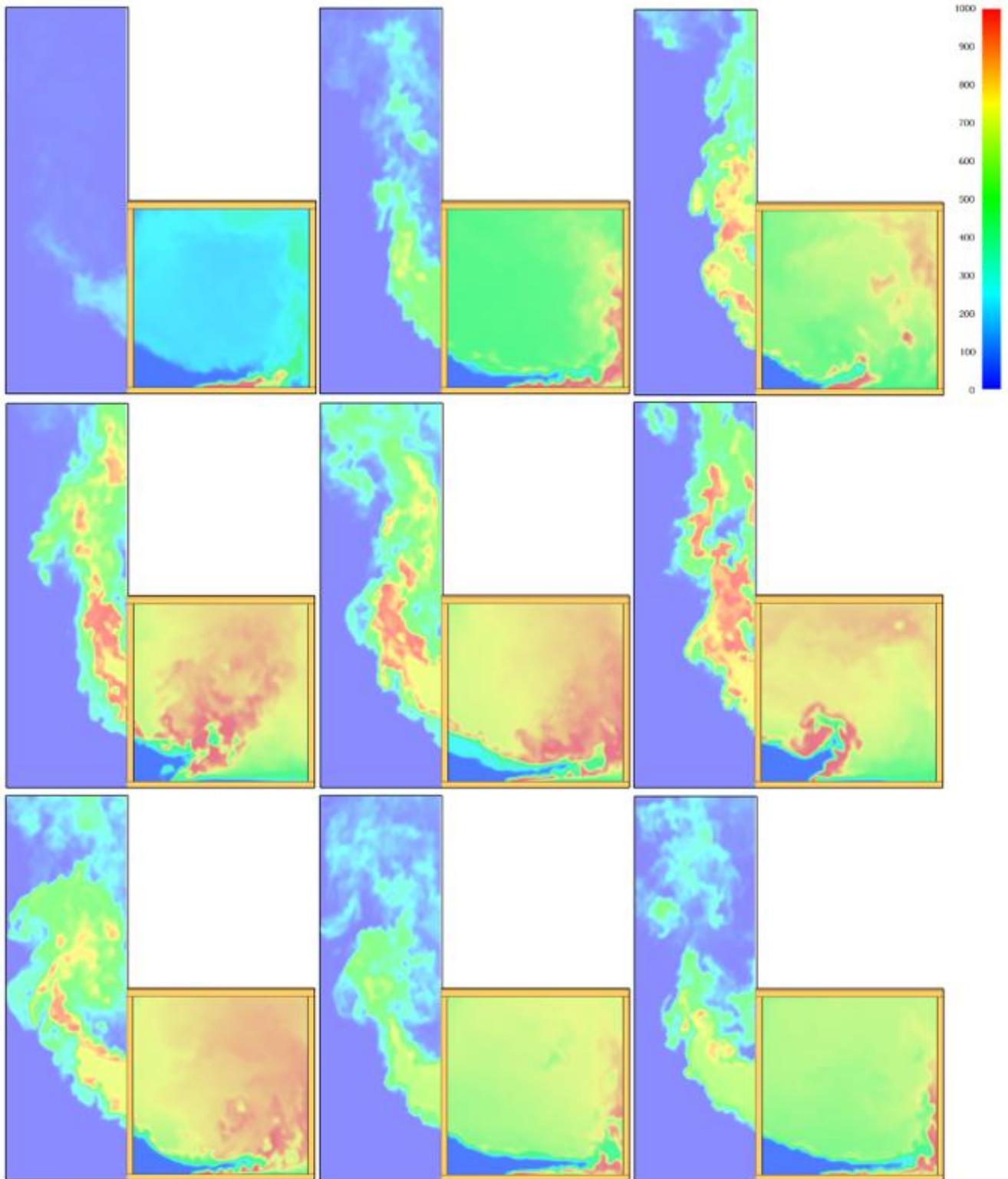
Figure 31 - Temperature slices in the compartment's middle are presented every 100 seconds, from 100s (top left) to 900s (bottom right)

5.2.2. Heat release rate

Figure 32 present the moving average of total HRR throughout the simulation, meaning both combustion inside the compartment and outside. From simulation start, the HRR shows an upward trend as the initial crib fire introduces volatiles into the compartment. The HRR ascends in accordance with the predefined release of volatiles, exhibiting an average increase of 5,7 kW/s until the 75-second mark. This point marks the onset of a more rapid growth phase, with the HRR accelerating at an average rate of 20 kW/s, escalating from 430 kW to 3000 kW within 125 seconds. The HRR continues to intensify until the 360-second mark (6 minutes), at which point it attains a brief stable peak.
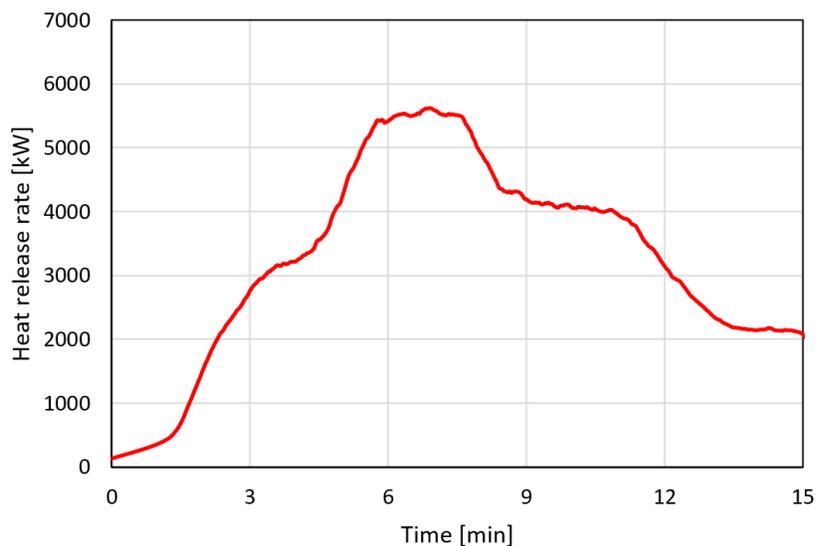
Figure 32 - Comparison between simulated and experimental total heat release rate

This transient stable peak averages at 5420 kW, lasting for about 100 seconds with the maximum recorded value hitting 6030 kW. The peak HRR coincides with the initial crib fire reaching its estimated maximum heat release rate of 3000 kW. During this phase, the pyrolyzates emanating from the timber surfaces contribute an additional 3000 kW to the HRR. This implies that up to 50% of the HRR can be attributed to the supplementary fuel sourced from CLT. This is illustrated in Figure 33 where the total HRR from the simulation is compared to the estimated HRR contributed by the crib fire.
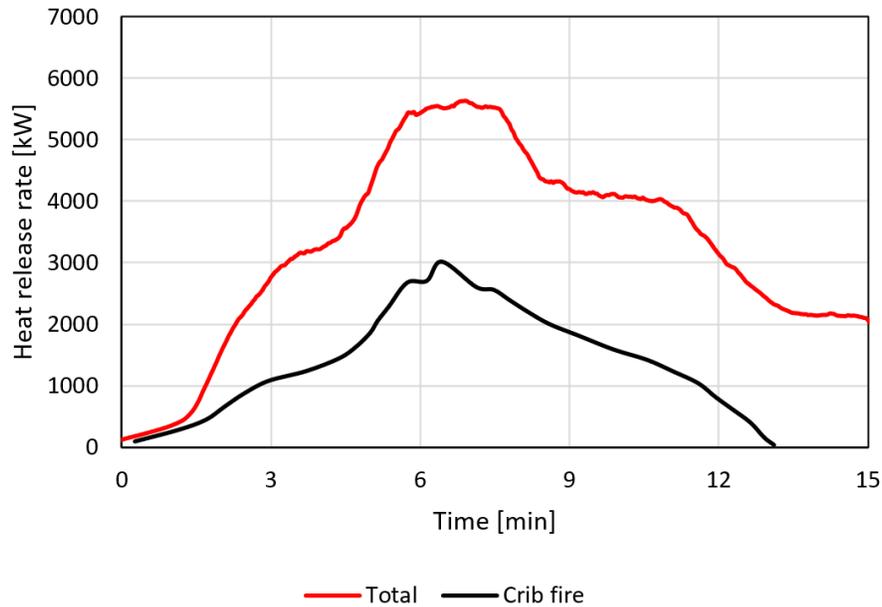
Figure 33 - Comparison between total HRR and estimated HRR from the crib fire

At the 460-second mark (7,6 minutes) of the simulation, there is a noticeable decline from the peak HRR plateau. The rate of this decrease mirrors the earlier rate of increase leading up to the peak. However, following 540 seconds (9 minutes) into the simulated fire, there is another brief period where the HRR appears to stabilize, maintaining an average HRR of around 4130 kW before it drops again to a plateau of 2100 kW. This lower plateau persists until the end of the simulation and indicate that the surfaces continue to even after the crib fire was extinguished.

5.2.3. Gas-phase temperature

Figure 34 presents the average gas phase temperature inside the compartment, 220 cm above floor level derived from nine points of measurements spread evenly in the plane. Described in chapter 3.3, flashover can be said to occur when the smoke layer reach 600 °C [60]. In the simulation, this temperature is attained at around 200 seconds (3,33 minutes) into the fire. The temperature then stabilizes to a slow growth to the 730-seconds mark (12,17 minutes) and the average temperature during this period is 745 °C. Peak temperatures are also reached in this period with 870 °C at around 680 seconds (11,33 minutes). The temperature decrease begins shortly after the peak temperatures have been reached with a slowly decreasing rate. The simulation is ended at 15 minutes where the temperature has dropped from the peak to 705 °C.

73
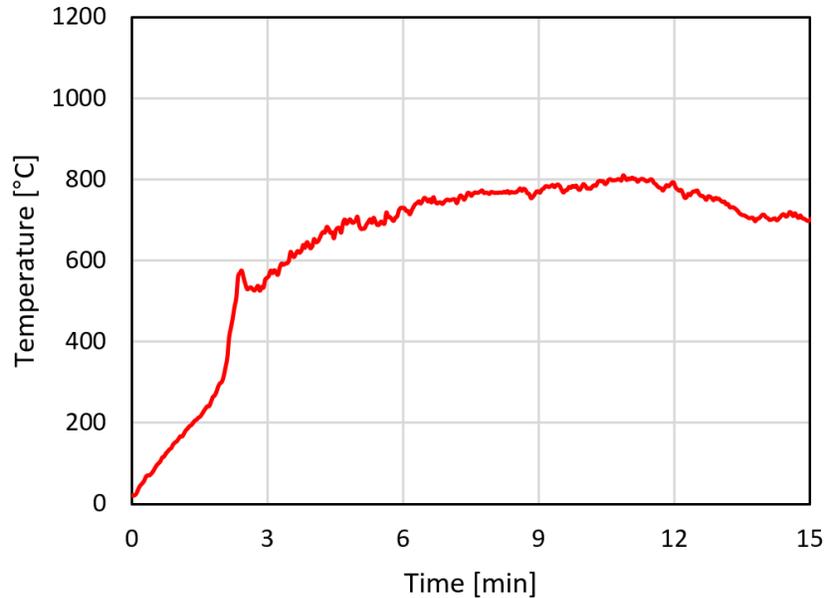
Figure 34 - Average gas temperature 220 cm above floor level from nine points of temperature measurements

5.2.4. Solid-phase temperature

Figure 35 presents the average temperatures at different depths for wall (left) and ceiling (right). The measured surface temperature for both exposed surfaces show a rapid increase in accordance with the heating of the compartment. The onset of temperature rise 9 mm into the elements are noticeably slower and first show an increase 4 minutes into the fire. Temperature measurements at 20 mm have a much slower increase and can be seen nearing 200 °C by the 15-minute mark. The 40 mm depth measurement for the wall and the 30 mm depth measurement for the ceiling has negligible rise in temperature and measurements deeper into the elements are therefore not included in the figures.

The wall surface reaches an average maximum of 823 °C around the 12-minute mark, while the ceiling surface reaches 773 °C at about the 11-minute mark. Both surface temperatures can be seen decreasing slowly after this peak. The peak average temperatures for the wall and ceiling at 9 mm depth occurs around the same time with temperatures of 526 °C and 489 °C, respectively.

The simulation results culminate with the termination of the simulation. The observable decrease towards the end is anticipated to persist in line with the diminishing HRR.
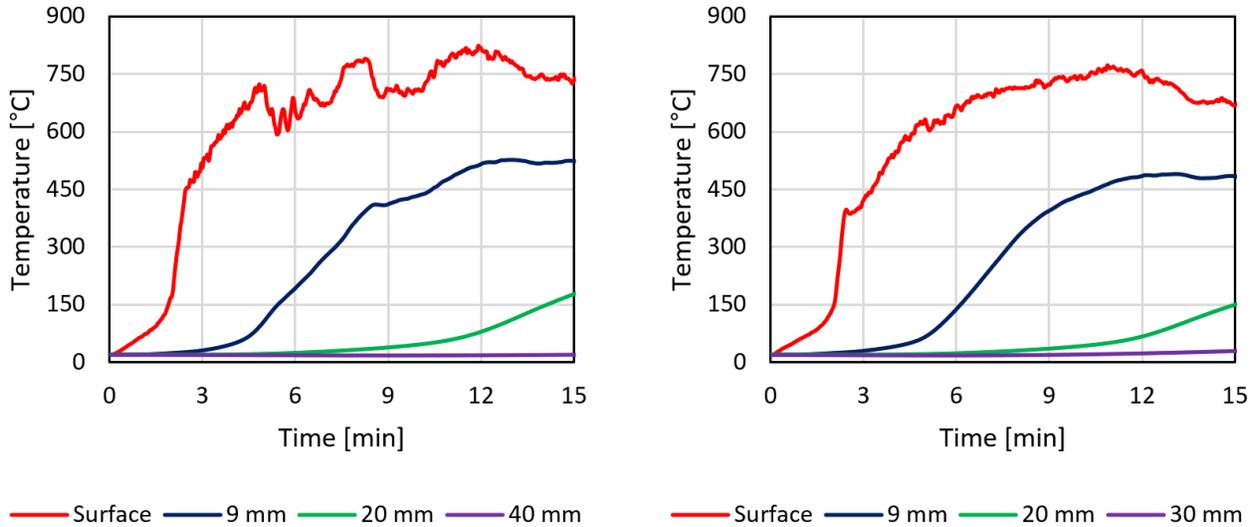
Figure 35 – Average of temperature profile for wall (left) and ceiling (right) at various depths

5.2.5. Incident radiative heat flux

Figure 36 present the average incident radiative heat flux which the exposed timber wall and ceiling receives. Both surfaces experience a similar increase in received heat flux, starting slow just before the 2-minute point and then increasing quickly to 40 and 30 kW/m² at the wall and ceiling respectively. After this, both rates of increase are the same, but the wall has higher values than the ceiling. By the 5-minute mark, the wall and ceiling have reached an average incident heat flux of 74 and 52 kW/m² respectively.
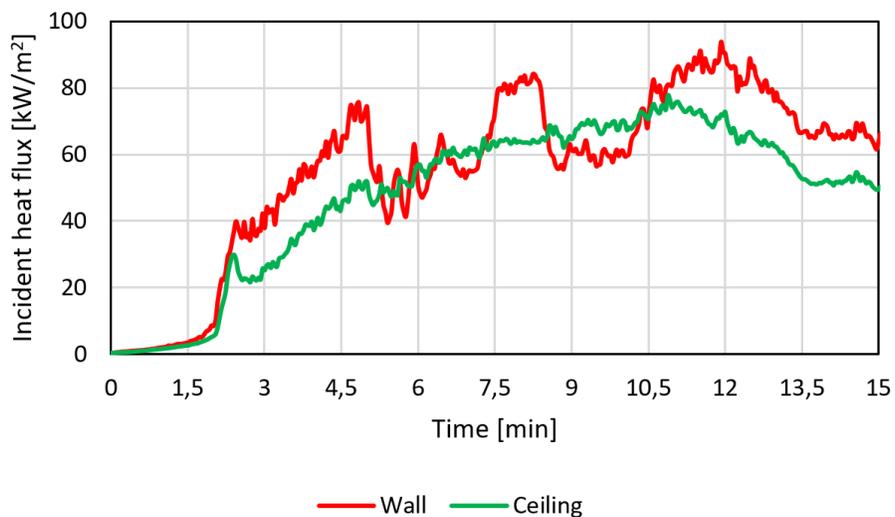
Figure 36 – Average incident heat flux received by the exposed timber wall and ceiling

At this point, a notable change occurs when the heat flux received by the wall suddenly drops to 39,50 kW/m², then starts to increase again with some fluctuations. This sudden drop in heat isn't seen in the heat flux absorbed by the ceiling. The reason for this difference may be the continuous smoke layer that covers the ceiling, while the wall first feels a strong heat impact from the initial crib fire. As the smoke layer moves lower inside the compartment, some of this heat is absorbed and held within the smoke layer, which lessens the direct heat affecting the wall.

5.2.6. Mass flux of volatiles

Figure 37 presents the mass flux of flammable pyrolyzates emerging into the compartment through the exposed timber wall and ceiling due to the predictive pyrolysis model. The release of pyrolyzates starts from the wall surface, which shows a quick increase in mass flux starting at the two-minute mark. In contrast, the release from the ceiling begins 15 seconds later and demonstrates a slower rate of increase.

Soon after the initial release, the peak mass flux from the wall is attained 146 seconds (2,43 minutes) into the fire, registering at 11,79 g/(m²s). Following this peak, the mass flux oscillates between 7,36 g/(m²s) and 11,32 g/(m²s) up until the five-minute mark. After this point, there is a significant reduction from 8,75 g/(m²s) to 3,62 g/(m²s) within a span of 30 seconds. From here the mass flux oscillates with an average increase leading up a local maximum 465 seconds in at 8,42 g/(m²s) before yet again dropping to a mass flux of 3,6 g/(m²s). At 15 minutes when the simulation ends the mass flux is at its lowest from start at 3,35 g/(m²s).

The mass flux of volatiles originating from the ceiling initially escalates at a more gradual pace in comparison to the wall mass flux. From initial release to 210 seconds (3,5 minutes) mass flux increase to 11,32 g/(m²s). Here the flux stabilizes for a brief period of 90 seconds before a drastic jump to 23,51 g/(m²s) which is the peak mass flux emerging from the ceiling. From here on, the mass flux lays quite stable, but with a slow decreasing average. At 15 minutes the mass flux has decreased to a value of no less than 17,20 g/(m²s).
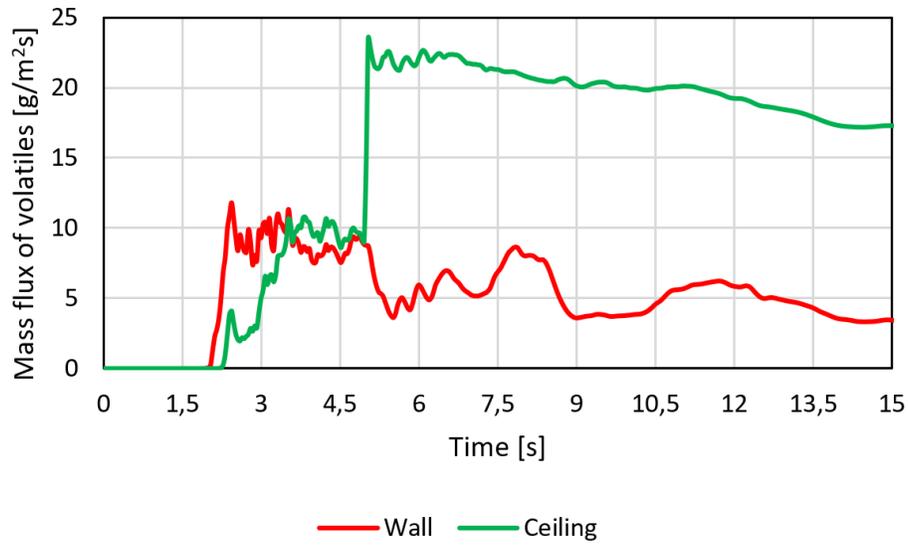
Figure 37 - Mass flux of combustible pyrolyzates emerging from the exposed wall and ceiling

6. Discussion

The purpose of this chapter is to discuss the findings presented in chapter 5 derived from the FDS simulation of a single-room compartment fire with exposed spruce CLT surfaces. The simulated output is compared to the experimental data to assess the simulations level of accuracy. Additionally, the chapter includes broadcasting any possible limitations within the model and proposing enhancements that could benefit future research undertakings.

The research questions guiding this analysis are as follows:

1. What is the model's level of accuracy to experimental data?
2. What are limitations of the model?
3. How can future models be improved for better results?

6.1. Heat Release Rate Analysis

Figure 38 offers a comparison between the total heat release rate as predicted by the simulation model and that derived from experimental data. To mitigate the effects of curve fluctuation, the simulated HRR is demonstrated as a moving average. Following necessary adjustments to account for the delayed ignition seen in the experimental setup (233 seconds delay), both the experimental and simulated HRRs commence their upward trajectory from the zero-second point. Like the simulated HRR, the experimental values initially exhibit a steady rate of increase, before an ensuing acceleration towards the peak HRR. This escalation transpires at 1,5 minutes in the simulation, 2,5 minutes sooner than the experimental data, which shows a swift incline beginning at the 4-minute mark. Thus, the model can be considered conservative in predicting the ignition timing of combustible surfaces contributing to the additional HRR.

The peak HRR, in terms of both its timing and magnitude within the simulation, corresponds closely to the experimental data. The experimental peak occurs at 315 seconds (5,25 minutes) with a value of 6000 kW, while the simulated peak happens at 427 seconds (7,12 minutes) with a value of 6030 kW.

Following the attainment of peak HRR, the experimental HRR begins a gradual decrease over the course of 405 seconds (6,75 minutes), resulting in a reduction of approximately 4500 kW. This decline accelerates shortly thereafter, marking the onset of the compartment fire's extinguishment. Conversely, the simulated HRR commences its descent almost immediately after peaking, at a rate nearly akin to its prior increase. This decrease is temporarily halted when the

HRR starts to plateau and stabilize around 4000 kW. This plateau persists for 150 seconds (2,5 minutes) before another downturn is observed, this time mirroring the pace of the experimental HRR's decline more closely.

Like the experiment, the simulation also portrays an ongoing fire after the crib fire 13 minutes after start. This indicate that the heat from the burning surface themselves is sufficient to sustain the pyrolysis processes for some time and a slower decrease in HRR is therefore observed.
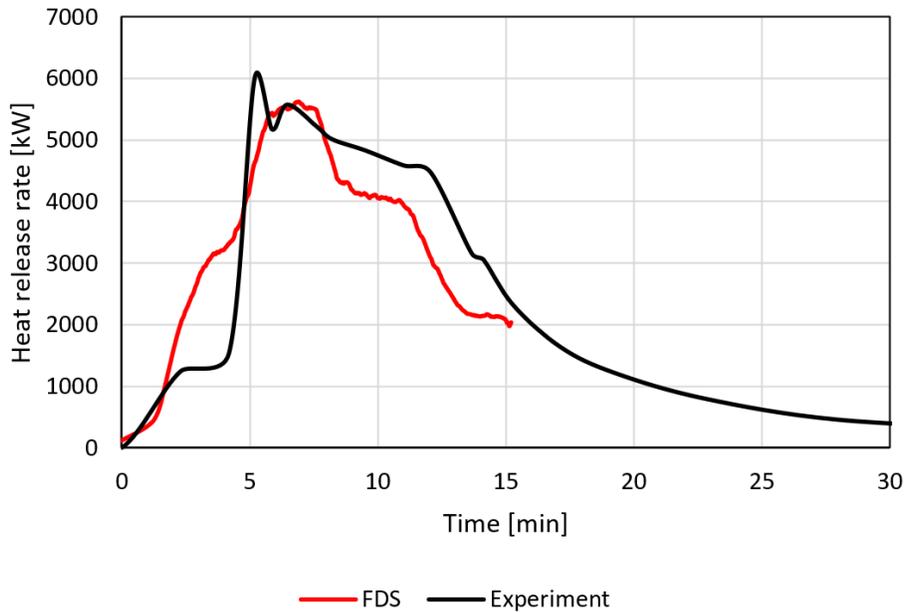
Figure 38 – Comparison between simulated and experimental total heat release rate

In evaluating the simulation's performance in comparison to the experimental data, several factors might be responsible for the observed divergences.

The model's premature prediction of ignition time might be influenced by multiple elements. The model parameters proposed by Rinta-Paavola & Hostikka may be overly reactive to the initial conditions, leading to a quicker response to the heat input. The moisture content used in the simulation may also have contributed to this early onset of fire for the burning surfaces. The experiment reported a moisture content of 12 % in the CLT elements, while the moisture content of the modelled spruce was set at 9 %. Along with other variations between simulated and experimental material properties like kinetic parameters, density, and specific heat, can have a significant impact on ignition timing. These factors may not have been completely or accurately replicated in the simulation, causing a disparity between the model and the experimental conditions.

The discrepancy observed between the simulated and experimental HRR post-peak could stem from the intricate dynamics of fire behavior and the intrinsic limitations of the simulation model, especially concerning the representation of the fire plume within the simulation domain. Notably, during the peak of the simulated fire, a portion of the fire plume was seen breaching the boundary of the simulated domain. This suggests that a taller domain might have allowed for additional combustion at these higher levels, which was not captured by the current model, thus contributing to an underestimation of the HRR.

Another contributory factor might be the lack of a model accounting for smouldering combustion in the char residue after spruce pyrolysis. In experimental conditions, the char layer left after spruce pyrolysis continues to smoulder, which adds to the total heat release and extends the HRR. The simulation, lacking this aspect, shows a swift drop in HRR post-primary combustion, leading to a significant underestimation of total HRR. Enhancing simulation accuracy could involve incorporating a separate model simulating the smouldering combustion process of the char layer. This would capture the extra heat released during this phase, providing a more comprehensive representation of the fire's evolution, and aligning the simulated HRR more closely with the experimental data.

Unfortunately, the mesh sensitivity in chapter 5.1 failed to identify a grid size of convergence and therefore it is not known if the grid cell size is affecting the total HRR. Rinta-Paavola & Hostikka used a grid cell size of 10 mm to accurately represent the pyrolysis within the CLT. If the simulation fails to accurately depict the amount of pyrolysis gases produced, the HRR might be underdetermined.

It should also be noted that another root for the discrepancy might be the choice of heat of combustion for the pyrolyzate gases emerging from the CLT elements. In accordance with Rinta-Paavola & Hostikka's model [2] the heat of combustion for the spruce pyrolyzates were 13,75 MJ/kg while Bartlett et al. assumed 17,5 MJ/kg. The experimental HRR data shown in Figure 38 is from calorimetry and should be accurate. The simulated peak HRR did also match the experimental data, if a higher heat of combustion had been chosen in the simulation model, the HRR might have been overestimated and is therefore not a certain reason for the discrepancy.

The discrepancies underscore the need for continual refinement of the model's parameters and assumptions. To summarize, possible reasons for discrepancies are (but not limited to):

- Choice of material properties including moisture content
- Choice of pyrolysis model

- Lack of a smouldering combustion model
- Volatiles leaving the simulation domain before combusted
- Choice of heat of combustion
- A too coarse grid resolution to capture the pyrolysis within the CLT elements

However, it is important to note that despite these discrepancies, the model demonstrates a promising correlation with the experimental data in terms of the progression of HRR. This observation is encouraging, suggesting that FDS possesses potential in accurately replicating HRR for such fires, provided the input parameters are carefully considered and calibrated.

6.2. Gas-Phase Temperature Analysis

Figure 39 presents a comparison between simulated and experimental data of the average gas-phase temperature inside the compartment at 220 cm above floor level. The simulated model yields peak temperatures of 810 °C, whereas the experimental data show a higher peak temperature of 1145 °C. This outcome suggests that the simulations underestimate the peak temperature by a significant margin of 335 °C. Compared to Šálek et al.'s [25] models which closest simulated temperature to experimental results was 300 °C, this thesis' model is 10,45 % less accurate in predicting gas-phase temperature. However, Šálek et al.'s model overestimates the gas-phase temperature while this model underestimate. Interestingly, the $\delta x = 0{,}025$ m simulation, despite generating the highest heat release rate among the simulations with different grid cell sizes, results in the lowest peak temperatures.

Flashover, as discussed in Section 3.3, is typically signified when the smoke layer attains a temperature of 600 °C [60]. In the simulation, this specific temperature is reached approximately 200 seconds (3,33 minutes) into the fire, which is earlier than what is recorded in the experimental data. After adjusting for the delayed ignition (233-second delay), the experimental data suggest that flashover occurs around 240 seconds into the fire. This discrepancy between simulation and experimental data indicates that the simulated model may be more conservative, predicting an earlier flashover than what is observed in the experimental data, a trend that aligns with the observations from the HRR analysis.
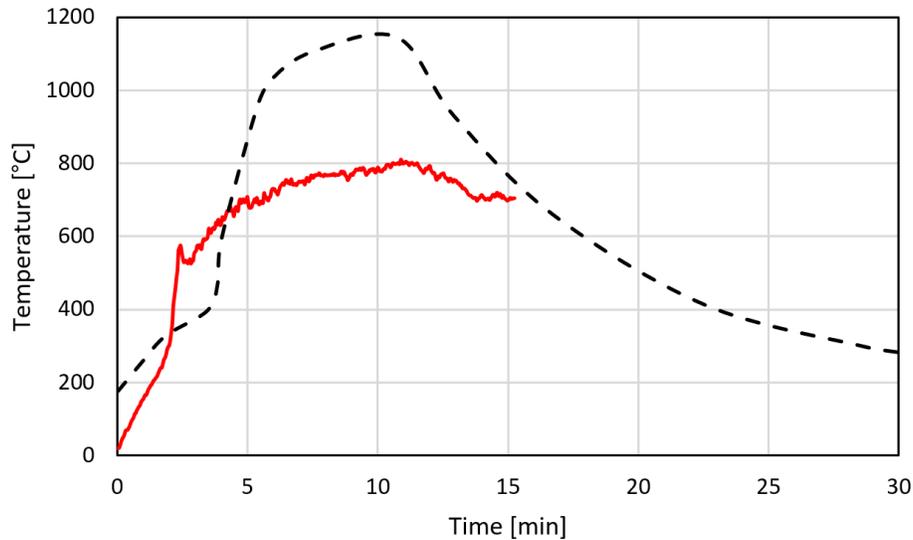
Figure 39 - Comparison between simulated and experimental compartment gas-phase temperature measurements 220 cm above floor level

Following the initial increase to 600 °C, the temperature in the simulation tends to stabilize, resulting in a gentle rise in the average temperature to 734 °C. This gradual increase lasts for about 450 seconds (10 minutes) until the peak temperature of 810 °C is achieved, after which a decline in temperature measurements commences. In contrast, the experimental data reveal a faster rate of temperature rise that persists until approximately 330 seconds (5,5 minutes). After this, the experiment also demonstrates a slower average temperature increase with an average temperature of 1060 °C. This phase persists for nearly the same duration, 330 seconds, culminating in the peak temperature of 1145 °C. Thereafter, the recorded temperature measurements begin to fall.

The decline in temperature in the simulated fire commences shortly after the peak temperatures have been attained. This trend aligns with the experimental results, with the location of the temperature decrease being similar in both the simulation and the experiments. Despite the discrepancies of conservative estimates for flashover and the underestimation of peak temperatures, the overall trends and behaviours in the simulated fires align well with the experimental observations. Unfortunately, the simulation results end at 15 minutes, and it is difficult to tell if the rate of temperature decline will align with the experimental data.

The temperature results from the simulation have shown to be inaccurate in replicating the experiment with a significant temperature difference in peak temperatures. This discrepancy is of great importance because gas-phase temperatures are often used as a measurement to decide fire resistance of structural elements and fire enclosing elements.

The significant difference between the experimental and simulated peak temperatures might be due to the heat of combustion value chosen for the simulation model's fuel. This critical parameter defines the total heat energy released when a specific amount of fuel fully burns. If the simulation's heat of combustion value is lower than the actual experimental value, it could lead to an underestimation of peak temperatures. A more accurate depiction of the heat of combustion in the simulation might align its predictions with the experimental data. Nonetheless, this idea requires further exploration and possible model recalibration.

Ventilation conditions, which influence oxygen availability for combustion, could also significantly impact the difference between simulated and experimental peak temperatures. If the simulation inaccurately reflected the experiment's actual ventilation conditions, the resulting temperatures could be affected. Underestimated ventilation could cause lower peak temperatures due to oxygen-limited combustion. This theory is supported by the simulation visualizations, which indicate that a lot of the combustions occur outside the compartment, even as far as 6 meters from it, which is the limit of the simulation domain. Further investigations are not included in the current paper but reviewing and adjusting the simulation's ventilation parameters might lead to better alignment with experimental data.

This prediction of temperature directly affects the heat transfer into the CLT elements and thereof the in-depth temperature of its components. These temperatures govern the pyrolysis processes, which in turn determine the mass flux of pyrolyzates from the surfaces. Consequently, the model underestimates the fuel entry into the simulated domain and affect the HRR. If the temperatures were higher, one might see an increase in HRR due to increased production of pyrolysis gases. This also might explain the discrepancies in HRR post peak.

However, it's important to note that these explanations are speculative at best. The true cause of the discrepancy in the gas-phase temperature predictions remains uncertain, making it challenging to ascertain whether it's due to a low heat of combustion for the chosen fuel, inaccurate representation of ventilation conditions, or a combination of these factors. Therefore, to conclusively identify the root cause of this temperature discrepancy, a more comprehensive investigation is necessary.

6.3. Solid-phase Temperature Analysis

Figure 40 presents a comparison of the average temperature progression in four scenarios: at the exposed timber wall surface (top left), at a depth of 9 mm in the wall (top right), at the exposed

ceiling surface (bottom left), and at a depth of 9 mm in the ceiling (bottom right). This comparison is drawn between the FDS output and the experimental data. Any deeper measurements do not provide a suitable comparison due to the challenges in extracting experimental data (as shown in in Figure 11, Section 2.6) and the negligible temperature increase in the simulation output (as illustrated in Figure 35, chapter 5.2.4).
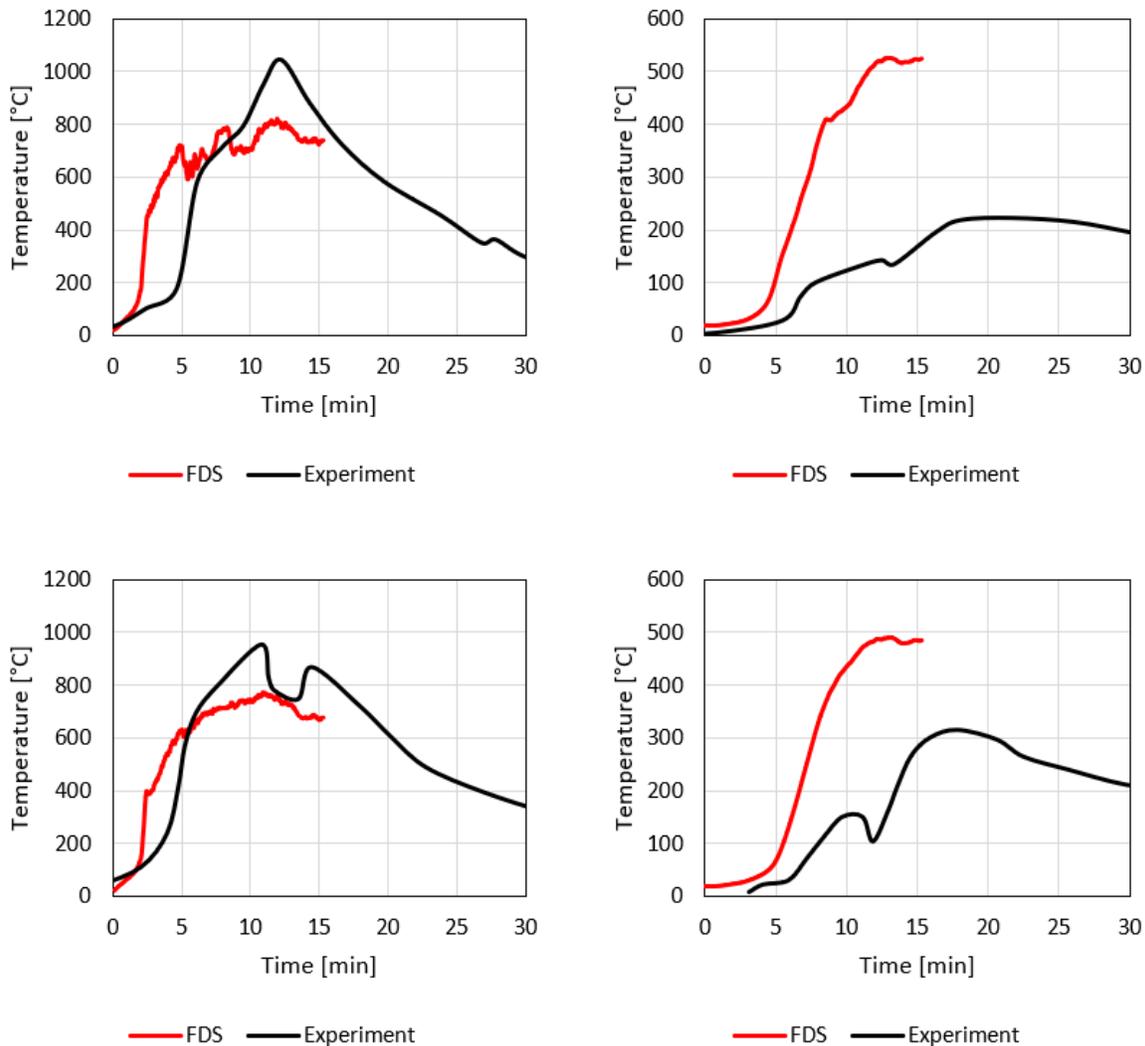
Figure 40 – Comparison of average temperature progression at the exposed timber wall surface (top left), at 9 mm depth in the wall (top right), at the exposed ceiling surface (bottom left), and at 9 mm depth in the ceiling (bottom right) between simulated and experimental results

The temperature increase, both at the surface and at 9 mm depth, initiates earlier in the simulation than in the experimental results, in line with the gas phase temperature increase reported in Section 6.2. One likely cause of this discrepancy is the choice of material properties for the spruce

surface in the simulation. While these properties were tailored for pyrolysis prediction, they may not accurately represent the behaviour of real-world materials, leading to potential inaccuracies in heat transfer through the timber. This is especially certain when it comes to choice of the thermal conductivity chosen for spruce and char which were 0.09 and 0,22 W/ (m K) respectively.

The simulation estimates peak average wall temperatures at 823 °C at the surface and 525 °C at a depth of 9mm, in contrast to the experimental findings of 1046 °C and 221 °C, respectively. As for the ceiling, the simulation predicts peak average temperatures of 773 °C at the surface and 488°C at 9mm depth, while the experiment reported 951 °C and 314 °C, respectively. These results suggest the simulation overestimates the heat transfer into the timber, given that it predicts a higher temperature than experimental data at 9mm depth, but the experiment showcase higher surface temperatures and lower in-depth temperatures. Also because the gas-phase temperature was highly underestimated, this will in turn be reflected in the solid-phase temperature.

To summarize, the simulation's inaccuracies in gas-phase temperatures extend to its predictions of solid-phase temperatures. Improved accuracy in gas-phase temperature prediction would consequently enhance the relevance of the solid-phase temperature outputs. The simulation's reliance on optimized values for pyrolysis prediction introduces inaccuracies in portraying heat transfer into the solid phase. Therefore, while the simulation provides some insight, it's crucial to exercise caution when extrapolating these results due to the inherent limitations.

6.4. Mass Flux of Volatiles Analysis

Figure 41 presents a comparison of the mass flux of volatile pyrolyzates emerging from the CLT wall (left and the ceiling (right) between Bartlett et al.'s estimations [1] and the FDS output.
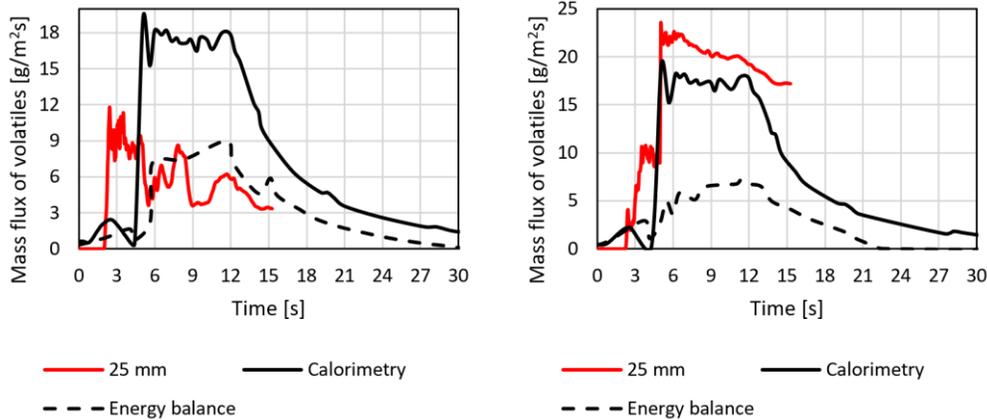
Figure 41 – Comparison between simulated and estimated experimental mass flux of pyrolyzates emerging from exposed timber wall left) and ceiling (right)

Wall Mass Flux

In the simulated model, the mass flux of volatiles from the wall commences around the 2-minute mark, demonstrating a sharp upward trend until it reaches its maximum at 11,78 g/(m²s). In contrast, the estimations from Bartlett et al. indicate the mass flux onset at the 0-second mark, likely due to the time adjustment for delayed ignition of the initial crib fire. However, this initial rise is marginal, with a similar substantial increase to the simulation observed 5 minutes into the experiment, or 3 minutes later than the simulation.

The significant divergence between the two estimation methods discussed in Sections 2.6 and 3.2 becomes evident during this rapid growth phase. While the energy balance method reaches and stabilizes at a mass flux of 7,47 g/(m²s), the calorimetry method achieves its peak flux of 19,17 g/(m²s) during the same period.

After its initial surge, the simulated mass flux from the wall begins to decline in a fluctuating manner. This downward trend persists for approximately 3 minutes, culminating in a mass flux of 3,72 g/(m²s) at the 330-second (5,5 minutes) mark. Notably, this coincides with the drastic reduction in the incident radiative heat flux discussed in chapter 5.2.5. The diminished heat flux received by the wall could significantly influence the heat transferred into the solid wall, consequently reducing the production of pyrolyzates. This decline in incident heat flux is theorized to result from a thickening smoke layer that absorbs much of the radiative heat generated by the

crib fire. However, this downward trend is not recorded to the same extent in Bartlett et al.'s estimations.

Following this, the mass flux from the wall experiences a fluctuating increase, reaching a local maximum of 8.04 g/(m²s) at approximately the 484-second mark (~8 minutes). This peak is followed by another decline, also correlating with a drop in incident heat flux. Figure 42 delineates the presumed correlation between the average incident heat flux received by the wall and the mass flux of volatiles emitted from the wall.
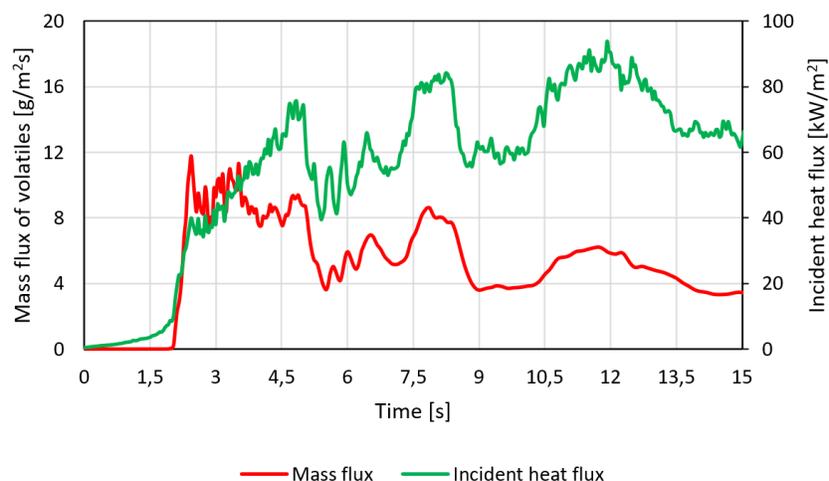
Figure 42 - Mass flux from exposed timber wall and average incident heat flux received by wall

The FDS simulation's estimation of mass flux from the wall doesn't align well with either of the estimation methods used by Bartlett et al. Moreover, it's challenging to assert the accuracy of these estimations in capturing the transient mass flux emerging from the wall. The simulated values align most closely with the energy balance method for estimating mass flux. If the timeline for the energy balance estimation were shifted forward by three minutes, the overall trends of the simulations could arguably align in terms of growth and subsequent decay, as depicted in Figure 43.
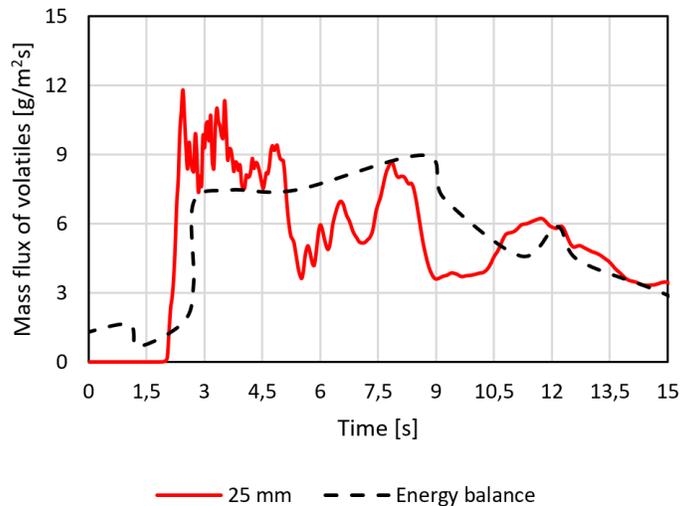
Figure 43 – Comparison between simulated and estimated mass flux from the wall with estimations being fast forwarded 3 minutes

Ceiling Mass Flux

The volatile mass flux originating from the ceiling in the simulation exhibited a markedly different pattern compared to the wall. The initial surge in mass flux begins at 165 seconds (2,75 minutes) in the simulation. Correspondingly, the estimations show a similar initial rise 255 seconds (4,25 minutes) into the experiment. This concurs with the overarching analysis that the simulation's material response to heat is prompter than what the experimental data indicates.

In the simulation, the mass flux undergoes a swift two-step surge before attaining its maximum level. Initially, it experiences a fluctuating rise, achieving 10,63 g/(m²s) at the 210-second (3,5 minutes) mark, during which it maintains a semi steady-state for a period of 90 seconds. Following this, it initiates its second increase, culminating in a peak mass flux of 23.51 g/(m²s). The timing of when the simulated mass flux reaches peak values overlap with the estimations made by Bartlett et al. using the calorimetry method.

Once the mass flux hits its peak, the graph steadies to a flow that slowly diminishes on average, which is also reflected in estimates made using the calorimetry method. However, the average value in this case is higher, averaging 21,06 g/(m²s) between the 5-minute and 12-minute marks. Meanwhile, the calorimetry method estimates a lower average of 17,41 g/(m²s) for the same duration.

Unlike the wall's impact on the fire environment, the ceiling experiences a more consistent exposure to incoming radiative heat, as detailed in chapter 5.2.5. Figure 44 displays both the mass flux from the ceiling and the incident heat flux. The steady mass flux that forms after the 5-minute mark is likely a result of the consistent and increasing exposure to radiative heat.
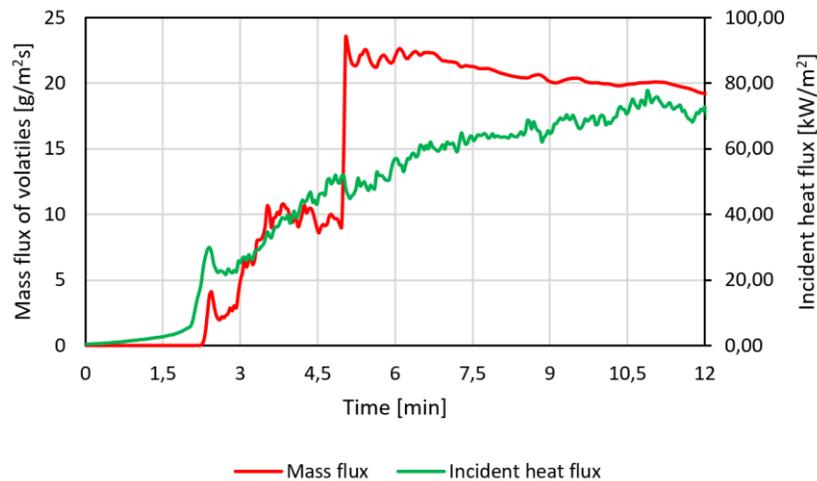
Figure 44 – Mass flux from exposed timber wall and average incident heat flux received by wall

The results from the mass flux analysis demonstrate that incorporating multiple reactions into the FDS simulation provides a more comprehensive understanding of pyrolysis in the CLT elements. This approach allows for the distinction and quantification of the mass loss of volatiles from different sources, namely the crib fire, the exposed wall, and the exposed ceiling.

The mass flux of pyrolyzates emerging from the wall and ceiling are tightly connected to the total HRR presented in Section 5.2.2. As more volatiles are introduced through the pyrolysis of spruce, the potential for more combustion reactions emerges. The analysis of both mass flux and HRR make it clear that the production of volatiles from the CLT elements significantly impacts the fire environment, mirroring the dynamics observed in the compartment experiment.

The simulation outcomes, while intriguing, are somewhat inconclusive. The simulated wall mass flux shows a better resemblance to estimations drawn from the energy balance method, though the correspondence isn't entirely accurate. Conversely, the ceiling mass flux in the simulation appears to align more closely with predictions from the calorimetry approach, albeit with some divergence. These differences underscore the limitations of the current simulation model in fully capturing the complex nature of a real fire event. Given these variations between the experimental and simulated estimations, the reliability of the simulated results is not without question. These

findings highlight the need for more rigorous research and model optimization for improved accuracy.

6.5. Simulation operation

As highlighted in the current thesis and by Dixon et al. [27], conducting simulations of enclosure fires involving exposed timber surfaces is notably time-consuming. There are many reasons why this is considered negative. Long simulation times can impact overall productivity and efficiency in research, development, and design processes. Researchers and engineers may experience delays in obtaining results, analysing data, and iteratively refining their models or designs. The need for fine mesh sizes to accurately capture the intricate pyrolysis processes within the elements largely contributes to this issue.

One proposed approach to decrease the simulation duration involves the utilization of multiple meshes, or MPI processes (parallel processing). By distributing the computations across multiple CPU cores that simultaneously operate on different areas of the simulation domain, the total simulation time can be significantly reduced. However, it's important to consider the potential trade-off involved. Beyond a certain threshold, the computational overhead associated with inter-mesh communication could outweigh the benefits of parallel processing, potentially leading to even longer simulation times than would be observed with fewer meshes.

An additional strategy to mitigate simulation time includes the application of variable mesh sizes (Adaptive Mesh Refinement). By employing finer meshes in areas where pyrolysis processes occur, and coarser meshes in areas where high mesh resolution is less critical, such as outside the compartment domain, computational efficiency can be significantly enhanced. Regrettably, this approach was not implemented in this thesis, which likely impacted the simulation duration. Future research should consider the implementation of these strategies to improve the simulation efficiency and accuracy.

Furthermore, the application of the flag `CELL_SIZE_FACTOR=0.8` notably extended the computational duration. This specific value was selected as it was found to be the minimum necessary to eliminate the oscillation in HRR output, while minimizing additional computational demand. It is important to note that other pyrolysis models may not require the application of this flag, thereby potentially offering more efficient simulations of the pyrolysis process. Future research should explore the use of alternative models or settings to strike an optimal balance between simulation accuracy and computational efficiency.

7. Conclusion

This chapter serves to summarize the key findings from the study in relation to the main objectives and research questions. Additionally, it will suggest further research work and provide final reflections from this thesis work.

7.1. Key findings

The primary objective of this study was to evaluate the model's accuracy. The final simulation outcomes exhibited limited alignment with the experimental findings. The HRR was the parameter that best reflected the experimental results. However, both the gas-phase and solid-phase temperature readings displayed significant discrepancies, with the latter being strongly influenced by the former. The production of volatile mass flux by the CLT demonstrated a degree of consistency with experimental data, indicating promising avenues for future research, but the current output isn't reliable enough for practical applications.

The second research question focused on identifying the model's limitations. The gas-phase temperature, a critical parameter influencing numerous aspects of compartment fires, was significantly underestimated. The exact reason behind this remains uncertain, but it is speculated to be due to either the selected heat of combustion values for the CLT pyrolyzates or the model's ability to accurately predict ventilation conditions within the compartment. If the gas-phase temperature had been more accurately modelled, the solid-phase temperature would be more relevant to study and the HRR might have exhibited closer correspondence to the experimental results. Moreover, the model's inability to account for the additional heat generated by smouldering combustion is seen as a significant limitation in achieving accurate results. This type of combustion was not included in the simulation, despite its potential for significantly affecting both HRR and gas-phase temperature. Lastly, the time-consuming nature of running the simulations is a limitation. This lengthy process restricts research flexibility and slows down the generation of results making it difficult to assess how different parameters influence the simulation output.

The final research question addressed potential enhancements for the model. These improvements could encompass mesh sensitivity analysis at sub 5 mm grid, methods to decrease extensive simulation times, such as parallel processing and Adaptive Mesh Refinement, and a more accurate depiction of material properties and pyrolysis models.

The mesh sensitivity analysis could not determine a resolution at which output would converge, leaving it unclear whether a 25 mm grid resolution was sufficient for such convergence. Thus, it remains inconclusive whether a finer grid might yield different results. It is therefore a suggestion for improvement that a mesh sensitivity analysis is conducted for grid sizes smaller than 25 mm.

Strategies to reduce computational time would substantially improve the outcome quality for such simulations, facilitating a faster process for verifying the model's accuracy and performing parameter sensitivity analysis. Given the advancements in computational power and software engineering over the past two decades, such models are likely to become more attractive for both research and fire engineering applications.

Material property representation and pyrolysis modelling are fundamental aspects for generating high-quality simulation outputs. The literature review revealed that these parameters are increasingly adopted in simulation applications and refining these models will enhance the accuracy of the results. Therefore, it is highly recommended to devote considerable effort to identifying parameters that are aptly suited for their respective tasks.

7.2. Future work

Continuing research based on this thesis could delve into various areas of potential enhancement. These improvements could bolster the precision and usability of fire simulation models such as FDS.

1. **Enhancement of Material Properties and Pyrolysis Model:** Future research could be dedicated to the advancement of material properties representation and the refinement of the pyrolysis model. This thesis used a pyrolysis model optimized to yield accurate cone calorimeter results in FDS. The parameters were thereof not aligned with real-world values. It is not clear if the model is suitable for large-scale application. Detailed material studies may improve the accuracy of fire behaviour predictions when incorporated into the pyrolysis model.

2. **Incorporation of Smouldering Combustion:** Smouldering combustion, overlooked in the current model, plays a natural role in fires involving exposed timber surfaces. Including this element in the simulation model may improve temperature and HRR predictions, thereby addressing some discrepancies observed in this study.

4. **Investigation of Grid Cell Size Effect:** In this study, identification of a suitable grid cell size leading to convergence was not achieved. Further research should delve into this issue, as grid cell size can significantly impact simulation results.

5. **Examination of Parallel Processing and Adaptive Mesh Refinement:** Decreasing computational times through strategies such as parallel processing or Adaptive Mesh Refinement could be a focus of future research. Shorter simulation times would allow for a more flexible research process and enable more detailed or varied simulations within the same timeframe.

6. **Enhanced Ventilation Modelling:** One of the identified limitations of the current model involves accurately capturing ventilation conditions within the compartment. Future studies should focus on improving this aspect of the model to enhance predictive capabilities.

7. **Practical Applications:** As simulations improve in accuracy and computational times decrease, future research should consider practical applications of these models in fire safety planning and post-fire analysis.

Focusing on these areas, researchers can improve the predictive capabilities of fire simulation models and their value in practical fire safety applications. While every model inevitably has limitations, it is through iterative cycles of development and refinement that fire simulation tools become more accurate and useful.

7.3. Final reflections

The journey of this thesis through the complexities of fire dynamics simulation has illuminated the multifaceted nature of this field. From the intricate details of the pyrolysis process, the nuances of grid resolution, to the intriguing behaviour of CLT under fire conditions. Even though the results yielded significant discrepancies, this thesis can be used as a guidance for further model development.

As the sector evolves to prioritize sustainable building materials, understanding the fire dynamics of materials like CLT is not just an academic pursuit, but a societal necessity. The challenges and limitations encountered in this thesis signal a call for further exploration. Strategies to enhance model efficiency, precision in material property representation, and a deeper comprehension of the pyrolysis process are just a few of the promising avenues for future research.

8. References

[1] Bartlett et al., "Auto-extinction of engineered timber: Application to compartment fires with exposed timber surfaces," *Fire Saf. J.,* Vol. 91, pp. 407-413, July 2017. doi: https://doi.org/10.1016/j.firesaf.2017.03.050.

[2] A. Rinta-Paavola and S. Hostikka, "A model for the pyrolysis of two Nordic structural timbers," *Fire Mater.,* vol. 46, pp. 55-68, February 2021. doi: https://doi.org/10.1002/fam.2947.

[3] United Nations Environment Programme, "2021 Global Status Report for Buildings and Construction: Towards a Zero-emmision, Efficient and Resillient Buildings and Construction Sector," Nairobi, 2021.

[4] R. Løvaas, "massivtrebygging" snl.no. Derived from: https://snl.no/massivtrebygging (Downloaded May 22nd 2023).

[5] C. Gorska, "Fire dynamics in multi-scale timber compartments," Ph.D. Dissertation, School of Civil Engineering, The University of Queensland, Brisbane, 2019.

[6] R. M. Hadden and A. Law, "Burnout means burnout," *SFPE Europe Digital Magazine, Q1,* 2017.

[7] A. Buchan and B. Östman, *Fire Safe Use of Wood in Buildings: Global Design Guide,* 1st ed., CRC Press, 2022.

[8] Hadden et al., "Effects of exposed cross laminated timber on compartment fire dynamics," *Fire Saf. J.,* Vol. 91, pp. 407-413, July 2017. doi: https://doi.org/10.1016/j.firesaf.2017.03.074.

[9] National Institute of Standards and Technology, "FDS and Smokeview" nist.gov. Derived from: URL: https://www.nist.gov/services-resources/software/fds-and-smokeview (Downloaded: December 12th 2022).

[10] Ankit Rohatgi, "WebPlotDigitizer", automeris.io. Derived from: https://automeris.io/WebPlotDigitizer/tutorial.html, (Downloaded: January 23rd 2023).

[11] D. Drysdale, "An Introduction to Fire Dynamics," 3rd ed.,University of Edinburgh, Scotland, UK, Wiley, 2011.

[12] H. Aarnes, "hemicelluloser", snl.no, Derived from: https://snl.no/hemicelluloser (Downloaded: May 3rd 2023).

[13] S. B. Manum, "ligning", snl.no, Derived from: https://snl.no/lignin (Downloaded: December 19th 2022).

[14] Norsk Treteknisk Institutt, "Håndbok - bygge med Massivtreelementer," Norsk Treteknisk Institutt, Oslo, 2006.

[15] "ANSI/APA PRG 320 - Standard for Performance-Rated Cross-Laminated Timber," The Engineered Wood Association, Tacoma, WA.

[16] TreFokus AS og Treteknisk, "Fokus på tre-serien: Nr. 20 - Massivtre," TreFokus AS og Treteknisk, Oslo, 2011.

[17] C. Pettersson, "Fire Safety in Timber Buildings - A review of existing knowledge," Brandforsk, Sweden, 2020.

[18] "Eurocode 5: Design of timber structures - Part 1-2: General - Structural fire design," NS-EN 1995-1-2:2004+NA:2010, 2010.

[19] *Eurocode 1: Actions on structures - Part 1-1: General actions - Densities, self-weight, imposed loads for buildings,* NS-EN 1991-1-2:2002+NA:2008, 2008.

[20] D. Barber, L. Sieverts, R. Dixon and J. Alston, "A methodology for quantifying fire resistance of exposed structural mass timber elements," Proceedings of the 10th International Conference on Structures in Fire, Belfast, UK, 2018.

[21] D. Brandon, "Fire Safety Challenges of Tall Wood Buildings – Phase 2: Task 4 Engineering Methods," NFPA,, Quincy, MA, No. FRPF-2018-04, 2018.

[22] D. Barber, R. Crielaard and X. Li, "Towards fire safety design of exposed timber in tall timber buildings," presented at Proceedings World Conference on Timber Engineering, Santiago, Chile, 2021.

[23] J. Schmid and A. Frangi, "Structural timber in compartment fires – The timber charring and heat storage model," *Open Eng.,* vol. 11, pp. 435-452, 2021, doi: https://doi.org/10.1515/eng-2021-0043.

[24] D. Nakrani, T. Wani and G. Srivastava, "Simulation of pyrolysis and combustion of pine wood using two-step reaction scheme," presented at the 11th International Conference on Structures in Fire, Brisbane, Australia, November 2020.

[25] V. Šálek, K. Cábová, F. Wald and M. Jahoda, "Numerical modelling of fire test with timber fire protection," *J. Struct. Fire Eng.,* vol. 13, no. 1, pp. 99-117, January 2022. doi: https://doi.org/10.1108/JSFE-04-2021-0017.

[26] S. Brunkhorst and J. Zehfuß, "Expiermental and Numerical Anlaysis of Fire Development in Compartment Fires with Immobile Fire Load," in *Wood & Fire Safety*, Braunschweig, Germany, Springer Nature Switzerland, 2020, pp. 185-190.

[27] R. Dixon, L. Sieverts, J. Alston and D. Barber, "A Methodology for Quantifying Fire Resistance Level of Buildings Containing Exposed Structural Timber Elements," presented at the Fire Safety Engineering Stream Conference: Quantification of Fire Safety, Australia, 2017.

[28] X. Wang, C. Fleischmann, M. Spearpoint and X. Huang, "The Application of Different Component Schemes to Predict Wood Pyrolysis and Fire Behaviour," presented at the International Fire Safety Symposium, Coimbra, Portugal, April 20-23, 2015.

[29] C. J. McGregor, "Contribution of Cross Laminated Timber Panles to Room Fires," Master thesis, Department of Civil and Environmental Engineering, Carleton University, Ottawa, 2013.

[30] T. J. Ohlemiller, G. W. Mulholland, A. Maranghides, J. J. Filliben and R. G. Gann, "World Trade Center Disaster Fire Tests of Single Office Workstations," NIST, NCSTAR 1-5C, 2005.

[31] A. H. Buchanan, "Fire engineering for a performance based code," *Fire Saf. J.,* Vol. 23, no. 1 pp. 1-16, 1994, doi: https://doi.org/10.1016/0379-7112(94)90058-2.

[32] A. Barlett, R. Hadden, L. Bisby and B. Lane, "Auto-Extinction of Engineered Timer as a Design Methodology," presented at the World Conference on Timber Engineering, Vienna, Austria, 2016.

[33] A. Bartlett, L. A. Bisby, R. Hadden and B. Lane, "Auto-extinction of engineered timber: the application of firepoint theory," presented at the 14th international conference Interflam, Royal Holloway College, UK, 2016.

[34] K. McGrattan, R. McDermott, M. Vanella and S. Hostikka, "Fire Dynamics Simulator User's Guide," 6th ed., National Institue of Standards and Technology, Marlyand, 2022.

[35] B. Fredlund, "A model for heat and mass transfer in timber structures during fire: A theoretical, numerical and experimental study," Ph.D. Dissetation, Department of Fire Safety Engineering, Lund Univerisity, Lund, 1988.

[36] A. Atreya, "Pyrolysis, Ignition and Fire Spread on Horizontal Surfaces of Wood," Ph.D. Dissertation, Division of Applied Sciences, Harvard University, Cambridge, 1983.

[37] M. Chaos, "Spectral Aspects of Bench-Scale Flammability Testing: Application to Hardwood Pyrolysis," *Fire Saf. Sci.,* vol. 11, pp. 165-178, July 2014. doi: 10.3801/IAFSS.FSS.11-165.

[38] M. Janssens, "Thermophysical Properties of Wood and their Role in Enclosure Fire Growth," The University of Ghent, Ghent, Belgium, 1991.

[39] N. Ryder and E. Weckman, "Effects of convective heat transfer coefficient in prediction of materials properties from cone calorimeter testing.," presented at Fire and Materials 13th International Conference and Exhibiton, London, 2012.

[40] T. Kashiwagi, J. Ohlemiller and K. Werner, "Effects of external radiant flux and ambient oxygen concentration on nonflaming gasification rates and evolved products of white pine," *Combust Flame,* vol. 69, issue 3, pp. 331-345, September 1987. doi: https://doi.org/10.1016/0010-2180(87)90125-8.

[41] G. SV and Z. SL, "Moisture relations and physical properties of wood:," in *Wood Handbook: Wood as an Engieering Material*, Centennial ed., Madison, USA, USDA Forest Service, 2010, Chapter 4.

[42] J. Torero, "Flaming Ignition of Solid Fuels," in *SFPE Handbook of Fire Protection Engineering*, 5th ed., Springer, 2016, pp. 633-661.

[43] A. Witkowski, A. A Stec and T. R. Hull, "Thermal Decomposition of Polymeric Materials," in *SFPE Handbook of Fire Protection Engineering*, 5th ed., Springer, 2016, pp. 167-254.

[44] Forest Products Laboratory, "Report 2136," United States Department of Agriculture, Forest Service, Madison, Wisconsin, 1958.

[45] A. I. Bartlett, R. M. Hadden and L. A. Bisby, "A Review of Factors Affecting the Burning Behaviour of Wood for Application to Tall Timber Construction," Fire Technol 55, 1–49, 2019, doi: https://doi.org/10.1007/s10694-018-0787-y..

[46] K. L. Friquin, "Material properties and external factors influencing the charring rate of solid wood and glue-laminated timber," *Fire Mater.,* vol. 35, issue 5, November 2010, doi: https://doi.org/10.1002/fam.1055.

[47] T. Kashiwagi, T. Ohlemiller and K. Werner, "Effects of external radiant flux and ambient oxygen concentration on nonflaming gasification rates and evolved products of white pine," *CombustFlame,* vol. 69, issue 3, pp. 331-345, 1987, doi: https://doi.org/10.1016/0010-2180(87)90125-8.

[48] I. S. Wichman and A. Atreya, "A simplified model for the pyrolysis of charring materials," *Combust Flame,* vol. 68, issue 3, pp. 231-247, 1987, doi: https://doi.org/10.1016/0010-2180(87)90002-2.

[49] M. G. Grønli and M. C. Melaaen, "Mathematical Model for Wood PyrolysisComparison of Experimental Measurements with Model Predictions," *Energy Fuels,* vol. 14, issue 4, pp. 791–800, May 2000, doi: https://doi.org/10.1021/ef990176q.

[50] C. Di Blasi, E. Gonzalez Hernandez and A. Santoro, "Radiative Pyrolysis of Single Moist Wood Particles," *Ind. Eng. Chem. Res,* vol. 39, issue 4, 2000, 873–882, doi: https://doi.org/10.1021/ie990720i.

[51] E. L. Schaffer, "Effect of pyrolytic temperatures on longitudinal strength of dry Douglas-fir," *J Test Eval,* vol. 1, issue 4, pp. 319-329, 1973, doi: 10.1520/JTE10025J.

[52] A. Inghelbrecht, "Evaluation of the burning behaviour of wood products in the context of structural fire design," Master thesis, Civil Engineering, The University of Queensland and Ghent University, Brisbane, 2014.

[53] P. W C Lau, R. White and I. Van Zealand, "Modelling the charring behaviour of structural lumber," *Fire Mater.,* vol. 23, pp. 209-216, 1999, doi: https://doi.org/10.1002/(SICI)1099-1018(199909/10)23:5<209::AID-FAM685>3.0.CO;2-A.

[54] R. V. Petrella, "The Mass Burning Rate and Mass Transfer Number of Selected Polymers, Wood, and Organic Liquids," *Polym Plast Technol Eng,* vol. 13, issue 1, pp. 83-103, January 1979, doi: 10.1080/03602557908067676.

[55] A. Tewarson and R. F. Pion, "Flammability of plastics—I. Burning intensity," *Combust Flame,* vol. 26, pp. 85-103, 1976, doi: https://doi.org/10.1016/0010-2180(76)90059-6.

[56] M. A. Delichatsios, "Piloted ignition times, critical heat fluxes and mass loss rates at reduced oxygen atmospheres," *Fre Saf. J.,* vol. 841, issue 3, pp. 197-212, 2005, doi: https://doi.org/10.1016/j.firesaf.2004.11.005.

[57] R. Emberley, T. Do, J. Yim and J. L. Torero, "Critical heat flux and mass loss rate for extinction of flaming combustion of timber," *Fire Saf. J.,* vol. 91, pp. 252-258, July, 2017, doi: https://doi.org/10.1016/j.firesaf.2017.03.008.

[58] B. Pedersen, "fordampningsvarme" snl.no, Derived from: https://snl.no/fordampingsvarme (Downloaded: December 6th 2022).

[59] B. Karlsson and J. G. Quintiere, *Enclosure Fire Dynamics,* 2nd ed., CRC Press, 2022.

[60] B. C. Hagen, *Grunnleggende brannteknikk,* 2nd ed., Norway, Bjarne Christian Hagen, 2018.

[61] E. D. Wormdahl, K. Hox, A. B. G. Steen-Hansen and M. K. Ulfsnes, "Brannsikkerhet i bygg med massivtre," SP Fire Research AS, Tiller, Norway, SPFR-rapport A17 20229:1, 2017.

[62] X. Li, C. McGregor, A. R. Medina, X. Sun, D. Barber and G. Hadjisophocleous.*presented at World Conference on Timber Engineering, Vienna University of Technology, Vienna, 2016.*

[63] M. Klippel and J. Schmid, "Guidance Document on the Verification of the Adhesive Performance in Fire," 2018, Switzerland, COST Action FP1404.

[64] D. Barber, R. Dixon, E. Rackauskaite and K. Looi, "A method for determining time equivalence for compartments with exposed mass timber, using iterative parametric curves," presentd at World Conference on Timber Engineering, Santiago, Chile, 2021.

[65] K. McGrattan, S. Hostikka, J. Floyd, R. McDermott and M. Vanella, "Fire Dynamics Simulator Techincal Reference Guide Volume 1: Mathematical model," 6th ed., National Institue of Standards and Technology, Maryland, 2022.

[66] Thunderhead Engineering, "Heat Conduction in Pyrosim", support.thunderheadeng.com. Derived from: https://support.thunderheadeng.com/tutorials/pyrosim/heat-conduction/ (Downloaded: January 28th 2023).

[67] Best Practice gruppen, "CFD Best Practice," 2009.

[68] K. McGrattan, R. McDermott and M. Vanella, "Fire Dynamics Simulator Technical Reference Guide Volume 3: Validation," 6th ed., National Institute of Standards and Technology, Maryland, 2022.

[69] A. Meunders, G. Baker, L. Arnold, B. Schröder, M. Spearpoint and D. Pau, "Parameter optimization and sensitivity analysis for fire spread modelling with FDS," presented at 10th International Conference on Performance-Based Codes and Fire Safety Design, Brisbane, Australia, 2014.

[70] L. Chiesa, Artist, *Thermogravimetric analyser (TGA)*. [Art]. Own work, 20 July 2006.

[71] E. Jamin, C. Wei-Hsin, T. Meisam, T. H. Anh, E. K. Eilhann, A. L. Kun-Yi and S. Ayyadurai, "Pyrolysis of lignocellulosic, algal, plastic, and other biomass wastes for biofuel

production and circular bioeconomy: A review of thermogravimetric analysis (TGA) approach," *Renewable Sustainable Energy Rev.,* vol. 169, November 2022, doi: https://doi.org/10.1016/j.rser.2022.112914.

[72] A. Dhaundiyal, S. Singh, M. M. Hanon and R. Rawat, "Determination of Kinetic Parameters for the Thermal Decomposition of Parthenium hysterophorus," *Environ. Clim. Technol,* vol.22, no.1, pp.5-21, 2018, doi: https://doi.org/10.1515/rtuect-2018-0001.

[73] *Reaction-to-fire tests — Heat release, smoke production and mass loss rate — Part 1: Heat release rate (cone calorimeter method) and smoke production rate (dynamic measurement),* ISO 5660-1:2015, 2015.

[74] American Society for Testing and Materials, *ASTM E1354-22b: Standard Test Method for Heat and Visible Smoke Release Rates for Materials and Products Using an Oxygen Consumption Calorimeter,* ASTM International, 2023.

[75] W. H. Twilley, *User's Guide for the Cone Calorimeter,* USA, U.S. Department of Commerce, National Bureau of Standards, 1988.

[76] J. P. Stensaas, "En eksperimentell undersøkelse av om sot- og tjæreansamlinger i isolasjonen i elementskorsteiner utgjør en brannfare," SINTEF Energi - Norges branntekniske laboratorium, Trondheim, STF84 A96601, 1996.

[77] A. Steen-Hansen, S. Fjær, K. Storesund and C. Sesseng, "Brann i snøoverbygg på Hallingskeid," SINTEF, Trondheim, NBL A12120, 2012.

[78] J. Hidalgo-Medina, "Performance-based Methodology for the Fire Safe Design of Insulation Materials in Energy Efficient Buildings," Ph.D. Dissertation, Fire Safety Engineering, The University of Edinburgh, Edinburgh, 2015.

[79] British Gypsum, "Gyproc FireLine Product Data Sheet," Saint-Gobain Construction Products, UK, 2016.

[80] I. Rahmanian, "Thermal and Mechanical Properties of Gypsum Boards and Their Influences on Fire Resistance of Gypsum Board Systems," Ph.D. Dissertation, Department

of Mechanical, Aerospace & Civil Engineering, The University of Manchester, Manchester, 2011.

Appendix

This appendix provides the FDS script that was used for simulating the results presented in chapter 5.2.

```
&HEAD CHID='025'/

&TIME T_END=2400.0, WALL_INCREMENT=1/

&DUMP DT_RESTART=60.0, DT_SL3D=0.25/

&MISC RESTART=.TRUE./


&MESH ID='MESH-01-01', IJK=40,58,60, XB=-1.5,-0.5,-1.46,-0.01,0.0,1.5/

&MESH ID='MESH-01-02', IJK=40,58,60, XB=-1.5,-0.5,-1.46,-0.01,1.5,3.0/

&MESH ID='MESH-01-03', IJK=40,58,60, XB=-1.5,-0.5,-0.01,1.44,0.0,1.5/

&MESH ID='MESH-01-04', IJK=40,58,60, XB=-1.5,-0.5,-0.01,1.44,1.5,3.0/

&MESH ID='MESH-01-05', IJK=40,58,60, XB=-0.5,0.5,-1.46,-0.01,0.0,1.5/

&MESH ID='MESH-01-06', IJK=40,58,60, XB=-0.5,0.5,-1.46,-0.01,1.5,3.0/

&MESH ID='MESH-01-07', IJK=40,58,60, XB=-0.5,0.5,-0.01,1.44,0.0,1.5/

&MESH ID='MESH-01-08', IJK=40,58,60, XB=-0.5,0.5,-0.01,1.44,1.5,3.0/

&MESH ID='MESH-01-09', IJK=40,58,60, XB=0.5,1.5,-1.46,-0.01,0.0,1.5/

&MESH ID='MESH-01-10', IJK=40,58,60, XB=0.5,1.5,-1.46,-0.01,1.5,3.0/

&MESH ID='MESH-01-11', IJK=40,58,60, XB=0.5,1.5,-0.01,1.44,0.0,1.5/

&MESH ID='MESH-01-12', IJK=40,58,60, XB=0.5,1.5,-0.01,1.44,1.5,3.0/

&MESH ID='MESH-03-merged-01', IJK=60,76,80, XB=-1.5,-3.108624E-15,1.44,3.34,0.0,2.0/

&MESH ID='MESH-03-merged-02', IJK=60,76,80, XB=-1.5,-3.108624E-15,1.44,3.34,2.0,4.0/

&MESH ID='MESH-03-merged-03', IJK=60,76,80, XB=-1.5,-3.108624E-15,1.44,3.34,4.0,6.0/

&MESH ID='MESH-03-merged-04', IJK=60,76,80, XB=-3.108624E-15,1.5,1.44,3.34,0.0,2.0/

&MESH ID='MESH-03-merged-05', IJK=60,76,80, XB=-3.108624E-15,1.5,1.44,3.34,2.0,4.0/

&MESH ID='MESH-03-merged-06', IJK=60,76,80, XB=-3.108624E-15,1.5,1.44,3.34,4.0,6.0/


&SPEC ID='WATER VAPOR'/

&SPEC ID='CEILING PYROLYZATE', FORMULA='C6H10O5'/

&SPEC ID='CRIB PYROLYZATE', FORMULA='C6H10O5'/

&SPEC ID='WALL PYROLYZATE', FORMULA='C6H10O5'/

&SPEC ID='CARBON MONOXIDE', FORMULA='CO'/

&SPEC ID='SOOT', FORMULA='C'/


&SPEC ID='PRODUCTS',

 SPEC_ID(1)='CARBON DIOXIDE',

 SPEC_ID(2)='CARBON MONOXIDE',

 SPEC_ID(3)='NITROGEN',

 SPEC_ID(4)='SOOT',

 SPEC_ID(5)='WATER VAPOR',

 VOLUME_FRACTION(1)=0.17482907047014,
```

```
VOLUME_FRACTION(2)=0.000699742487043609,

VOLUME_FRACTION(3)=0.659261428591368,

VOLUME_FRACTION(4)=0.00611949877078569,

VOLUME_FRACTION(5)=0.159090259680663/


&REAC ID='CRIB PYROLYZATE', HEAT_OF_COMBUSTION=1.75E+4, FUEL='CRIB PYROLYZATE', SPEC_ID_NU='AIR','CRIB PYROLYZATE','PRODUCTS', NU=-
27.8760872419788,-1.0,33.0901597290989/


&REAC ID='BACK WALL PYROLYZATE', HEAT_OF_COMBUSTION=1.375E+4, FUEL='WALL PYROLYZATE', SPEC_ID_NU='AIR','WALL PYROLYZATE','PRODUCTS',
NU=-27.8760872419788,-1.0,33.0901597290989/


&REAC   ID='CEILING   PYROLYZATE',   HEAT_OF_COMBUSTION=1.375E+4,   FUEL='CEILING   PYROLYZATE',   SPEC_ID_NU='AIR','CEILING
PYROLYZATE','PRODUCTS', NU=-27.8760872419788,-1.0,33.0901597290989/


&DEVC ID='MID_MID_EC_HRRPUA', QUANTITY='HRRPUA', XYZ=2.220446E-16,-6.661338E-16,2.87, IOR=-3/

&DEVC ID='MID_MID_EC_INCHF', QUANTITY='INCIDENT HEAT FLUX', XYZ=2.220446E-16,-6.661338E-16,2.87, IOR=-3/

&DEVC ID='MID_MID_EC_TEMP', QUANTITY='WALL TEMPERATURE', XYZ=2.220446E-16,-6.661338E-16,2.87, IOR=-3/

&DEVC ID='MID_MID_EC_TEMP09', DEPTH=9.0E-3, QUANTITY='INSIDE WALL TEMPERATURE', XYZ=2.220446E-16,-6.661338E-16,2.87, IOR=-3/

&DEVC ID='MID_MID_EC_TEMP20', DEPTH=0.02, QUANTITY='INSIDE WALL TEMPERATURE', XYZ=2.220446E-16,2.220446E-16,2.87, IOR=-3/

&DEVC ID='MID_MID_EC_TEMP30', DEPTH=0.03, QUANTITY='INSIDE WALL TEMPERATURE', XYZ=2.220446E-16,2.220446E-16,2.87, IOR=-3/

&DEVC ID='MID_MID_EC_TEMP40', DEPTH=0.04, QUANTITY='INSIDE WALL TEMPERATURE', XYZ=2.220446E-16,2.220446E-16,2.87, IOR=-3/

&DEVC ID='MID_MID_EC_TEMP60', DEPTH=0.06, QUANTITY='INSIDE WALL TEMPERATURE', XYZ=2.220446E-16,2.220446E-16,2.87, IOR=-3/

&DEVC ID='MID_UP01_EC_HRRPUA', QUANTITY='HRRPUA', XYZ=2.220446E-16,0.5,2.87, IOR=-3/

&DEVC ID='MID_UP01_EC_INCHF01', QUANTITY='INCIDENT HEAT FLUX', XYZ=2.220446E-16,0.5,2.87, IOR=-3/

&DEVC ID='MID_UP01_EC_TEMP', QUANTITY='WALL TEMPERATURE', XYZ=2.220446E-16,0.5,2.87, IOR=-3/

&DEVC ID='MID_UP01_EC_TEMP09', DEPTH=9.0E-3, QUANTITY='INSIDE WALL TEMPERATURE', XYZ=2.220446E-16,0.5,2.87, IOR=-3/

&DEVC ID='MID_UP01_EC_TEMP20', DEPTH=0.02, QUANTITY='INSIDE WALL TEMPERATURE', XYZ=2.220446E-16,0.5,2.87, IOR=-3/

&DEVC ID='MID_UP01_EC_TEMP30', DEPTH=0.03, QUANTITY='INSIDE WALL TEMPERATURE', XYZ=2.220446E-16,0.5,2.87, IOR=-3/

&DEVC ID='MID_UP01_EC_TEMP40', DEPTH=0.04, QUANTITY='INSIDE WALL TEMPERATURE', XYZ=2.220446E-16,0.5,2.87, IOR=-3/

&DEVC ID='MID_UP01_EC_TEMP60', DEPTH=0.06, QUANTITY='INSIDE WALL TEMPERATURE', XYZ=2.220446E-16,0.5,2.87, IOR=-3/

&DEVC ID='MID_UP02_EC_HRRPUA', QUANTITY='HRRPUA', XYZ=2.220446E-16,1.0,2.87, IOR=-3/

&DEVC ID='MID_UP02_EC_INCHF', QUANTITY='INCIDENT HEAT FLUX', XYZ=2.220446E-16,1.0,2.87, IOR=-3/

&DEVC ID='MID_UP02_EC_TEMP', QUANTITY='WALL TEMPERATURE', XYZ=2.220446E-16,1.0,2.87, IOR=-3/

&DEVC ID='MID_UP02_EC_TEMP09', DEPTH=9.0E-3, QUANTITY='INSIDE WALL TEMPERATURE', XYZ=2.220446E-16,1.0,2.87, IOR=-3/

&DEVC ID='MID_UP02_EC_TEMP20', DEPTH=0.02, QUANTITY='INSIDE WALL TEMPERATURE', XYZ=2.220446E-16,1.0,2.87, IOR=-3/

&DEVC ID='MID_UP02_EC_TEMP30', DEPTH=0.03, QUANTITY='INSIDE WALL TEMPERATURE', XYZ=2.220446E-16,1.0,2.87, IOR=-3/

&DEVC ID='MID_UP02_EC_TEMP40', DEPTH=0.04, QUANTITY='INSIDE WALL TEMPERATURE', XYZ=2.220446E-16,1.0,2.87, IOR=-3/

&DEVC ID='MID_UP02_EC_TEMP60', DEPTH=0.06, QUANTITY='INSIDE WALL TEMPERATURE', XYZ=2.220446E-16,1.0,2.87, IOR=-3/

&DEVC ID='MID_DOWN01_EC_HRRPUA', QUANTITY='HRRPUA', XYZ=2.220446E-16,-0.5,2.87, IOR=-3/

&DEVC ID='MID_DOWN01_EC_INCHF', QUANTITY='INCIDENT HEAT FLUX', XYZ=2.220446E-16,-0.5,2.87, IOR=-3/

&DEVC ID='MID_DOWN01_EC_TEMP', QUANTITY='WALL TEMPERATURE', XYZ=2.220446E-16,-0.5,2.87, IOR=-3/

&DEVC ID='MID_DOWN01_EC_TEMP09', DEPTH=9.0E-3, QUANTITY='INSIDE WALL TEMPERATURE', XYZ=2.220446E-16,-0.5,2.87, IOR=-3/

&DEVC ID='MID_DOWN01_EC_TEMP20', DEPTH=0.02, QUANTITY='INSIDE WALL TEMPERATURE', XYZ=2.220446E-16,-0.5,2.87, IOR=-3/

&DEVC ID='MID_DOWN01_EC_TEMP30', DEPTH=0.03, QUANTITY='INSIDE WALL TEMPERATURE', XYZ=2.220446E-16,-0.5,2.87, IOR=-3/

&DEVC ID='MID_DOWN01_EC_TEMP40', DEPTH=0.04, QUANTITY='INSIDE WALL TEMPERATURE', XYZ=2.220446E-16,-0.5,2.87, IOR=-3/
```

B

```
&DEVC ID='MID_DOWN01_EC_TEMP60', DEPTH=0.06, QUANTITY='INSIDE WALL TEMPERATURE', XYZ=2.220446E-16,-0.5,2.87, IOR=-3/

&DEVC ID='MID_DOWN02_EC_HRRPUA', QUANTITY='HRRPUA', XYZ=2.220446E-16,-1.0,2.87, IOR=-3/

&DEVC ID='MID_DOWN02_EC_INCHF', QUANTITY='INCIDENT HEAT FLUX', XYZ=2.220446E-16,-1.0,2.87, IOR=-3/

&DEVC ID='MID_DOWN02_EC_TEMP', QUANTITY='WALL TEMPERATURE', XYZ=2.220446E-16,-1.0,2.87, IOR=-3/

&DEVC ID='MID_DOWN02_EC_TEMP09', DEPTH=9.0E-3, QUANTITY='INSIDE WALL TEMPERATURE', XYZ=2.220446E-16,-1.0,2.87, IOR=-3/

&DEVC ID='MID_DOWN02_EC_TEMP20', DEPTH=0.02, QUANTITY='INSIDE WALL TEMPERATURE', XYZ=2.220446E-16,-1.0,2.87, IOR=-3/

&DEVC ID='MID_DOWN02_EC_TEMP30', DEPTH=0.03, QUANTITY='INSIDE WALL TEMPERATURE', XYZ=2.220446E-16,-1.0,2.87, IOR=-3/

&DEVC ID='MID_DOWN02_EC_TEMP40', DEPTH=0.04, QUANTITY='INSIDE WALL TEMPERATURE', XYZ=2.220446E-16,-1.0,2.87, IOR=-3/

&DEVC ID='MID_DOWN02_EC_TEMP60', DEPTH=0.06, QUANTITY='INSIDE WALL TEMPERATURE', XYZ=2.220446E-16,-1.0,2.87, IOR=-3/

&DEVC ID='LEFT_UP_EC_HRRPUA', QUANTITY='HRRPUA', XYZ=1.06,1.0,2.87, IOR=-3/

&DEVC ID='LEFT_UP_EC_INCHF', QUANTITY='INCIDENT HEAT FLUX', XYZ=1.06,1.0,2.87, IOR=-3/

&DEVC ID='LEFT_UP_EC_TEMP', QUANTITY='WALL TEMPERATURE', XYZ=1.06,1.0,2.87, IOR=-3/

&DEVC ID='LEFT_UP_EC_TEMP09', DEPTH=9.0E-3, QUANTITY='INSIDE WALL TEMPERATURE', XYZ=1.06,1.0,2.87, IOR=-3/

&DEVC ID='LEFT_UP_EC_TEMP20', DEPTH=0.02, QUANTITY='INSIDE WALL TEMPERATURE', XYZ=1.06,1.0,2.87, IOR=-3/

&DEVC ID='LEFT_UP_EC_TEMP30', DEPTH=0.03, QUANTITY='INSIDE WALL TEMPERATURE', XYZ=1.06,1.0,2.87, IOR=-3/

&DEVC ID='LEFT_UP_EC_TEMP40', DEPTH=0.04, QUANTITY='INSIDE WALL TEMPERATURE', XYZ=1.06,1.0,2.87, IOR=-3/

&DEVC ID='LEFT_UP_EC_TEMP60', DEPTH=0.06, QUANTITY='INSIDE WALL TEMPERATURE', XYZ=1.06,1.0,2.87, IOR=-3/

&DEVC ID='LEFT_MID_EC_HRRPUA', QUANTITY='HRRPUA', XYZ=1.06,2.220446E-16,2.87, IOR=-3/

&DEVC ID='LEFT_MID_EC_INCHF', QUANTITY='INCIDENT HEAT FLUX', XYZ=1.06,-6.661338E-16,2.87, IOR=-3/

&DEVC ID='LEFT_MID_EC_TEMP', QUANTITY='WALL TEMPERATURE', XYZ=1.06,-6.661338E-16,2.87, IOR=-3/

&DEVC ID='LEFT_MID_EC_TEMP09', DEPTH=9.0E-3, QUANTITY='INSIDE WALL TEMPERATURE', XYZ=1.06,-6.661338E-16,2.87, IOR=-3/

&DEVC ID='LEFT_MID_EC_TEMP20', DEPTH=0.02, QUANTITY='INSIDE WALL TEMPERATURE', XYZ=1.06,2.220446E-16,2.87, IOR=-3/

&DEVC ID='LEFT_MID_EC_TEMP30', DEPTH=0.03, QUANTITY='INSIDE WALL TEMPERATURE', XYZ=1.06,2.220446E-16,2.87, IOR=-3/

&DEVC ID='LEFT_MID_EC_TEMP40', DEPTH=0.04, QUANTITY='INSIDE WALL TEMPERATURE', XYZ=1.06,2.220446E-16,2.87, IOR=-3/

&DEVC ID='LEFT_MID_EC_TEMP60', DEPTH=0.06, QUANTITY='INSIDE WALL TEMPERATURE', XYZ=1.06,2.220446E-16,2.87, IOR=-3/

&DEVC ID='LEFT_DOWN_EC_HRRPUA', QUANTITY='HRRPUA', XYZ=1.06,-1.0,2.87, IOR=-3/

&DEVC ID='LEFT_DOWN_EC_INCHF', QUANTITY='INCIDENT HEAT FLUX', XYZ=1.06,-1.0,2.87, IOR=-3/

&DEVC ID='LEFT_DOWN_EC_TEMP', QUANTITY='WALL TEMPERATURE', XYZ=1.06,-1.0,2.87, IOR=-3/

&DEVC ID='LEFT_DOWN_EC_TEMP09', DEPTH=9.0E-3, QUANTITY='INSIDE WALL TEMPERATURE', XYZ=1.06,-1.0,2.87, IOR=-3/

&DEVC ID='LEFT_DOWN_EC_TEMP20', DEPTH=0.02, QUANTITY='INSIDE WALL TEMPERATURE', XYZ=1.06,-1.0,2.87, IOR=-3/

&DEVC ID='LEFT_DOWN_EC_TEMP30', DEPTH=0.03, QUANTITY='INSIDE WALL TEMPERATURE', XYZ=1.06,-1.0,2.87, IOR=-3/

&DEVC ID='LEFT_DOWN_EC_TEMP40', DEPTH=0.04, QUANTITY='INSIDE WALL TEMPERATURE', XYZ=1.06,-1.0,2.87, IOR=-3/

&DEVC ID='LEFT_DOWN_EC_TEMP60', DEPTH=0.06, QUANTITY='INSIDE WALL TEMPERATURE', XYZ=1.06,-1.0,2.87, IOR=-3/

&DEVC ID='RIGHT_UP02_EC_HRRPUA', QUANTITY='HRRPUA', XYZ=-1.06,1.0,2.87, IOR=-3/

&DEVC ID='RIGHT_UP02_EC_INCHF', QUANTITY='INCIDENT HEAT FLUX', XYZ=-1.06,1.0,2.87, IOR=-3/

&DEVC ID='RIGHT_UP02_EC_TEMP', QUANTITY='WALL TEMPERATURE', XYZ=-1.06,1.0,2.87, IOR=-3/

&DEVC ID='RIGHT_UP02_EC_TEMP09', DEPTH=9.0E-3, QUANTITY='INSIDE WALL TEMPERATURE', XYZ=-1.06,1.0,2.87, IOR=-3/

&DEVC ID='RIGHT_UP02_EC_TEMP20', DEPTH=0.02, QUANTITY='INSIDE WALL TEMPERATURE', XYZ=-1.06,1.0,2.87, IOR=-3/

&DEVC ID='RIGHT_UP02_EC_TEMP30', DEPTH=0.03, QUANTITY='INSIDE WALL TEMPERATURE', XYZ=-1.06,1.0,2.87, IOR=-3/

&DEVC ID='RIGHT_UP02_EC_TEMP40', DEPTH=0.04, QUANTITY='INSIDE WALL TEMPERATURE', XYZ=-1.06,1.0,2.87, IOR=-3/

&DEVC ID='RIGHT_UP02_EC_TEMP60', DEPTH=0.06, QUANTITY='INSIDE WALL TEMPERATURE', XYZ=-1.06,1.0,2.87, IOR=-3/

&DEVC ID='RIGHT_UP01_EC_HRRPUA', QUANTITY='HRRPUA', XYZ=-1.06,0.5,2.87, IOR=-3/

&DEVC ID='RIGHT_UP01_EC_INCHF', QUANTITY='INCIDENT HEAT FLUX', XYZ=-1.06,0.5,2.87, IOR=-3/
```

c

```
&DEVC ID='RIGHT_UP01_EC_TEMP', QUANTITY='WALL TEMPERATURE', XYZ=-1.06,0.5,2.87, IOR=-3/

&DEVC ID='RIGHT_UP01_EC_TEMP09', DEPTH=9.0E-3, QUANTITY='INSIDE WALL TEMPERATURE', XYZ=-1.06,0.5,2.87, IOR=-3/

&DEVC ID='RIGHT_UP01_EC_TEMP20', DEPTH=0.02, QUANTITY='INSIDE WALL TEMPERATURE', XYZ=-1.06,0.5,2.87, IOR=-3/

&DEVC ID='RIGHT_UP01_EC_TEMP30', DEPTH=0.03, QUANTITY='INSIDE WALL TEMPERATURE', XYZ=-1.06,0.5,2.87, IOR=-3/

&DEVC ID='RIGHT_UP01_EC_TEMP40', DEPTH=0.04, QUANTITY='INSIDE WALL TEMPERATURE', XYZ=-1.06,0.5,2.87, IOR=-3/

&DEVC ID='RIGHT_UP01_EC_TEMP60', DEPTH=0.06, QUANTITY='INSIDE WALL TEMPERATURE', XYZ=-1.06,0.5,2.87, IOR=-3/

&DEVC ID='LEFT_EC_HRRPUA', QUANTITY='HRRPUA', XYZ=-1.06,-4.440892E-16,2.87, IOR=-3/

&DEVC ID='LEFT_EC_INCHF', QUANTITY='INCIDENT HEAT FLUX', XYZ=-1.06,-6.661338E-16,2.87, IOR=-3/

&DEVC ID='LEFT_EC_TEMP', QUANTITY='WALL TEMPERATURE', XYZ=-1.06,-6.661338E-16,2.87, IOR=-3/

&DEVC ID='LEFT_EC_TEMP09', DEPTH=9.0E-3, QUANTITY='INSIDE WALL TEMPERATURE', XYZ=-1.06,2.220446E-16,2.87, IOR=-3/

&DEVC ID='LEFT_EC_TEMP20', DEPTH=0.02, QUANTITY='INSIDE WALL TEMPERATURE', XYZ=-1.06,2.220446E-16,2.87, IOR=-3/

&DEVC ID='LEFT_EC_TEMP30', DEPTH=0.03, QUANTITY='INSIDE WALL TEMPERATURE', XYZ=-1.06,2.220446E-16,2.87, IOR=-3/

&DEVC ID='LEFT_EC_TEMP40', DEPTH=0.04, QUANTITY='INSIDE WALL TEMPERATURE', XYZ=-1.06,2.220446E-16,2.87, IOR=-3/

&DEVC ID='LEFT_EC_TEMP60', DEPTH=0.06, QUANTITY='INSIDE WALL TEMPERATURE', XYZ=-1.06,2.220446E-16,2.87, IOR=-3/

&DEVC ID='RIGHT_DOWN01_EC_HRRPUA', QUANTITY='HRRPUA', XYZ=-1.06,-0.5,2.87, IOR=-3/

&DEVC ID='RIGHT_DOWN01_EC_INCHF', QUANTITY='INCIDENT HEAT FLUX', XYZ=-1.06,-0.5,2.87, IOR=-3/

&DEVC ID='RIGHT_DOWN01_EC_TEMP', QUANTITY='WALL TEMPERATURE', XYZ=-1.06,-0.5,2.87, IOR=-3/

&DEVC ID='RIGHT_DOWN01_EC_TEMP09', DEPTH=9.0E-3, QUANTITY='INSIDE WALL TEMPERATURE', XYZ=-1.06,-0.5,2.87, IOR=-3/

&DEVC ID='RIGHT_DOWN01_EC_TEMP20', DEPTH=0.02, QUANTITY='INSIDE WALL TEMPERATURE', XYZ=-1.06,-0.5,2.87, IOR=-3/

&DEVC ID='RIGHT_DOWN01_EC_TEMP30', DEPTH=0.03, QUANTITY='INSIDE WALL TEMPERATURE', XYZ=-1.06,-0.5,2.87, IOR=-3/

&DEVC ID='RIGHT_DOWN01_EC_TEMP40', DEPTH=0.04, QUANTITY='INSIDE WALL TEMPERATURE', XYZ=-1.06,-0.5,2.87, IOR=-3/

&DEVC ID='RIGHT_DOWN01_EC_TEMP60', DEPTH=0.06, QUANTITY='INSIDE WALL TEMPERATURE', XYZ=-1.06,-0.5,2.87, IOR=-3/

&DEVC ID='RIGHT_DOWN02_EC_HRRPUA', QUANTITY='HRRPUA', XYZ=-1.06,-1.0,2.87, IOR=-3/

&DEVC ID='RIGHT_DOWN02_EC_INCHF', QUANTITY='INCIDENT HEAT FLUX', XYZ=-1.06,-1.0,2.87, IOR=-3/

&DEVC ID='RIGHT_DOWN02_EC_TEMP', QUANTITY='WALL TEMPERATURE', XYZ=-1.06,-1.0,2.87, IOR=-3/

&DEVC ID='RIGHT_DOWN02_EC_TEMP09', DEPTH=9.0E-3, QUANTITY='INSIDE WALL TEMPERATURE', XYZ=-1.06,-1.0,2.87, IOR=-3/

&DEVC ID='RIGHT_DOWN02_EC_TEMP20', DEPTH=0.02, QUANTITY='INSIDE WALL TEMPERATURE', XYZ=-1.06,-1.0,2.87, IOR=-3/

&DEVC ID='RIGHT_DOWN02_EC_TEMP30', DEPTH=0.03, QUANTITY='INSIDE WALL TEMPERATURE', XYZ=-1.06,-1.0,2.87, IOR=-3/

&DEVC ID='RIGHT_DOWN02_EC_TEMP40', DEPTH=0.04, QUANTITY='INSIDE WALL TEMPERATURE', XYZ=-1.06,-1.0,2.87, IOR=-3/

&DEVC ID='RIGHT_DOWN02_EC_TEMP60', DEPTH=0.06, QUANTITY='INSIDE WALL TEMPERATURE', XYZ=-1.06,-1.0,2.87, IOR=-3/

&DEVC ID='MID_UP02_EW_HRRPUA', QUANTITY='HRRPUA', XYZ=2.220446E-16,-1.36,2.5, IOR=2/

&DEVC ID='MID_UP02_EW_INCHF', QUANTITY='INCIDENT HEAT FLUX', XYZ=2.220446E-16,-1.36,2.5, IOR=2/

&DEVC ID='MID_UP02_EW_RADHF', QUANTITY='RADIATIVE HEAT FLUX', XYZ=2.220446E-16,-1.36,2.5, IOR=2/

&DEVC ID='MID_UP02_EW_TEMP', QUANTITY='WALL TEMPERATURE', XYZ=2.220446E-16,-1.36,2.5, IOR=2/

&DEVC ID='MID_UP02_EW_TEMP09', DEPTH=9.0E-3, QUANTITY='INSIDE WALL TEMPERATURE', XYZ=2.220446E-16,-1.36,2.5, IOR=2/

&DEVC ID='MID_UP02_EW_TEMP20', DEPTH=0.02, QUANTITY='INSIDE WALL TEMPERATURE', XYZ=2.220446E-16,-1.36,2.5, IOR=2/

&DEVC ID='MID_UP02_EW_TEMP40', DEPTH=0.04, QUANTITY='INSIDE WALL TEMPERATURE', XYZ=2.220446E-16,-1.36,2.5, IOR=2/

&DEVC ID='MID_UP02_EW_TEMP60', DEPTH=0.06, QUANTITY='INSIDE WALL TEMPERATURE', XYZ=2.220446E-16,-1.36,2.5, IOR=2/

&DEVC ID='MID_UP02_EW_TEMP80', DEPTH=0.08, QUANTITY='INSIDE WALL TEMPERATURE', XYZ=2.220446E-16,-1.36,2.5, IOR=2/

&DEVC ID='MID_UP01_EW_HRRPUA', QUANTITY='HRRPUA', XYZ=2.220446E-16,-1.36,2.05, IOR=2/

&DEVC ID='MID_UP01_EW_INCHF', QUANTITY='INCIDENT HEAT FLUX', XYZ=2.220446E-16,-1.36,2.05, IOR=2/

&DEVC ID='MID_UP01_EW_RADHF', QUANTITY='RADIATIVE HEAT FLUX', XYZ=2.220446E-16,-1.36,2.05, IOR=2/

&DEVC ID='MID_UP01_EW_TEMP', QUANTITY='WALL TEMPERATURE', XYZ=2.220446E-16,-1.36,2.05, IOR=2/
```

D

```
&DEVC ID='MID_UP01_EW_TEMP09', DEPTH=9.0E-3, QUANTITY='INSIDE WALL TEMPERATURE', XYZ=2.220446E-16,-1.36,2.05, IOR=2/

&DEVC ID='MID_UP01_EW_TEMP20', DEPTH=0.02, QUANTITY='INSIDE WALL TEMPERATURE', XYZ=2.220446E-16,-1.36,2.05, IOR=2/

&DEVC ID='MID_UP01_EW_TEMP40', DEPTH=0.04, QUANTITY='INSIDE WALL TEMPERATURE', XYZ=2.220446E-16,-1.36,2.05, IOR=2/

&DEVC ID='MID_UP01_EW_TEMP60', DEPTH=0.06, QUANTITY='INSIDE WALL TEMPERATURE', XYZ=2.220446E-16,-1.36,2.05, IOR=2/

&DEVC ID='MID_UP01_EW_TEMP80', DEPTH=0.08, QUANTITY='INSIDE WALL TEMPERATURE', XYZ=2.220446E-16,-1.36,2.05, IOR=2/

&DEVC ID='MID_MID_EW_HRRPUA', QUANTITY='HRRPUA', XYZ=2.220446E-16,-1.36,1.6, IOR=2/

&DEVC ID='MID_MID_EW_INCHF', QUANTITY='INCIDENT HEAT FLUX', XYZ=2.220446E-16,-1.36,1.6, IOR=2/

&DEVC ID='MID_MID_EW_RADHF', QUANTITY='RADIATIVE HEAT FLUX', XYZ=2.220446E-16,-1.36,1.6, IOR=2/

&DEVC ID='MID_MID_EW_TEMP', QUANTITY='WALL TEMPERATURE', XYZ=2.220446E-16,-1.36,1.6, IOR=2/

&DEVC ID='MID_MID_EW_TEMP09', DEPTH=9.0E-3, QUANTITY='INSIDE WALL TEMPERATURE', XYZ=2.220446E-16,-1.36,1.6, IOR=2/

&DEVC ID='MID_MID_EW_TEMP20', DEPTH=0.02, QUANTITY='INSIDE WALL TEMPERATURE', XYZ=2.220446E-16,-1.36,1.6, IOR=2/

&DEVC ID='MID_MID_EW_TEMP40', DEPTH=0.04, QUANTITY='INSIDE WALL TEMPERATURE', XYZ=2.220446E-16,-1.36,1.6, IOR=2/

&DEVC ID='MID_MID_EW_TEMP60', DEPTH=0.06, QUANTITY='INSIDE WALL TEMPERATURE', XYZ=2.220446E-16,-1.36,1.6, IOR=2/

&DEVC ID='MID_MID_EW_TEMP80', DEPTH=0.08, QUANTITY='INSIDE WALL TEMPERATURE', XYZ=2.220446E-16,-1.36,1.6, IOR=2/

&DEVC ID='MID_DOWN01_EW_HRRPUA', QUANTITY='HRRPUA', XYZ=2.220446E-16,-1.36,1.15, IOR=2/

&DEVC ID='MID_DOWN01_EW_INCHF', QUANTITY='INCIDENT HEAT FLUX', XYZ=2.220446E-16,-1.36,1.15, IOR=2/

&DEVC ID='MID_DOWN01_EW_RADHF', QUANTITY='RADIATIVE HEAT FLUX', XYZ=2.220446E-16,-1.36,1.15, IOR=2/

&DEVC ID='MID_DOWN01_EW_TEMP', QUANTITY='WALL TEMPERATURE', XYZ=2.220446E-16,-1.36,1.15, IOR=2/

&DEVC ID='MID_DOWN01_EW_TEMP09', DEPTH=9.0E-3, QUANTITY='INSIDE WALL TEMPERATURE', XYZ=2.220446E-16,-1.36,1.15, IOR=2/

&DEVC ID='MID_DOWN01_EW_TEMP20', DEPTH=0.02, QUANTITY='INSIDE WALL TEMPERATURE', XYZ=2.220446E-16,-1.36,1.15, IOR=2/

&DEVC ID='MID_DOWN01_EW_TEMP40', DEPTH=0.04, QUANTITY='INSIDE WALL TEMPERATURE', XYZ=2.220446E-16,-1.36,1.15, IOR=2/

&DEVC ID='MID_DOWN01_EW_TEMP60', DEPTH=0.06, QUANTITY='INSIDE WALL TEMPERATURE', XYZ=2.220446E-16,-1.36,1.15, IOR=2/

&DEVC ID='MID_DOWN01_EW_TEMP80', DEPTH=0.08, QUANTITY='INSIDE WALL TEMPERATURE', XYZ=2.220446E-16,-1.36,1.15, IOR=2/

&DEVC ID='MID_DOWN02_EW_HRRPUA', QUANTITY='HRRPUA', XYZ=2.220446E-16,-1.36,0.7, IOR=2/

&DEVC ID='MID_DOWN02_EW_INCHF', QUANTITY='INCIDENT HEAT FLUX', XYZ=2.220446E-16,-1.36,0.7, IOR=2/

&DEVC ID='MID_DOWN02_EW_RADHF', QUANTITY='RADIATIVE HEAT FLUX', XYZ=2.220446E-16,-1.36,0.7, IOR=2/

&DEVC ID='MID_DOWN02_EW_TEMP', QUANTITY='WALL TEMPERATURE', XYZ=2.220446E-16,-1.36,0.7, IOR=2/

&DEVC ID='MID_DOWN02_EW_TEMP09', DEPTH=9.0E-3, QUANTITY='INSIDE WALL TEMPERATURE', XYZ=2.220446E-16,-1.36,0.7, IOR=2/

&DEVC ID='MID_DOWN02_EW_TEMP20', DEPTH=0.02, QUANTITY='INSIDE WALL TEMPERATURE', XYZ=2.220446E-16,-1.36,0.7, IOR=2/

&DEVC ID='MID_DOWN02_EW_TEMP40', DEPTH=0.04, QUANTITY='INSIDE WALL TEMPERATURE', XYZ=2.220446E-16,-1.36,0.7, IOR=2/

&DEVC ID='MID_DOWN02_EW_TEMP60', DEPTH=0.06, QUANTITY='INSIDE WALL TEMPERATURE', XYZ=2.220446E-16,-1.36,0.7, IOR=2/

&DEVC ID='MID_DOWN02_EW_TEMP80', DEPTH=0.08, QUANTITY='INSIDE WALL TEMPERATURE', XYZ=2.220446E-16,-1.36,0.7, IOR=2/

&DEVC ID='RIGHT_UP02_EW_HRRPUA', QUANTITY='HRRPUA', XYZ=-1.06,-1.36,2.5, IOR=2/

&DEVC ID='RIGHT_UP02_EW_INCHF', QUANTITY='INCIDENT HEAT FLUX', XYZ=-1.06,-1.36,2.5, IOR=2/

&DEVC ID='RIGHT_UP02_EW_RADHF', QUANTITY='RADIATIVE HEAT FLUX', XYZ=-1.06,-1.36,2.5, IOR=2/

&DEVC ID='RIGHT_UP02_EW_TEMP', QUANTITY='WALL TEMPERATURE', XYZ=-1.06,-1.36,2.5, IOR=2/

&DEVC ID='RIGHT_UP02_EW_TEMP09', DEPTH=9.0E-3, QUANTITY='INSIDE WALL TEMPERATURE', XYZ=-1.06,-1.36,2.5, IOR=2/

&DEVC ID='RIGHT_UP02_EW_TEMP20', DEPTH=0.02, QUANTITY='INSIDE WALL TEMPERATURE', XYZ=-1.06,-1.36,2.5, IOR=2/

&DEVC ID='RIGHT_UP02_EW_TEMP40', DEPTH=0.04, QUANTITY='INSIDE WALL TEMPERATURE', XYZ=-1.06,-1.36,2.5, IOR=2/

&DEVC ID='RIGHT_UP02_EW_TEMP60', DEPTH=0.06, QUANTITY='INSIDE WALL TEMPERATURE', XYZ=-1.06,-1.36,2.5, IOR=2/

&DEVC ID='RIGHT_UP02_EW_TEMP80', DEPTH=0.08, QUANTITY='INSIDE WALL TEMPERATURE', XYZ=-1.06,-1.36,2.5, IOR=2/

&DEVC ID='RIGHT_UP01_EW_HRRPUA', QUANTITY='HRRPUA', XYZ=-1.06,-1.36,2.05, IOR=2/

&DEVC ID='RIGHT_UP01_EW_INCHF', QUANTITY='INCIDENT HEAT FLUX', XYZ=-1.06,-1.36,2.05, IOR=2/
```

E

```
&DEVC ID='RIGHT_UP01_EW_RADHF', QUANTITY='RADIATIVE HEAT FLUX', XYZ=-1.06,-1.36,2.05, IOR=2/

&DEVC ID='RIGHT_UP01_EW_TEMP', QUANTITY='WALL TEMPERATURE', XYZ=-1.06,-1.36,2.05, IOR=2/

&DEVC ID='RIGHT_UP01_EW_TEMP09', DEPTH=9.0E-3, QUANTITY='INSIDE WALL TEMPERATURE', XYZ=-1.06,-1.36,2.05, IOR=2/

&DEVC ID='RIGHT_UP01_EW_TEMP20', DEPTH=0.02, QUANTITY='INSIDE WALL TEMPERATURE', XYZ=-1.06,-1.36,2.05, IOR=2/

&DEVC ID='RIGHT_UP01_EW_TEMP40', DEPTH=0.04, QUANTITY='INSIDE WALL TEMPERATURE', XYZ=-1.06,-1.36,2.05, IOR=2/

&DEVC ID='RIGHT_UP01_EW_TEMP60', DEPTH=0.06, QUANTITY='INSIDE WALL TEMPERATURE', XYZ=-1.06,-1.36,2.05, IOR=2/

&DEVC ID='RIGHT_UP01_EW_TEMP80', DEPTH=0.08, QUANTITY='INSIDE WALL TEMPERATURE', XYZ=-1.06,-1.36,2.05, IOR=2/

&DEVC ID='RIGHT_MID_EW_HRRPUA', QUANTITY='HRRPUA', XYZ=-1.06,-1.36,1.6, IOR=2/

&DEVC ID='RIGHT_MID_EW_INCHF', QUANTITY='INCIDENT HEAT FLUX', XYZ=-1.06,-1.36,1.6, IOR=2/

&DEVC ID='RIGHT_MID_EW_RADHF', QUANTITY='RADIATIVE HEAT FLUX', XYZ=-1.06,-1.36,1.6, IOR=2/

&DEVC ID='RIGHT_MID_EW_TEMP', QUANTITY='WALL TEMPERATURE', XYZ=-1.06,-1.36,1.6, IOR=2/

&DEVC ID='RIGHT_MID_EW_TEMP09', DEPTH=9.0E-3, QUANTITY='INSIDE WALL TEMPERATURE', XYZ=-1.06,-1.36,1.6, IOR=2/

&DEVC ID='RIGHT_MID_EW_TEMP20', DEPTH=0.02, QUANTITY='INSIDE WALL TEMPERATURE', XYZ=-1.06,-1.36,1.6, IOR=2/

&DEVC ID='RIGHT_MID_EW_TEMP40', DEPTH=0.04, QUANTITY='INSIDE WALL TEMPERATURE', XYZ=-1.06,-1.36,1.6, IOR=2/

&DEVC ID='RIGHT_MID_EW_TEMP60', DEPTH=0.06, QUANTITY='INSIDE WALL TEMPERATURE', XYZ=-1.06,-1.36,1.6, IOR=2/

&DEVC ID='RIGHT_MID_EW_TEMP80', DEPTH=0.08, QUANTITY='INSIDE WALL TEMPERATURE', XYZ=-1.06,-1.36,1.6, IOR=2/

&DEVC ID='RIGHT_DOWN01_EW_HRRPUA', QUANTITY='HRRPUA', XYZ=-1.06,-1.36,1.15, IOR=2/

&DEVC ID='RIGHT_DOWN01_EW_INCHF', QUANTITY='INCIDENT HEAT FLUX', XYZ=-1.06,-1.36,1.15, IOR=2/

&DEVC ID='RIGHT_DOWN01_EW_RADHF', QUANTITY='RADIATIVE HEAT FLUX', XYZ=-1.06,-1.36,1.15, IOR=2/

&DEVC ID='RIGHT_DOWN01_EW_TEMP', QUANTITY='WALL TEMPERATURE', XYZ=-1.06,-1.36,1.15, IOR=2/

&DEVC ID='RIGHT_DOWN01_EW_TEMP09', DEPTH=9.0E-3, QUANTITY='INSIDE WALL TEMPERATURE', XYZ=-1.06,-1.36,1.15, IOR=2/

&DEVC ID='RIGHT_DOWN01_EW_TEMP20', DEPTH=0.02, QUANTITY='INSIDE WALL TEMPERATURE', XYZ=-1.06,-1.36,1.15, IOR=2/

&DEVC ID='RIGHT_DOWN01_EW_TEMP40', DEPTH=0.04, QUANTITY='INSIDE WALL TEMPERATURE', XYZ=-1.06,-1.36,1.15, IOR=2/

&DEVC ID='RIGHT_DOWN01_EW_TEMP60', DEPTH=0.06, QUANTITY='INSIDE WALL TEMPERATURE', XYZ=-1.06,-1.36,1.15, IOR=2/

&DEVC ID='RIGHT_DOWN01_EW_TEMP80', DEPTH=0.08, QUANTITY='INSIDE WALL TEMPERATURE', XYZ=-1.06,-1.36,1.15, IOR=2/

&DEVC ID='RIGHT_DOWN02_EW_HRRPUA', QUANTITY='HRRPUA', XYZ=-1.06,-1.36,0.7, IOR=2/

&DEVC ID='RIGHT_DOWN02_EW_INCHF', QUANTITY='INCIDENT HEAT FLUX', XYZ=-1.06,-1.36,0.7, IOR=2/

&DEVC ID='RIGHT_DOWN02_EW_RADHF', QUANTITY='RADIATIVE HEAT FLUX', XYZ=-1.06,-1.36,0.7, IOR=2/

&DEVC ID='RIGHT_DOWN02_EW_TEMP', QUANTITY='WALL TEMPERATURE', XYZ=-1.06,-1.36,0.7, IOR=2/

&DEVC ID='RIGHT_DOWN02_EW_TEMP09', DEPTH=9.0E-3, QUANTITY='INSIDE WALL TEMPERATURE', XYZ=-1.06,-1.36,0.7, IOR=2/

&DEVC ID='RIGHT_DOWN02_EW_TEMP20', DEPTH=0.02, QUANTITY='INSIDE WALL TEMPERATURE', XYZ=-1.06,-1.36,0.7, IOR=2/

&DEVC ID='RIGHT_DOWN02_EW_TEMP40', DEPTH=0.04, QUANTITY='INSIDE WALL TEMPERATURE', XYZ=-1.06,-1.36,0.7, IOR=2/

&DEVC ID='RIGHT_DOWN02_EW_TEMP60', DEPTH=0.06, QUANTITY='INSIDE WALL TEMPERATURE', XYZ=-1.06,-1.36,0.7, IOR=2/

&DEVC ID='RIGHT_DOWN02_EW_TEMP80', DEPTH=0.08, QUANTITY='INSIDE WALL TEMPERATURE', XYZ=-1.06,-1.36,0.7, IOR=2/

&DEVC ID='LEFT_MID_EW_HRRPUA', QUANTITY='HRRPUA', XYZ=1.06,-1.36,1.6, IOR=2/

&DEVC ID='LEFT_MID_EW_INCHF', QUANTITY='INCIDENT HEAT FLUX', XYZ=1.06,-1.36,1.6, IOR=2/

&DEVC ID='LEFT_MID_EW_RADHF', QUANTITY='RADIATIVE HEAT FLUX', XYZ=1.06,-1.36,1.6, IOR=2/

&DEVC ID='LEFT_MID_EW_TEMP', QUANTITY='WALL TEMPERATURE', XYZ=1.06,-1.36,1.6, IOR=2/

&DEVC ID='LEFT_MID_EW_TEMP09', DEPTH=9.0E-3, QUANTITY='INSIDE WALL TEMPERATURE', XYZ=1.06,-1.36,1.6, IOR=2/

&DEVC ID='LEFT_MID_EW_TEMP20', DEPTH=0.02, QUANTITY='INSIDE WALL TEMPERATURE', XYZ=1.06,-1.36,1.6, IOR=2/

&DEVC ID='LEFT_MID_EW_TEMP40', DEPTH=0.04, QUANTITY='INSIDE WALL TEMPERATURE', XYZ=1.06,-1.36,1.6, IOR=2/

&DEVC ID='LEFT_MID_EW_TEMP60', DEPTH=0.06, QUANTITY='INSIDE WALL TEMPERATURE', XYZ=1.06,-1.36,1.6, IOR=2/

&DEVC ID='LEFT_MID_EW_TEMP80', DEPTH=0.08, QUANTITY='INSIDE WALL TEMPERATURE', XYZ=1.06,-1.36,1.6, IOR=2/
```

F

```
&DEVC ID='LEFT_UP_EW_HRRPUA', QUANTITY='HRRPUA', XYZ=1.06,-1.36,2.5, IOR=2/

&DEVC ID='LEFT_UP_EW_INCHF', QUANTITY='INCIDENT HEAT FLUX', XYZ=1.06,-1.36,2.5, IOR=2/

&DEVC ID='LEFT_UP_EW_RADHF', QUANTITY='RADIATIVE HEAT FLUX', XYZ=1.06,-1.36,2.5, IOR=2/

&DEVC ID='LEFT_UP_EW_TEMP', QUANTITY='WALL TEMPERATURE', XYZ=1.06,-1.36,2.5, IOR=2/

&DEVC ID='LEFT_UP_EW_TEMP09', DEPTH=9.0E-3, QUANTITY='INSIDE WALL TEMPERATURE', XYZ=1.06,-1.36,2.5, IOR=2/

&DEVC ID='LEFT_UP_EW_TEMP20', DEPTH=0.02, QUANTITY='INSIDE WALL TEMPERATURE', XYZ=1.06,-1.36,2.5, IOR=2/

&DEVC ID='LEFT_UP_EW_TEMP40', DEPTH=0.04, QUANTITY='INSIDE WALL TEMPERATURE', XYZ=1.06,-1.36,2.5, IOR=2/

&DEVC ID='LEFT_UP_EW_TEMP60', DEPTH=0.06, QUANTITY='INSIDE WALL TEMPERATURE', XYZ=1.06,-1.36,2.5, IOR=2/

&DEVC ID='LEFT_UP_EW_TEMP80', DEPTH=0.08, QUANTITY='INSIDE WALL TEMPERATURE', XYZ=1.06,-1.36,2.5, IOR=2/

&DEVC ID='LEFT_DOWN_EW_HRRPUA', QUANTITY='HRRPUA', XYZ=1.06,-1.36,0.7, IOR=2/

&DEVC ID='LEFT_DOWN_EW_INCHF', QUANTITY='INCIDENT HEAT FLUX', XYZ=1.06,-1.36,0.7, IOR=2/

&DEVC ID='LEFT_DOWN_EW_RADHF', QUANTITY='RADIATIVE HEAT FLUX', XYZ=1.06,-1.36,0.7, IOR=2/

&DEVC ID='LEFT_DOWN_EW_TEMP', QUANTITY='WALL TEMPERATURE', XYZ=1.06,-1.36,0.7, IOR=2/

&DEVC ID='LEFT_DOWN_EW_TEMP09', DEPTH=9.0E-3, QUANTITY='INSIDE WALL TEMPERATURE', XYZ=1.06,-1.36,0.7, IOR=2/

&DEVC ID='LEFT_DOWN_EW_TEMP20', DEPTH=0.02, QUANTITY='INSIDE WALL TEMPERATURE', XYZ=1.06,-1.36,0.7, IOR=2/

&DEVC ID='LEFT_DOWN_EW_TEMP40', DEPTH=0.04, QUANTITY='INSIDE WALL TEMPERATURE', XYZ=1.06,-1.36,0.7, IOR=2/

&DEVC ID='LEFT_DOWN_EW_TEMP60', DEPTH=0.06, QUANTITY='INSIDE WALL TEMPERATURE', XYZ=1.06,-1.36,0.7, IOR=2/

&DEVC ID='LEFT_DOWN_EW_TEMP80', DEPTH=0.08, QUANTITY='INSIDE WALL TEMPERATURE', XYZ=1.06,-1.36,0.7, IOR=2/

&DEVC ID='MID_LEN_HRRPUA', QUANTITY='HRRPUA', XYZ=1.36,0.0,1.485, IOR=-1/

&DEVC ID='MID_LEN_INCHF', QUANTITY='INCIDENT HEAT FLUX', XYZ=1.36,0.0,1.485, IOR=-1/

&DEVC ID='MID_LEN_RADHF', QUANTITY='RADIATIVE HEAT FLUX', XYZ=1.36,0.0,1.485, IOR=-1/

&DEVC ID='MID_LEN_TEMP', QUANTITY='WALL TEMPERATURE', XYZ=1.36,2.220446E-16,1.485, IOR=-1/

&DEVC ID='MID_LEN_TEMP25', DEPTH=0.025, QUANTITY='INSIDE WALL TEMPERATURE', XYZ=1.36,2.220446E-16,1.485, IOR=-1/

&DEVC ID='MID_LEN_TEMP45', DEPTH=0.045, QUANTITY='INSIDE WALL TEMPERATURE', XYZ=1.36,2.220446E-16,1.485, IOR=-1/

&DEVC ID='MID_LEN_TEMP65', DEPTH=0.065, QUANTITY='INSIDE WALL TEMPERATURE', XYZ=1.36,2.220446E-16,1.485, IOR=-1/

&DEVC ID='MID_LEN_TEMP85', DEPTH=0.085, QUANTITY='INSIDE WALL TEMPERATURE', XYZ=1.36,2.220446E-16,1.485, IOR=-1/

&DEVC ID='MID_LEN_TEMP105', DEPTH=0.105, QUANTITY='INSIDE WALL TEMPERATURE', XYZ=1.36,2.220446E-16,1.485, IOR=-1/

&DEVC ID='LEFT_LEN_HRRPUA', QUANTITY='HRRPUA', XYZ=1.36,0.8875,1.485, IOR=-1/

&DEVC ID='LEFT_LEN_INCHF', QUANTITY='INCIDENT HEAT FLUX', XYZ=1.36,0.8875,1.485, IOR=-1/

&DEVC ID='LEFT_LEN_RADHF', QUANTITY='RADIATIVE HEAT FLUX', XYZ=1.36,0.8875,1.485, IOR=-1/

&DEVC ID='LEFT_LEN_TEMP', QUANTITY='WALL TEMPERATURE', XYZ=1.36,0.8875,1.485, IOR=-1/

&DEVC ID='LEFT_LEN_TEMP25', DEPTH=0.025, QUANTITY='INSIDE WALL TEMPERATURE', XYZ=1.36,0.8875,1.485, IOR=-1/

&DEVC ID='LEFT_LEN_TEMP45', DEPTH=0.045, QUANTITY='INSIDE WALL TEMPERATURE', XYZ=1.36,0.8875,1.485, IOR=-1/

&DEVC ID='LEFT_LEN_TEMP65', DEPTH=0.065, QUANTITY='INSIDE WALL TEMPERATURE', XYZ=1.36,0.8875,1.485, IOR=-1/

&DEVC ID='LEFT_LEN_TEMP85', DEPTH=0.085, QUANTITY='INSIDE WALL TEMPERATURE', XYZ=1.36,0.8875,1.485, IOR=-1/

&DEVC ID='LEFT_LEN_TEMP105', DEPTH=0.105, QUANTITY='INSIDE WALL TEMPERATURE', XYZ=1.36,0.8875,1.485, IOR=-1/

&DEVC ID='RIGHT_LEN_HRRPUA', QUANTITY='HRRPUA', XYZ=1.36,-0.8875,1.485, IOR=-1/

&DEVC ID='RIGHT_LEN_INCHF', QUANTITY='INCIDENT HEAT FLUX', XYZ=1.36,-0.8875,1.485, IOR=-1/

&DEVC ID='RIGHT_LEN_RADHF', QUANTITY='RADIATIVE HEAT FLUX', XYZ=1.36,-0.8875,1.485, IOR=-1/

&DEVC ID='RIGHT_LEN_TEMP', QUANTITY='WALL TEMPERATURE', XYZ=1.36,-0.8875,1.485, IOR=-1/

&DEVC ID='RIGHT_LEN_TEMP25', DEPTH=0.025, QUANTITY='INSIDE WALL TEMPERATURE', XYZ=1.36,-0.8875,1.485, IOR=-1/

&DEVC ID='RIGHT_LEN_TEMP45', DEPTH=0.045, QUANTITY='INSIDE WALL TEMPERATURE', XYZ=1.36,-0.8875,1.485, IOR=-1/

&DEVC ID='RIGHT_LEN_TEMP65', DEPTH=0.065, QUANTITY='INSIDE WALL TEMPERATURE', XYZ=1.36,-0.8875,1.485, IOR=-1/
```

G

```
&DEVC ID='RIGHT_LEN_TEMP85', DEPTH=0.085, QUANTITY='INSIDE WALL TEMPERATURE', XYZ=1.36,-0.8875,1.485, IOR=-1/

&DEVC ID='RIGHT_LEN_TEMP105', DEPTH=0.105, QUANTITY='INSIDE WALL TEMPERATURE', XYZ=1.36,-0.8875,1.485, IOR=-1/

&DEVC ID='UP_LEN_HRRPUA', QUANTITY='HRRPUA', XYZ=1.36,0.0,2.3825, IOR=-1/

&DEVC ID='UP_LEN_INCHF', QUANTITY='INCIDENT HEAT FLUX', XYZ=1.36,0.0,2.3825, IOR=-1/

&DEVC ID='UP_LEN_RADHF', QUANTITY='RADIATIVE HEAT FLUX', XYZ=1.36,0.0,2.3825, IOR=-1/

&DEVC ID='UP_LEN_TEMP', QUANTITY='WALL TEMPERATURE', XYZ=1.36,2.220446E-16,2.3825, IOR=-1/

&DEVC ID='UP_LEN_TEMP25', DEPTH=0.025, QUANTITY='INSIDE WALL TEMPERATURE', XYZ=1.36,2.220446E-16,2.3825, IOR=-1/

&DEVC ID='UP_LEN_TEMP45', DEPTH=0.045, QUANTITY='INSIDE WALL TEMPERATURE', XYZ=1.36,2.220446E-16,2.3825, IOR=-1/

&DEVC ID='UP_LEN_TEMP65', DEPTH=0.065, QUANTITY='INSIDE WALL TEMPERATURE', XYZ=1.36,2.220446E-16,2.3825, IOR=-1/

&DEVC ID='UP_LEN_TEMP85', DEPTH=0.085, QUANTITY='INSIDE WALL TEMPERATURE', XYZ=1.36,2.220446E-16,2.3825, IOR=-1/

&DEVC ID='UP_LEN_TEMP105', DEPTH=0.105, QUANTITY='INSIDE WALL TEMPERATURE', XYZ=1.36,2.220446E-16,2.3825, IOR=-1/

&DEVC ID='DOWN_LEN_HRRPUA', QUANTITY='HRRPUA', XYZ=1.36,0.0,0.5875, IOR=-1/

&DEVC ID='DOWN_LEN_INCHF', QUANTITY='INCIDENT HEAT FLUX', XYZ=1.36,0.0,0.5875, IOR=-1/

&DEVC ID='DOWN_LEN_RADHF', QUANTITY='RADIATIVE HEAT FLUX', XYZ=1.36,0.0,0.5875, IOR=-1/

&DEVC ID='DOWN_LEN_TEMP', QUANTITY='WALL TEMPERATURE', XYZ=1.36,0.0,0.5875, IOR=-1/

&DEVC ID='DOWN_LEN_TEMP25', DEPTH=0.025, QUANTITY='INSIDE WALL TEMPERATURE', XYZ=1.36,2.220446E-16,0.5875, IOR=-1/

&DEVC ID='DOWN_LEN_TEMP45', DEPTH=0.045, QUANTITY='INSIDE WALL TEMPERATURE', XYZ=1.36,2.220446E-16,0.5875, IOR=-1/

&DEVC ID='DOWN_LEN_TEMP65', DEPTH=0.065, QUANTITY='INSIDE WALL TEMPERATURE', XYZ=1.36,2.220446E-16,0.5875, IOR=-1/

&DEVC ID='DOWN_LEN_TEMP85', DEPTH=0.085, QUANTITY='INSIDE WALL TEMPERATURE', XYZ=1.36,2.220446E-16,0.5875, IOR=-1/

&DEVC ID='DOWN_LEN_TEMP105', DEPTH=0.105, QUANTITY='INSIDE WALL TEMPERATURE', XYZ=1.36,2.220446E-16,0.5875, IOR=-1/

&DEVC ID='MID_REN_HRRPUA', QUANTITY='HRRPUA', XYZ=-1.36,0.0,1.485, IOR=1/

&DEVC ID='MID_REN_INCHF', QUANTITY='INCIDENT HEAT FLUX', XYZ=-1.36,0.0,1.485, IOR=1/

&DEVC ID='MID_REN_RADHF', QUANTITY='RADIATIVE HEAT FLUX', XYZ=-1.36,0.0,1.485, IOR=1/

&DEVC ID='MID_REN_TEMP', QUANTITY='WALL TEMPERATURE', XYZ=-1.36,0.0,1.485, IOR=1/

&DEVC ID='MID_REN_TEMP25', DEPTH=0.025, QUANTITY='INSIDE WALL TEMPERATURE', XYZ=-1.36,2.220446E-16,1.485, IOR=1/

&DEVC ID='MID_REN_TEMP45', DEPTH=0.045, QUANTITY='INSIDE WALL TEMPERATURE', XYZ=-1.36,2.220446E-16,1.485, IOR=1/

&DEVC ID='MID_REN_TEMP65', DEPTH=0.065, QUANTITY='INSIDE WALL TEMPERATURE', XYZ=-1.36,2.220446E-16,1.485, IOR=1/

&DEVC ID='MID_REN_TEMP85', DEPTH=0.085, QUANTITY='INSIDE WALL TEMPERATURE', XYZ=-1.36,2.220446E-16,1.485, IOR=1/

&DEVC ID='MID_REN_TEMP105', DEPTH=0.105, QUANTITY='INSIDE WALL TEMPERATURE', XYZ=-1.36,2.220446E-16,1.485, IOR=1/

&DEVC ID='RIGHT_REN_HRRPUA', QUANTITY='HRRPUA', XYZ=-1.36,0.8875,1.485, IOR=1/

&DEVC ID='RIGHT_REN_INCHF', QUANTITY='INCIDENT HEAT FLUX', XYZ=-1.36,0.8875,1.485, IOR=1/

&DEVC ID='RIGHT_REN_RADHF', QUANTITY='RADIATIVE HEAT FLUX', XYZ=-1.36,0.8875,1.485, IOR=1/

&DEVC ID='RIGHT_REN_TEMP', QUANTITY='WALL TEMPERATURE', XYZ=-1.36,0.8875,1.485, IOR=1/

&DEVC ID='RIGHT_REN_TEMP25', DEPTH=0.025, QUANTITY='INSIDE WALL TEMPERATURE', XYZ=-1.36,0.8875,1.485, IOR=1/

&DEVC ID='RIGHT_REN_TEMP45', DEPTH=0.045, QUANTITY='INSIDE WALL TEMPERATURE', XYZ=-1.36,0.8875,1.485, IOR=1/

&DEVC ID='RIGHT_REN_TEMP65', DEPTH=0.065, QUANTITY='INSIDE WALL TEMPERATURE', XYZ=-1.36,0.8875,1.485, IOR=1/

&DEVC ID='RIGHT_REN_TEMP85', DEPTH=0.085, QUANTITY='INSIDE WALL TEMPERATURE', XYZ=-1.36,0.8875,1.485, IOR=1/

&DEVC ID='RIGHT_REN_TEMP105', DEPTH=0.105, QUANTITY='INSIDE WALL TEMPERATURE', XYZ=-1.36,0.8875,1.485, IOR=1/

&DEVC ID='LEFT_REN_HRRPUA', QUANTITY='HRRPUA', XYZ=-1.36,-0.8875,1.485, IOR=1/

&DEVC ID='LEFT_REN_INCHF', QUANTITY='INCIDENT HEAT FLUX', XYZ=-1.36,-0.8875,1.485, IOR=1/

&DEVC ID='LEFT_REN_RADHF', QUANTITY='RADIATIVE HEAT FLUX', XYZ=-1.36,-0.8875,1.485, IOR=1/

&DEVC ID='LEFT_REN_TEMP', QUANTITY='WALL TEMPERATURE', XYZ=-1.36,-0.8875,1.485, IOR=1/

&DEVC ID='LEFT_REN_TEMP25', DEPTH=0.025, QUANTITY='INSIDE WALL TEMPERATURE', XYZ=-1.36,-0.8875,1.485, IOR=1/
```

H

```
&DEVC ID='LEFT_REN_TEMP45', DEPTH=0.045, QUANTITY='INSIDE WALL TEMPERATURE', XYZ=-1.36,-0.8875,1.485, IOR=1/

&DEVC ID='LEFT_REN_TEMP65', DEPTH=0.065, QUANTITY='INSIDE WALL TEMPERATURE', XYZ=-1.36,-0.8875,1.485, IOR=1/

&DEVC ID='LEFT_REN_TEMP85', DEPTH=0.085, QUANTITY='INSIDE WALL TEMPERATURE', XYZ=-1.36,-0.8875,1.485, IOR=1/

&DEVC ID='LEFT_REN_TEMP105', DEPTH=0.105, QUANTITY='INSIDE WALL TEMPERATURE', XYZ=-1.36,-0.8875,1.485, IOR=1/

&DEVC ID='UP_REN_HRRPUA', QUANTITY='HRRPUA', XYZ=-1.36,0.0,2.3825, IOR=1/

&DEVC ID='UP_REN_INCHF', QUANTITY='INCIDENT HEAT FLUX', XYZ=-1.36,0.0,2.3825, IOR=1/

&DEVC ID='UP_REN_RADHF', QUANTITY='RADIATIVE HEAT FLUX', XYZ=-1.36,0.0,2.3825, IOR=1/

&DEVC ID='UP_REN_TEMP', QUANTITY='WALL TEMPERATURE', XYZ=-1.36,0.0,2.3825, IOR=1/

&DEVC ID='UP_REN_TEMP25', DEPTH=0.025, QUANTITY='INSIDE WALL TEMPERATURE', XYZ=-1.36,2.220446E-16,2.3825, IOR=1/

&DEVC ID='UP_REN_TEMP45', DEPTH=0.045, QUANTITY='INSIDE WALL TEMPERATURE', XYZ=-1.36,2.220446E-16,2.3825, IOR=1/

&DEVC ID='UP_REN_TEMP65', DEPTH=0.065, QUANTITY='INSIDE WALL TEMPERATURE', XYZ=-1.36,2.220446E-16,2.3825, IOR=1/

&DEVC ID='UP_REN_TEMP85', DEPTH=0.085, QUANTITY='INSIDE WALL TEMPERATURE', XYZ=-1.36,2.220446E-16,2.3825, IOR=1/

&DEVC ID='UP_REN_TEMP105', DEPTH=0.105, QUANTITY='INSIDE WALL TEMPERATURE', XYZ=-1.36,2.220446E-16,2.3825, IOR=1/

&DEVC ID='DOWN_REN_HRRPUA', QUANTITY='HRRPUA', XYZ=-1.36,0.0,0.5875, IOR=1/

&DEVC ID='DOWN_REN_INCHF', QUANTITY='INCIDENT HEAT FLUX', XYZ=-1.36,0.0,0.5875, IOR=1/

&DEVC ID='DOWN_REN_RADHF', QUANTITY='RADIATIVE HEAT FLUX', XYZ=-1.36,0.0,0.5875, IOR=1/

&DEVC ID='DOWN_REN_TEMP', QUANTITY='WALL TEMPERATURE', XYZ=-1.36,0.0,0.5875, IOR=1/

&DEVC ID='DOWN_REN_TEMP25', DEPTH=0.025, QUANTITY='INSIDE WALL TEMPERATURE', XYZ=-1.36,2.220446E-16,0.5875, IOR=1/

&DEVC ID='DOWN_REN_TEMP45', DEPTH=0.045, QUANTITY='INSIDE WALL TEMPERATURE', XYZ=-1.36,2.220446E-16,0.5875, IOR=1/

&DEVC ID='DOWN_REN_TEMP65', DEPTH=0.065, QUANTITY='INSIDE WALL TEMPERATURE', XYZ=-1.36,2.220446E-16,0.5875, IOR=1/

&DEVC ID='DOWN_REN_TEMP85', DEPTH=0.085, QUANTITY='INSIDE WALL TEMPERATURE', XYZ=-1.36,2.220446E-16,0.5875, IOR=1/

&DEVC ID='DOWN_REN_TEMP105', DEPTH=0.105, QUANTITY='INSIDE WALL TEMPERATURE', XYZ=-1.36,2.220446E-16,0.5875, IOR=1/

&DEVC ID='MID_UP_GAS_TEMP270', QUANTITY='TEMPERATURE', XYZ=2.220446E-16,-1.075,2.7/

&DEVC ID='MID_UP_GAS_TEMP220', QUANTITY='TEMPERATURE', XYZ=2.220446E-16,-1.075,2.2/

&DEVC ID='MID_UP_GAS_TEMP170', QUANTITY='TEMPERATURE', XYZ=2.220446E-16,-1.075,1.7/

&DEVC ID='MID_UP_GAS_TEMP120', QUANTITY='TEMPERATURE', XYZ=2.220446E-16,-1.075,1.2/

&DEVC ID='MID_UP_GAS_TEMP070', QUANTITY='TEMPERATURE', XYZ=2.220446E-16,-1.075,0.7/

&DEVC ID='MID_DOWN_GAS_TEMP270', QUANTITY='TEMPERATURE', XYZ=2.220446E-16,1.075,2.7/

&DEVC ID='MID_DOWN_GAS_TEMP220', QUANTITY='TEMPERATURE', XYZ=2.220446E-16,1.075,2.2/

&DEVC ID='MID_DOWN_GAS_TEMP170', QUANTITY='TEMPERATURE', XYZ=2.220446E-16,1.075,1.7/

&DEVC ID='MID_DOWN_GAS_TEMP120', QUANTITY='TEMPERATURE', XYZ=2.220446E-16,1.075,1.2/

&DEVC ID='MID_DOWN_GAS_TEMP070', QUANTITY='TEMPERATURE', XYZ=2.220446E-16,1.075,0.7/

&DEVC ID='MID_MID_GAS_TEMP270', QUANTITY='TEMPERATURE', XYZ=2.220446E-16,0.0,2.7/

&DEVC ID='MID_MID_GAS_TEMP220', QUANTITY='TEMPERATURE', XYZ=2.220446E-16,0.0,2.2/

&DEVC ID='MID_MID_GAS_TEMP170', QUANTITY='TEMPERATURE', XYZ=2.220446E-16,0.0,1.7/

&DEVC ID='MID_MID_GAS_TEMP120', QUANTITY='TEMPERATURE', XYZ=2.220446E-16,0.0,1.2/

&DEVC ID='MID_MID_GAS_TEMP070', QUANTITY='TEMPERATURE', XYZ=2.220446E-16,0.0,0.7/

&DEVC ID='LEFT_UP_GAS_TEMP270', QUANTITY='TEMPERATURE', XYZ=1.075,-1.075,2.7/

&DEVC ID='LEFT_UP_GAS_TEMP220', QUANTITY='TEMPERATURE', XYZ=1.075,-1.075,2.2/

&DEVC ID='LEFT_UP_GAS_TEMP170', QUANTITY='TEMPERATURE', XYZ=1.075,-1.075,1.7/

&DEVC ID='LEFT_UP_GAS_TEMP120', QUANTITY='TEMPERATURE', XYZ=1.075,-1.075,1.2/

&DEVC ID='LEFT_UP_GAS_TEMP070', QUANTITY='TEMPERATURE', XYZ=1.075,-1.075,0.7/

&DEVC ID='LEFT_MID_GAS_TEMP270', QUANTITY='TEMPERATURE', XYZ=1.075,0.0,2.7/
```

I

```
&DEVC ID='LEFT_MID_GAS_TEMP220', QUANTITY='TEMPERATURE', XYZ=1.075,0.0,2.2/

&DEVC ID='LEFT_MID_GAS_TEMP170', QUANTITY='TEMPERATURE', XYZ=1.075,0.0,1.7/

&DEVC ID='LEFT_MID_GAS_TEMP120', QUANTITY='TEMPERATURE', XYZ=1.075,0.0,1.2/

&DEVC ID='LEFT_MID_GAS_TEMP070', QUANTITY='TEMPERATURE', XYZ=1.075,0.0,0.7/

&DEVC ID='LEFT_DOWN_GAS_TEMP270', QUANTITY='TEMPERATURE', XYZ=1.075,1.075,2.7/

&DEVC ID='LEFT_DOWN_GAS_TEMP220', QUANTITY='TEMPERATURE', XYZ=1.075,1.075,2.2/

&DEVC ID='LEFT_DOWN_GAS_TEMP170', QUANTITY='TEMPERATURE', XYZ=1.075,1.075,1.7/

&DEVC ID='LEFT_DOWN_GAS_TEMP120', QUANTITY='TEMPERATURE', XYZ=1.075,1.075,1.2/

&DEVC ID='LEFT_DOWN_GAS_TEMP070', QUANTITY='TEMPERATURE', XYZ=1.075,1.075,0.7/

&DEVC ID='RIGHT_MID_GAS_TEMP270', QUANTITY='TEMPERATURE', XYZ=-1.075,0.0,2.7/

&DEVC ID='RIGHT_MID_GAS_TEMP220', QUANTITY='TEMPERATURE', XYZ=-1.075,0.0,2.2/

&DEVC ID='RIGHT_MID_GAS_TEMP170', QUANTITY='TEMPERATURE', XYZ=-1.075,0.0,1.7/

&DEVC ID='RIGHT_MID_GAS_TEMP120', QUANTITY='TEMPERATURE', XYZ=-1.075,0.0,1.2/

&DEVC ID='RIGHT_MID_GAS_TEMP070', QUANTITY='TEMPERATURE', XYZ=-1.075,0.0,0.7/

&DEVC ID='RIGHT_UP_GAS_TEMP270', QUANTITY='TEMPERATURE', XYZ=-1.075,-1.075,2.7/

&DEVC ID='RIGHT_UP_GAS_TEMP220', QUANTITY='TEMPERATURE', XYZ=-1.075,-1.075,2.2/

&DEVC ID='RIGHT_UP_GAS_TEMP170', QUANTITY='TEMPERATURE', XYZ=-1.075,-1.075,1.7/

&DEVC ID='RIGHT_UP_GAS_TEMP120', QUANTITY='TEMPERATURE', XYZ=-1.075,-1.075,1.2/

&DEVC ID='RIGHT_UP_GAS_TEMP070', QUANTITY='TEMPERATURE', XYZ=-1.075,-1.075,0.7/

&DEVC ID='RIGHT_DOWN_GAS_TEMP270', QUANTITY='TEMPERATURE', XYZ=-1.075,1.075,2.7/

&DEVC ID='RIGHT_DOWN_GAS_TEMP220', QUANTITY='TEMPERATURE', XYZ=-1.075,1.075,2.2/

&DEVC ID='RIGHT_DOWN_GAS_TEMP170', QUANTITY='TEMPERATURE', XYZ=-1.075,1.075,1.7/

&DEVC ID='RIGHT_DOWN_GAS_TEMP120', QUANTITY='TEMPERATURE', XYZ=-1.075,1.075,1.2/

&DEVC ID='RIGHT_DOWN_GAS_TEMP070', QUANTITY='TEMPERATURE', XYZ=-1.075,1.075,0.7/


&MATL ID='SPRUCE CEILING',

    FYI='Hostikka - Nordic structural timber',

    SPECIFIC_HEAT_RAMP='SPRUCE CEILING_SPECIFIC_HEAT_RAMP',

    CONDUCTIVITY=0.09,

    DENSITY=408.0,

    N_REACTIONS=1,

    HEAT_OF_REACTION=19.0,

    MATL_ID(1,1)='CHAR',

    NU_MATL(1,1)=0.16,

    SPEC_ID(1,1)='CEILING PYROLYZATE',

    NU_SPEC(1,1)=0.84,

    N_S=1.89,

    A=2.19311E+11,

    E=1.905E+5/

&RAMP ID='SPRUCE CEILING_SPECIFIC_HEAT_RAMP', T=30.0, F=0.92/

&RAMP ID='SPRUCE CEILING_SPECIFIC_HEAT_RAMP', T=50.0, F=1.008/

&RAMP ID='SPRUCE CEILING_SPECIFIC_HEAT_RAMP', T=70.0, F=1.096/

&RAMP ID='SPRUCE CEILING_SPECIFIC_HEAT_RAMP', T=90.0, F=1.184/
```

J

```
&RAMP ID='SPRUCE CEILING_SPECIFIC_HEAT_RAMP', T=110.0, F=1.272/

&RAMP ID='SPRUCE CEILING_SPECIFIC_HEAT_RAMP', T=130.0, F=1.36/

&RAMP ID='SPRUCE CEILING_SPECIFIC_HEAT_RAMP', T=150.0, F=1.448/

&RAMP ID='SPRUCE CEILING_SPECIFIC_HEAT_RAMP', T=170.0, F=1.536/

&RAMP ID='SPRUCE CEILING_SPECIFIC_HEAT_RAMP', T=190.0, F=1.624/

&RAMP ID='SPRUCE CEILING_SPECIFIC_HEAT_RAMP', T=210.0, F=1.712/

&RAMP ID='SPRUCE CEILING_SPECIFIC_HEAT_RAMP', T=230.0, F=1.8/

&RAMP ID='SPRUCE CEILING_SPECIFIC_HEAT_RAMP', T=250.0, F=1.888/

&RAMP ID='SPRUCE CEILING_SPECIFIC_HEAT_RAMP', T=270.0, F=1.976/

&RAMP ID='SPRUCE CEILING_SPECIFIC_HEAT_RAMP', T=290.0, F=2.064/

&RAMP ID='SPRUCE CEILING_SPECIFIC_HEAT_RAMP', T=310.0, F=2.152/

&RAMP ID='SPRUCE CEILING_SPECIFIC_HEAT_RAMP', T=330.0, F=2.24/

&RAMP ID='SPRUCE CEILING_SPECIFIC_HEAT_RAMP', T=350.0, F=2.328/

&RAMP ID='SPRUCE CEILING_SPECIFIC_HEAT_RAMP', T=370.0, F=2.416/

&RAMP ID='SPRUCE CEILING_SPECIFIC_HEAT_RAMP', T=390.0, F=2.504/

&RAMP ID='SPRUCE CEILING_SPECIFIC_HEAT_RAMP', T=410.0, F=2.592/

&RAMP ID='SPRUCE CEILING_SPECIFIC_HEAT_RAMP', T=430.0, F=2.68/

&RAMP ID='SPRUCE CEILING_SPECIFIC_HEAT_RAMP', T=450.0, F=2.768/

&RAMP ID='SPRUCE CEILING_SPECIFIC_HEAT_RAMP', T=470.0, F=2.856/

&RAMP ID='SPRUCE CEILING_SPECIFIC_HEAT_RAMP', T=490.0, F=2.944/

&RAMP ID='SPRUCE CEILING_SPECIFIC_HEAT_RAMP', T=510.0, F=3.032/

&RAMP ID='SPRUCE CEILING_SPECIFIC_HEAT_RAMP', T=530.0, F=3.12/

&RAMP ID='SPRUCE CEILING_SPECIFIC_HEAT_RAMP', T=550.0, F=3.208/

&RAMP ID='SPRUCE CEILING_SPECIFIC_HEAT_RAMP', T=570.0, F=3.296/

&RAMP ID='SPRUCE CEILING_SPECIFIC_HEAT_RAMP', T=590.0, F=3.384/

&RAMP ID='SPRUCE CEILING_SPECIFIC_HEAT_RAMP', T=610.0, F=3.472/

&RAMP ID='SPRUCE CEILING_SPECIFIC_HEAT_RAMP', T=630.0, F=3.56/

&RAMP ID='SPRUCE CEILING_SPECIFIC_HEAT_RAMP', T=650.0, F=3.648/

&RAMP ID='SPRUCE CEILING_SPECIFIC_HEAT_RAMP', T=670.0, F=3.736/

&RAMP ID='SPRUCE CEILING_SPECIFIC_HEAT_RAMP', T=690.0, F=3.824/

&RAMP ID='SPRUCE CEILING_SPECIFIC_HEAT_RAMP', T=710.0, F=3.912/

&RAMP ID='SPRUCE CEILING_SPECIFIC_HEAT_RAMP', T=730.0, F=4.0/

&RAMP ID='SPRUCE CEILING_SPECIFIC_HEAT_RAMP', T=750.0, F=4.088/

&RAMP ID='SPRUCE CEILING_SPECIFIC_HEAT_RAMP', T=770.0, F=4.176/

&RAMP ID='SPRUCE CEILING_SPECIFIC_HEAT_RAMP', T=790.0, F=4.264/

&RAMP ID='SPRUCE CEILING_SPECIFIC_HEAT_RAMP', T=810.0, F=4.352/

&MATL ID='CHAR',

    FYI='Hostikka - Nordic structural timber',

    SPECIFIC_HEAT_RAMP='CHAR_SPECIFIC_HEAT_RAMP',

    CONDUCTIVITY=0.22,

    DENSITY=59.0,

    EMISSIVITY=0.85/

&RAMP ID='CHAR_SPECIFIC_HEAT_RAMP', T=0.0, F=0.545879/
```

K

```
&RAMP ID='CHAR_SPECIFIC_HEAT_RAMP', T=50.0, F=0.843743/

&RAMP ID='CHAR_SPECIFIC_HEAT_RAMP', T=100.0, F=1.036761/

&RAMP ID='CHAR_SPECIFIC_HEAT_RAMP', T=150.0, F=1.171407/

&RAMP ID='CHAR_SPECIFIC_HEAT_RAMP', T=200.0, F=1.270994/

&RAMP ID='CHAR_SPECIFIC_HEAT_RAMP', T=250.0, F=1.348258/

&RAMP ID='CHAR_SPECIFIC_HEAT_RAMP', T=300.0, F=1.410638/

&RAMP ID='CHAR_SPECIFIC_HEAT_RAMP', T=350.0, F=1.462712/

&RAMP ID='CHAR_SPECIFIC_HEAT_RAMP', T=400.0, F=1.507426/

&RAMP ID='CHAR_SPECIFIC_HEAT_RAMP', T=450.0, F=1.546742/

&RAMP ID='CHAR_SPECIFIC_HEAT_RAMP', T=500.0, F=1.582011/

&RAMP ID='CHAR_SPECIFIC_HEAT_RAMP', T=550.0, F=1.614186/

&RAMP ID='CHAR_SPECIFIC_HEAT_RAMP', T=600.0, F=1.643955/

&RAMP ID='CHAR_SPECIFIC_HEAT_RAMP', T=650.0, F=1.671824/

&RAMP ID='CHAR_SPECIFIC_HEAT_RAMP', T=700.0, F=1.698173/

&RAMP ID='CHAR_SPECIFIC_HEAT_RAMP', T=750.0, F=1.723293/

&RAMP ID='CHAR_SPECIFIC_HEAT_RAMP', T=800.0, F=1.747407/

&RAMP ID='CHAR_SPECIFIC_HEAT_RAMP', T=850.0, F=1.770691/

&RAMP ID='CHAR_SPECIFIC_HEAT_RAMP', T=900.0, F=1.793281/

&RAMP ID='CHAR_SPECIFIC_HEAT_RAMP', T=950.0, F=1.815291/

&RAMP ID='CHAR_SPECIFIC_HEAT_RAMP', T=1000.0, F=1.836808/

&RAMP ID='CHAR_SPECIFIC_HEAT_RAMP', T=1050.0, F=1.857907/

&RAMP ID='CHAR_SPECIFIC_HEAT_RAMP', T=1100.0, F=1.878646/

&RAMP ID='CHAR_SPECIFIC_HEAT_RAMP', T=1150.0, F=1.899076/

&RAMP ID='CHAR_SPECIFIC_HEAT_RAMP', T=1200.0, F=1.919238/

&MATL ID='WATER',

    FYI='Hostikka - Nordic structural timber',

    SPECIFIC_HEAT_RAMP='WATER_SPECIFIC_HEAT_RAMP',

    CONDUCTIVITY=0.6,

    DENSITY=1000.0,

    N_REACTIONS=1,

    HEAT_OF_REACTION=2500.0,

    SPEC_ID(1,1)='WATER VAPOR',

    NU_SPEC(1,1)=1.0,

    N_S=3.31,

    A=1.12438E+16,

    E=1.36E+5/

&RAMP ID='WATER_SPECIFIC_HEAT_RAMP', T=20.0, F=4.7/

&RAMP ID='WATER_SPECIFIC_HEAT_RAMP', T=100.0, F=6.7/

&MATL ID='SPRUCE WALL',

    FYI='Hostikka - Nordic structural timber',

    SPECIFIC_HEAT_RAMP='SPRUCE WALL_SPECIFIC_HEAT_RAMP',

    CONDUCTIVITY=0.09,

    DENSITY=408.0,
```

L

```
    N_REACTIONS=1,

    HEAT_OF_REACTION=19.0,

    MATL_ID(1,1)='CHAR',

    NU_MATL(1,1)=0.16,

    SPEC_ID(1,1)='WALL PYROLYZATE',

    NU_SPEC(1,1)=0.84,

    N_S=1.89,

    A=2.19311E+11,

    E=1.905E+5/
```

&RAMP ID='SPRUCE WALL_SPECIFIC_HEAT_RAMP', T=30.0, F=0.92/

&RAMP ID='SPRUCE WALL_SPECIFIC_HEAT_RAMP', T=50.0, F=1.008/

&RAMP ID='SPRUCE WALL_SPECIFIC_HEAT_RAMP', T=70.0, F=1.096/

&RAMP ID='SPRUCE WALL_SPECIFIC_HEAT_RAMP', T=90.0, F=1.184/

&RAMP ID='SPRUCE WALL_SPECIFIC_HEAT_RAMP', T=110.0, F=1.272/

&RAMP ID='SPRUCE WALL_SPECIFIC_HEAT_RAMP', T=130.0, F=1.36/

&RAMP ID='SPRUCE WALL_SPECIFIC_HEAT_RAMP', T=150.0, F=1.448/

&RAMP ID='SPRUCE WALL_SPECIFIC_HEAT_RAMP', T=170.0, F=1.536/

&RAMP ID='SPRUCE WALL_SPECIFIC_HEAT_RAMP', T=190.0, F=1.624/

&RAMP ID='SPRUCE WALL_SPECIFIC_HEAT_RAMP', T=210.0, F=1.712/

&RAMP ID='SPRUCE WALL_SPECIFIC_HEAT_RAMP', T=230.0, F=1.8/

&RAMP ID='SPRUCE WALL_SPECIFIC_HEAT_RAMP', T=250.0, F=1.888/

&RAMP ID='SPRUCE WALL_SPECIFIC_HEAT_RAMP', T=270.0, F=1.976/

&RAMP ID='SPRUCE WALL_SPECIFIC_HEAT_RAMP', T=290.0, F=2.064/

&RAMP ID='SPRUCE WALL_SPECIFIC_HEAT_RAMP', T=310.0, F=2.152/

&RAMP ID='SPRUCE WALL_SPECIFIC_HEAT_RAMP', T=330.0, F=2.24/

&RAMP ID='SPRUCE WALL_SPECIFIC_HEAT_RAMP', T=350.0, F=2.328/

&RAMP ID='SPRUCE WALL_SPECIFIC_HEAT_RAMP', T=370.0, F=2.416/

&RAMP ID='SPRUCE WALL_SPECIFIC_HEAT_RAMP', T=390.0, F=2.504/

&RAMP ID='SPRUCE WALL_SPECIFIC_HEAT_RAMP', T=410.0, F=2.592/

&RAMP ID='SPRUCE WALL_SPECIFIC_HEAT_RAMP', T=430.0, F=2.68/

&RAMP ID='SPRUCE WALL_SPECIFIC_HEAT_RAMP', T=450.0, F=2.768/

&RAMP ID='SPRUCE WALL_SPECIFIC_HEAT_RAMP', T=470.0, F=2.856/

&RAMP ID='SPRUCE WALL_SPECIFIC_HEAT_RAMP', T=490.0, F=2.944/

&RAMP ID='SPRUCE WALL_SPECIFIC_HEAT_RAMP', T=510.0, F=3.032/

&RAMP ID='SPRUCE WALL_SPECIFIC_HEAT_RAMP', T=530.0, F=3.12/

&RAMP ID='SPRUCE WALL_SPECIFIC_HEAT_RAMP', T=550.0, F=3.208/

&RAMP ID='SPRUCE WALL_SPECIFIC_HEAT_RAMP', T=570.0, F=3.296/

&RAMP ID='SPRUCE WALL_SPECIFIC_HEAT_RAMP', T=590.0, F=3.384/

&RAMP ID='SPRUCE WALL_SPECIFIC_HEAT_RAMP', T=610.0, F=3.472/

&RAMP ID='SPRUCE WALL_SPECIFIC_HEAT_RAMP', T=630.0, F=3.56/

&RAMP ID='SPRUCE WALL_SPECIFIC_HEAT_RAMP', T=650.0, F=3.648/

&RAMP ID='SPRUCE WALL_SPECIFIC_HEAT_RAMP', T=670.0, F=3.736/

&RAMP ID='SPRUCE WALL_SPECIFIC_HEAT_RAMP', T=690.0, F=3.824/

M

```
&RAMP ID='SPRUCE WALL_SPECIFIC_HEAT_RAMP', T=710.0, F=3.912/

&RAMP ID='SPRUCE WALL_SPECIFIC_HEAT_RAMP', T=730.0, F=4.0/

&RAMP ID='SPRUCE WALL_SPECIFIC_HEAT_RAMP', T=750.0, F=4.088/

&RAMP ID='SPRUCE WALL_SPECIFIC_HEAT_RAMP', T=770.0, F=4.176/

&RAMP ID='SPRUCE WALL_SPECIFIC_HEAT_RAMP', T=790.0, F=4.264/

&RAMP ID='SPRUCE WALL_SPECIFIC_HEAT_RAMP', T=810.0, F=4.352/

&MATL ID='TYPE F PLASTERBOARD',

    FYI='Bartlett - Effects of exposed cross laminated timber on compartment fire dynamics',

    SPECIFIC_HEAT=0.95,

    CONDUCTIVITY=0.24,

    DENSITY=784.0/

&MATL ID='STONE WOOL',

    FYI='Bartlett - Effects of exposed cross laminated timber on compartment fire dynamics',

    SPECIFIC_HEAT=0.7,

    CONDUCTIVITY=0.039,

    DENSITY=164.0/


&SURF ID='CRIB FIRE',

    FYI='MLRPUA: Bartlett - Effects of exposed cross laminated timber on compartment fire dynamics',

    RGB=226,0,16,

    TMP_FRONT=0.0,

    MASS_FLUX=0.17,

    SPEC_ID='CRIB PYROLYZATE',

    RAMP_MF='CRIB FIRE_RAMP_MF'/

&RAMP ID='CRIB FIRE_RAMP_MF', T=0.0, F=0.0/

&RAMP ID='CRIB FIRE_RAMP_MF', T=10.0, F=0.02824/

&RAMP ID='CRIB FIRE_RAMP_MF', T=20.0, F=0.038919/

&RAMP ID='CRIB FIRE_RAMP_MF', T=30.0, F=0.049772/

&RAMP ID='CRIB FIRE_RAMP_MF', T=40.0, F=0.060892/

&RAMP ID='CRIB FIRE_RAMP_MF', T=50.0, F=0.072446/

&RAMP ID='CRIB FIRE_RAMP_MF', T=60.0, F=0.08464/

&RAMP ID='CRIB FIRE_RAMP_MF', T=70.0, F=0.097598/

&RAMP ID='CRIB FIRE_RAMP_MF', T=80.0, F=0.111243/

&RAMP ID='CRIB FIRE_RAMP_MF', T=90.0, F=0.125672/

&RAMP ID='CRIB FIRE_RAMP_MF', T=100.0, F=0.144727/

&RAMP ID='CRIB FIRE_RAMP_MF', T=110.0, F=0.174599/

&RAMP ID='CRIB FIRE_RAMP_MF', T=120.0, F=0.210554/

&RAMP ID='CRIB FIRE_RAMP_MF', T=130.0, F=0.240919/

&RAMP ID='CRIB FIRE_RAMP_MF', T=140.0, F=0.273427/

&RAMP ID='CRIB FIRE_RAMP_MF', T=150.0, F=0.300214/

&RAMP ID='CRIB FIRE_RAMP_MF', T=160.0, F=0.319182/

&RAMP ID='CRIB FIRE_RAMP_MF', T=170.0, F=0.347307/

&RAMP ID='CRIB FIRE_RAMP_MF', T=180.0, F=0.372185/
```

N

```
&RAMP ID='CRIB FIRE_RAMP_MF', T=190.0, F=0.388631/

&RAMP ID='CRIB FIRE_RAMP_MF', T=200.0, F=0.398089/

&RAMP ID='CRIB FIRE_RAMP_MF', T=210.0, F=0.403686/

&RAMP ID='CRIB FIRE_RAMP_MF', T=220.0, F=0.408921/

&RAMP ID='CRIB FIRE_RAMP_MF', T=230.0, F=0.417164/

&RAMP ID='CRIB FIRE_RAMP_MF', T=240.0, F=0.429733/

&RAMP ID='CRIB FIRE_RAMP_MF', T=250.0, F=0.446338/

&RAMP ID='CRIB FIRE_RAMP_MF', T=260.0, F=0.467806/

&RAMP ID='CRIB FIRE_RAMP_MF', T=270.0, F=0.499918/

&RAMP ID='CRIB FIRE_RAMP_MF', T=280.0, F=0.543201/

&RAMP ID='CRIB FIRE_RAMP_MF', T=290.0, F=0.590341/

&RAMP ID='CRIB FIRE_RAMP_MF', T=300.0, F=0.636274/

&RAMP ID='CRIB FIRE_RAMP_MF', T=310.0, F=0.689401/

&RAMP ID='CRIB FIRE_RAMP_MF', T=320.0, F=0.762319/

&RAMP ID='CRIB FIRE_RAMP_MF', T=330.0, F=0.825406/

&RAMP ID='CRIB FIRE_RAMP_MF', T=340.0, F=0.864216/

&RAMP ID='CRIB FIRE_RAMP_MF', T=350.0, F=0.928293/

&RAMP ID='CRIB FIRE_RAMP_MF', T=360.0, F=0.996338/

&RAMP ID='CRIB FIRE_RAMP_MF', T=370.0, F=1.042767/

&RAMP ID='CRIB FIRE_RAMP_MF', T=380.0, F=1.041998/

&RAMP ID='CRIB FIRE_RAMP_MF', T=390.0, F=0.970718/

&RAMP ID='CRIB FIRE_RAMP_MF', T=400.0, F=0.918449/

&RAMP ID='CRIB FIRE_RAMP_MF', T=410.0, F=0.917735/

&RAMP ID='CRIB FIRE_RAMP_MF', T=420.0, F=0.914804/

&RAMP ID='CRIB FIRE_RAMP_MF', T=430.0, F=0.901623/

&RAMP ID='CRIB FIRE_RAMP_MF', T=440.0, F=0.880741/

&RAMP ID='CRIB FIRE_RAMP_MF', T=450.0, F=0.854706/

&RAMP ID='CRIB FIRE_RAMP_MF', T=460.0, F=0.826005/

&RAMP ID='CRIB FIRE_RAMP_MF', T=470.0, F=0.79665/

&RAMP ID='CRIB FIRE_RAMP_MF', T=480.0, F=0.768372/

&RAMP ID='CRIB FIRE_RAMP_MF', T=490.0, F=0.734496/

&RAMP ID='CRIB FIRE_RAMP_MF', T=500.0, F=0.703634/

&RAMP ID='CRIB FIRE_RAMP_MF', T=510.0, F=0.680048/

&RAMP ID='CRIB FIRE_RAMP_MF', T=520.0, F=0.6594/

&RAMP ID='CRIB FIRE_RAMP_MF', T=530.0, F=0.64002/

&RAMP ID='CRIB FIRE_RAMP_MF', T=540.0, F=0.623843/

&RAMP ID='CRIB FIRE_RAMP_MF', T=550.0, F=0.611886/

&RAMP ID='CRIB FIRE_RAMP_MF', T=560.0, F=0.597059/

&RAMP ID='CRIB FIRE_RAMP_MF', T=570.0, F=0.571518/

&RAMP ID='CRIB FIRE_RAMP_MF', T=580.0, F=0.547644/

&RAMP ID='CRIB FIRE_RAMP_MF', T=590.0, F=0.534573/

&RAMP ID='CRIB FIRE_RAMP_MF', T=600.0, F=0.524055/

&RAMP ID='CRIB FIRE_RAMP_MF', T=610.0, F=0.509245/
```

O

```
&RAMP ID='CRIB FIRE_RAMP_MF', T=620.0, F=0.492617/

&RAMP ID='CRIB FIRE_RAMP_MF', T=630.0, F=0.479242/

&RAMP ID='CRIB FIRE_RAMP_MF', T=640.0, F=0.469093/

&RAMP ID='CRIB FIRE_RAMP_MF', T=650.0, F=0.452937/

&RAMP ID='CRIB FIRE_RAMP_MF', T=660.0, F=0.425357/

&RAMP ID='CRIB FIRE_RAMP_MF', T=670.0, F=0.397983/

&RAMP ID='CRIB FIRE_RAMP_MF', T=680.0, F=0.377152/

&RAMP ID='CRIB FIRE_RAMP_MF', T=690.0, F=0.362642/

&RAMP ID='CRIB FIRE_RAMP_MF', T=700.0, F=0.348058/

&RAMP ID='CRIB FIRE_RAMP_MF', T=710.0, F=0.320918/

&RAMP ID='CRIB FIRE_RAMP_MF', T=720.0, F=0.268206/

&RAMP ID='CRIB FIRE_RAMP_MF', T=730.0, F=0.234606/

&RAMP ID='CRIB FIRE_RAMP_MF', T=740.0, F=0.207328/

&RAMP ID='CRIB FIRE_RAMP_MF', T=750.0, F=0.175702/

&RAMP ID='CRIB FIRE_RAMP_MF', T=760.0, F=0.131468/

&RAMP ID='CRIB FIRE_RAMP_MF', T=770.0, F=0.10753/

&RAMP ID='CRIB FIRE_RAMP_MF', T=780.0, F=0.052541/

&RAMP ID='CRIB FIRE_RAMP_MF', T=790.0, F=8.255963E-3/

&SURF ID='SPRUCE CEILING',

    FYI='Compostion: Bartlett - Effects of exposed cross laminated timber on compartment fire dynamics',

    RGB=187,152,116,

    HEAT_TRANSFER_COEFFICIENT=15.0,

    BACKING='VOID',

    MATL_ID(1,1:2)='SPRUCE CEILING','WATER',

    MATL_MASS_FRACTION(1,1:2)=0.91,0.09,

    THICKNESS(1)=0.1,

    CELL_SIZE_FACTOR=0.8,

    STRETCH_FACTOR(1)=1.0/

&SURF ID='SPRUCE WALL',

    RGB=187,152,116,

    HEAT_TRANSFER_COEFFICIENT=15.0,

    BACKING='VOID',

    MATL_ID(1,1:2)='SPRUCE WALL','WATER',

    MATL_MASS_FRACTION(1,1:2)=0.91,0.09,

    THICKNESS(1)=0.1,

    CELL_SIZE_FACTOR=0.8,

    STRETCH_FACTOR(1)=1.0/

&SURF ID='ENCAPSULATION',

    FYI='Compositon: Bartlett - Effects of exposed cross laminated timber on compartment fire dynamics',

    RGB=148,222,255,

    BACKING='VOID',

    MATL_ID(1,1)='TYPE F PLASTERBOARD',

    MATL_ID(2,1)='SPRUCE WALL',
```

P

```
    MATL_MASS_FRACTION(1,1)=1.0,

    MATL_MASS_FRACTION(2,1)=1.0,

    THICKNESS(1:2)=0.025,0.1/


&OBST ID='BACK WALL', XB=-1.36,1.36,-1.46,-1.36,0.1,2.87, SURF_ID6='INERT','INERT','INERT','SPRUCE WALL','INERT','INERT'/

&OBST ID='RIGHT WALL', XB=1.36,1.46,-1.46,1.46,0.1,2.87, SURF_ID6='ENCAPSULATION','INERT','INERT','INERT','INERT','INERT'/

&OBST ID='FRONT WALL', XB=-1.36,1.36,1.36,1.46,0.1,2.87, SURF_ID6='INERT','INERT','ENCAPSULATION','INERT','INERT','INERT'/

&OBST ID='LEFT WALL', XB=-1.46,-1.36,-1.46,1.46,0.1,2.87, SURF_ID6='INERT','INERT','ENCAPSULATION','INERT','INERT','INERT'/

&OBST ID='CEILING', XB=-1.46,1.46,-1.46,1.46,2.87,2.97, SURF_IDS='INERT','INERT','SPRUCE CEILING'/

&OBST ID='FLOOR', XB=-1.46,1.46,-1.46,1.46,0.0,0.1/

&OBST ID='Obstruction', XB=-1.46,1.5,-1.46,1.46,2.97,3.0/

&OBST ID='Obstruction', XB=-1.5,-1.46,-1.46,1.46,0.0,3.0/

&OBST ID='Obstruction', XB=1.46,1.5,-1.46,1.46,0.0,2.97/

&OBST ID='Obstruction', XB=-1.5,1.5,-1.46,1.46,3.0,6.0/


&HOLE ID='OPENING', XB=-0.38,0.38,1.26,1.56,0.1,1.94/


&VENT ID='Mesh Vent: MESH-01-01 [XMIN]', SURF_ID='OPEN', XB=-1.5,-1.5,-1.46,-0.01,0.0,1.5/

&VENT ID='Mesh Vent: MESH-01-01 [YMIN]', SURF_ID='OPEN', XB=-1.5,-0.5,-1.46,-1.46,0.0,1.5/

&VENT ID='Mesh Vent: MESH-01-01 [ZMIN]', SURF_ID='OPEN', XB=-1.5,-0.5,-1.46,-0.01,0.0,0.0/

&VENT ID='Mesh Vent: MESH-01-02 [XMIN]', SURF_ID='OPEN', XB=-1.5,-1.5,-1.46,-0.01,1.5,3.0/

&VENT ID='Mesh Vent: MESH-01-02 [YMIN]', SURF_ID='OPEN', XB=-1.5,-0.5,-1.46,-1.46,1.5,3.0/

&VENT ID='Mesh Vent: MESH-01-02 [ZMAX]', SURF_ID='OPEN', XB=-1.5,-0.5,-1.46,-0.01,3.0,3.0/

&VENT ID='Mesh Vent: MESH-01-03 [XMIN]', SURF_ID='OPEN', XB=-1.5,-1.5,-0.01,1.44,0.0,1.5/

&VENT ID='Mesh Vent: MESH-01-03 [ZMIN]', SURF_ID='OPEN', XB=-1.5,-0.5,-0.01,1.44,0.0,0.0/

&VENT ID='Mesh Vent: MESH-01-04 [XMIN]', SURF_ID='OPEN', XB=-1.5,-1.5,-0.01,1.44,1.5,3.0/

&VENT ID='Mesh Vent: MESH-01-04 [ZMAX]', SURF_ID='OPEN', XB=-1.5,-0.5,-0.01,1.44,3.0,3.0/

&VENT ID='Mesh Vent: MESH-01-05 [YMIN]', SURF_ID='OPEN', XB=-0.5,0.5,-1.46,-1.46,0.0,1.5/

&VENT ID='Mesh Vent: MESH-01-05 [ZMIN]', SURF_ID='OPEN', XB=-0.5,0.5,-1.46,-0.01,0.0,0.0/

&VENT ID='Mesh Vent: MESH-01-06 [YMIN]', SURF_ID='OPEN', XB=-0.5,0.5,-1.46,-1.46,1.5,3.0/

&VENT ID='Mesh Vent: MESH-01-06 [ZMAX]', SURF_ID='OPEN', XB=-0.5,0.5,-1.46,-0.01,3.0,3.0/

&VENT ID='Mesh Vent: MESH-01-07 [ZMIN]', SURF_ID='OPEN', XB=-0.5,0.5,-0.01,1.44,0.0,0.0/

&VENT ID='Mesh Vent: MESH-01-08 [ZMAX]', SURF_ID='OPEN', XB=-0.5,0.5,-0.01,1.44,3.0,3.0/

&VENT ID='Mesh Vent: MESH-01-09 [XMAX]', SURF_ID='OPEN', XB=1.5,1.5,-1.46,-0.01,0.0,1.5/

&VENT ID='Mesh Vent: MESH-01-09 [YMIN]', SURF_ID='OPEN', XB=0.5,1.5,-1.46,-1.46,0.0,1.5/

&VENT ID='Mesh Vent: MESH-01-09 [ZMIN]', SURF_ID='OPEN', XB=0.5,1.5,-1.46,-0.01,0.0,0.0/

&VENT ID='Mesh Vent: MESH-01-10 [XMAX]', SURF_ID='OPEN', XB=1.5,1.5,-1.46,-0.01,1.5,3.0/

&VENT ID='Mesh Vent: MESH-01-10 [YMIN]', SURF_ID='OPEN', XB=0.5,1.5,-1.46,-1.46,1.5,3.0/

&VENT ID='Mesh Vent: MESH-01-10 [ZMAX]', SURF_ID='OPEN', XB=0.5,1.5,-1.46,-0.01,3.0,3.0/

&VENT ID='Mesh Vent: MESH-01-11 [XMAX]', SURF_ID='OPEN', XB=1.5,1.5,-0.01,1.44,0.0,1.5/

&VENT ID='Mesh Vent: MESH-01-11 [ZMIN]', SURF_ID='OPEN', XB=0.5,1.5,-0.01,1.44,0.0,0.0/

&VENT ID='Mesh Vent: MESH-01-12 [XMAX]', SURF_ID='OPEN', XB=1.5,1.5,-0.01,1.44,1.5,3.0/

&VENT ID='Mesh Vent: MESH-01-12 [ZMAX]', SURF_ID='OPEN', XB=0.5,1.5,-0.01,1.44,3.0,3.0/
```

Q

```
&VENT ID='Mesh Vent: MESH-03-merged-01 [XMIN]', SURF_ID='OPEN', XB=-1.5,-1.5,1.44,3.34,0.0,2.0/

&VENT ID='Mesh Vent: MESH-03-merged-01 [YMAX]', SURF_ID='OPEN', XB=-1.5,-3.108624E-15,3.34,3.34,0.0,2.0/

&VENT ID='Mesh Vent: MESH-03-merged-02 [XMIN]', SURF_ID='OPEN', XB=-1.5,-1.5,1.44,3.34,2.0,4.0/

&VENT ID='Mesh Vent: MESH-03-merged-02 [YMAX]', SURF_ID='OPEN', XB=-1.5,-3.108624E-15,3.34,3.34,2.0,4.0/

&VENT ID='Mesh Vent: MESH-03-merged-02 [YMIN]', SURF_ID='OPEN', XB=-1.5,-3.108624E-15,1.44,1.44,3.0,4.0/

&VENT ID='Mesh Vent: MESH-03-merged-03 [XMIN]', SURF_ID='OPEN', XB=-1.5,-1.5,1.44,3.34,4.0,6.0/

&VENT ID='Mesh Vent: MESH-03-merged-03 [YMAX]', SURF_ID='OPEN', XB=-1.5,-3.108624E-15,3.34,3.34,4.0,6.0/

&VENT ID='Mesh Vent: MESH-03-merged-03 [YMIN]', SURF_ID='OPEN', XB=-1.5,-3.108624E-15,1.44,1.44,4.0,6.0/

&VENT ID='Mesh Vent: MESH-03-merged-03 [ZMAX]', SURF_ID='OPEN', XB=-1.5,-3.108624E-15,1.44,3.34,6.0,6.0/

&VENT ID='Mesh Vent: MESH-03-merged-04 [XMAX]', SURF_ID='OPEN', XB=1.5,1.5,1.44,3.34,0.0,2.0/

&VENT ID='Mesh Vent: MESH-03-merged-04 [YMAX]', SURF_ID='OPEN', XB=-3.108624E-15,1.5,3.34,3.34,0.0,2.0/

&VENT ID='Mesh Vent: MESH-03-merged-05 [XMAX]', SURF_ID='OPEN', XB=1.5,1.5,1.44,3.34,2.0,4.0/

&VENT ID='Mesh Vent: MESH-03-merged-05 [YMAX]', SURF_ID='OPEN', XB=-3.108624E-15,1.5,3.34,3.34,2.0,4.0/

&VENT ID='Mesh Vent: MESH-03-merged-05 [YMIN]', SURF_ID='OPEN', XB=-3.108624E-15,1.5,1.44,1.44,3.0,4.0/

&VENT ID='Mesh Vent: MESH-03-merged-06 [XMAX]', SURF_ID='OPEN', XB=1.5,1.5,1.44,3.34,4.0,6.0/

&VENT ID='Mesh Vent: MESH-03-merged-06 [YMAX]', SURF_ID='OPEN', XB=-3.108624E-15,1.5,3.34,3.34,4.0,6.0/

&VENT ID='Mesh Vent: MESH-03-merged-06 [YMIN]', SURF_ID='OPEN', XB=-3.108624E-15,1.5,1.44,1.44,4.0,6.0/

&VENT ID='Mesh Vent: MESH-03-merged-06 [ZMAX]', SURF_ID='OPEN', XB=-3.108624E-15,1.5,1.44,3.34,6.0,6.0/

&VENT ID='CRIB', SURF_ID='CRIB FIRE', XB=-0.5,0.5,-0.5,0.5,0.1,0.1/


&BNDF QUANTITY='MASS FLUX', SPEC_ID='CEILING PYROLYZATE'/

&BNDF QUANTITY='MASS FLUX', SPEC_ID='WALL PYROLYZATE'/

&BNDF QUANTITY='INCIDENT HEAT FLUX'/


&PROF ID='CEILING TEMP', XYZ=0.0,0.0,2.87, IOR=-3, QUANTITY='TEMPERATURE'/

&PROF ID='BACK WALL TEMP', XYZ=0.0,-1.36,1.435, IOR=2, QUANTITY='TEMPERATURE'/


&SLCF QUANTITY='TEMPERATURE', ID='TEMP Y', PBY=0.0/

&SLCF QUANTITY='TEMPERATURE', ID='TEMP X', PBX=0.0/

&SLCF QUANTITY='CONDUCTIVITY', ID='CONDUCTIVITY', PBY=0.0/

&SLCF QUANTITY='VELOCITY', VECTOR=.TRUE., CELL_CENTERED=.TRUE., ID='VELOCITY Y', PBY=0.0/

&SLCF QUANTITY='VELOCITY', VECTOR=.TRUE., CELL_CENTERED=.TRUE., ID='VELOCITY X', PBX=0.0/

&SLCF QUANTITY='TEMPERATURE', ID='3D Slice', XB=-1.5,1.5,-1.46,3.34,0.0,6.0/

&SLCF QUANTITY='HRRPUV', ID='3D Slice', XB=-1.5,1.5,-1.46,3.34,0.0,6.0/


&TAIL /
```

R